SR AND U ISOTOPES REVEAL INTERACTIONS OF SURFACE WATER AND GROUNDWATER ALONG THE MOUNTAIN HEADWATERS TO INTERMOUNTAIN BASIN TRANSITION (HYALITE CANYON AND GALLATIN VALLEY, MT)

by

Florence Rita Miller

A thesis submitted in partial fulfillment
of the requirements for the degree

of

Master of Science

in

Land Resources and Environmental Sciences

MONTANA STATE UNIVERSITY
Bozeman, Montana

August 2018

ACKNOWLEDGEMENTS

I would like to thank my advisor, Dr. Stephanie Ewing for her guidance and mentorship; and for allowing me the opportunity of conducting novel research in the beautiful landscapes of Hyalite Canyon and the Gallatin Valley. Her dedication and passion for producing quality research is inspirational, all while passing on her knowledge on the intricacies of isotope systems, geochemistry, and pedology. I would like to thank committee member Dr. Rob Payn for offering countless hours of guidance on coding, and for providing valuable insight on hydrology and the nuances of scientific writing. I would like to thank committee member Dr. Jim Paces for his geochemical expertise, including running a multitude of isotope analysis while patiently passing on his knowledge from the analytical chemistry to interpretation and writing of results. I would like to extend my gratitude to Dr. Steve Custer and Tom Michalek for their wisdom on hydrology and geology systems in the Gallatin Valley, often presenting the key to the understanding and interpretation of our research.

Thank you to the USGS Grant 104g Water Resources Competitive Grants Program, the Nielsen Fellowship, and the Montana Agriculture Experiment Station for offering financial support and ideological inspiration for my research and degree.

Thank you to my Ewing Lab mates Ethan Wologo, Sam Leuthold, Joe Capella, and Adam Sigler for their collaboration, support, and friendship. Thank you to my friends and family for their support, fun, and grounding presence throughout this process. And finally, thank you to my mom and dad for listing to ideas and reading countless drafts all while providing unwavering support.

TABLE OF CONTENTS

TABLE OF CONTENTS CONTINUED

TABLE OF CONTENTS CONTINUED

LIST OF TABLES

Table Page

LIST OF FIGURES

LIST OF FIGURES CONTINUED

Figure Page

ABSTRACT

Mountainous regions of the western United States are characterized by steep, rapidly eroding mountain headwater streams transitioning to more depositional intermountain basins. The character and flux of water across these process domains is subject to projected changes in mountain headwater snowpack and agricultural and urban land use in rapidly developing intermountain basins. Here we evaluate controls on water/rock, water/substrate, and surface/groundwater interactions within Hyalite Creek and the Gallatin Valley of southwest Montana. We use solute loads and geochemical tracers ($^{87}Sr/^{86}Sr$, Ca/Sr, and $[^{234}U/^{238}U]$) as indicators of such interactions. Surface water, groundwater, and soil samples were collected between 2016 and 2018. Stream water in upper Hyalite Creek had low $^{87}Sr/^{86}Sr$ values typical of volcanic and sedimentary host rock units, and low $[^{234}U/^{238}U]$ values consistent with shorter flow path soil, shallow aquifer or runoff water. Middle Hyalite Creek had increased $[^{234}U/^{238}U]$ values, reflecting groundwater inflows from the Madison Group limestones. Lower Hyalite Creek had an increase in $^{87}Sr/^{86}Sr$ values and decrease in $[^{234}U/^{238}U]$ values, indicated contributions from Archean gneiss fracture flow. Using mixing models, we estimate inflows from the Madison contribute ~4% during summer baseflow conditions and inflows from the Archean contribute ~2% to ~8% of streamflow during summer and winter baseflow conditions. At the mountain front, diverse Ca/Sr, $^{87}Sr/^{86}Sr$, and $[^{234}U/^{238}U]$ ratios were observed as a result of convergent flow in mountain headwaters catchments. In the intermountain basin, divergent flow at the mountain front recharges valley aquifers and combines with infiltration through soils. With distance down-valley, we observe intermediate values of Ca/Sr, $^{87}Sr/^{86}Sr$, and $[^{234}U/^{238}U]$, suggesting mixing of diverse source waters. Higher concentrations of Sr, alkalinity, and Ca/Sr and $^{87}Sr/^{86}Sr$ ratios consistent with soil carbonates suggest water infiltration through soil facilitated the influence of soil secondary carbonates on groundwater geochemistry. Additionally, increased water movement through soil facilitates the increase in anthropogenic loading of NO_3^- and Cl^- in surface and groundwaters. Our results provide novel quantification of groundwater contribution to streamflow in mountain headwaters, and elucidate water quality and quantity controls from the mountain front across the intermountain basin, including valley aquifer recharge, infiltration through soils, and anthropogenic solute influxes to groundwater.

CHAPTER ONE

GENERAL INTRODUCTION

Mountain headwaters supply surface water and groundwater to the rivers and aquifers of intermountain basins, where ecosystems, agriculture, and urban communities rely on this mountain front water supply (Hoylman et al. 2018; Payn et al. 2012; Silverman & Maneta 2016). Mountain headwater streams undergo exchange with groundwater. These gains and losses influence the stream's solute composition and alluvial aquifer recharge. At the mountain front transition, stream water solute chemistry reflects water interaction with rock and soil through substrate weathering and water flow path (Covino & McGlynn 2007; Capell et al. 2011; Yang et al. 2017; Jasechko & Kirchner 2016; Payn et al. 2009). This water-rock and water-soil interaction imparts a geochemical fingerprint on water, reflecting lithologic water source and flow path. Thus, the transition from mountain headwaters to intermountain basin marks a key shift in process domains as conceived by Montgomery (1999). This transition controls streamflow and water quality, as the water emerging at the mountain front provides an input signal that is defined by the mountain catchment that delivers it. Within the valley aquifer and surface waters, geochemical tracers and solutes record the influence of snowmelt recharge, infiltration through soils, and anthropogenic inputs to groundwater by virtue of land use.

In this thesis, I use $^{234}U/^{238}U$ activity ratios and $^{87}Sr/^{86}Sr$ ratios, along with water balance, discharge patterns, and solute composition, to characterize the interaction of

groundwater and surface water, its influence on stream chemistry, and alluvial aquifer recharge in the mountain headwaters to intermountain basin transition of Hyalite Creek and the Gallatin Valley, within the Upper Missouri River Headwaters (Figure 1.1). My goals with this work are to (1) improve understanding of water storage, flow and exchange in mountain headwaters to intermountain basin weathering environments, and (2) characterize the contribution of weathering in soils, alluvium and bedrock across this transition using surface water and groundwater chemistry.

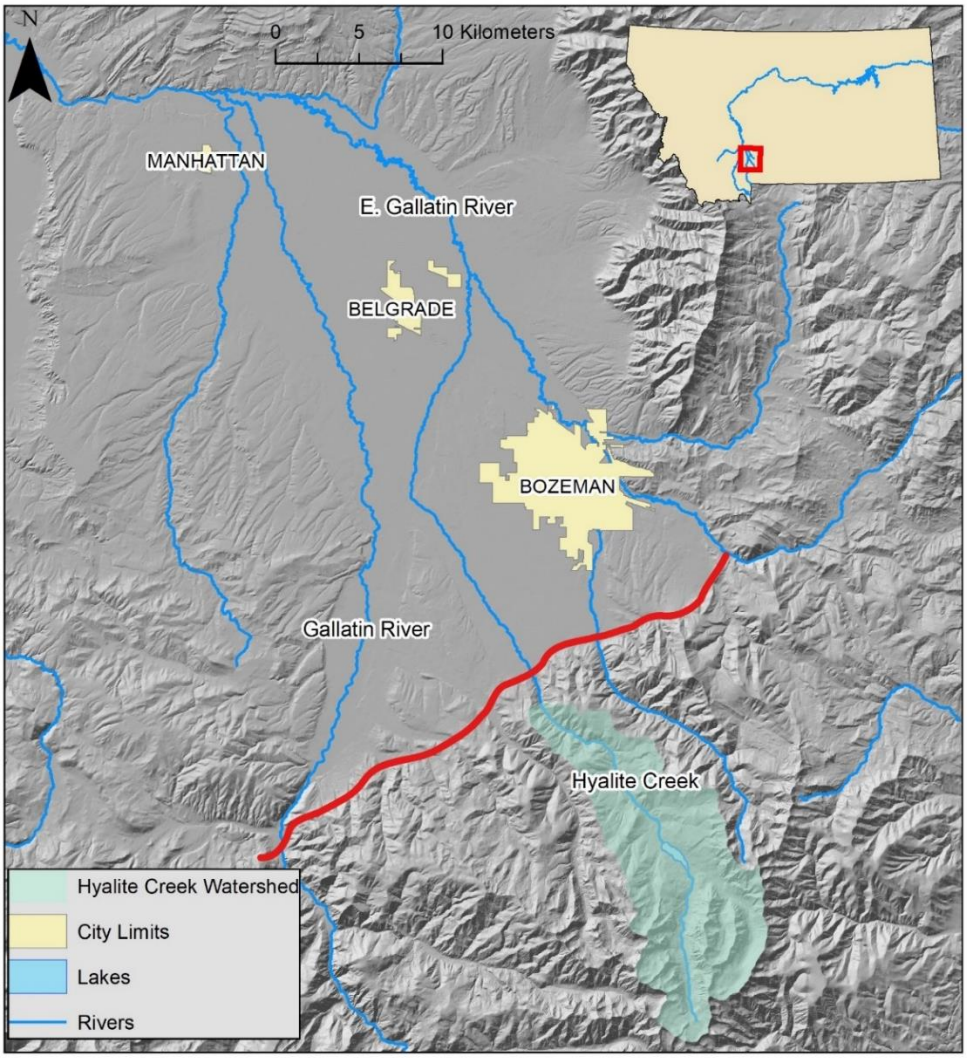

Figure 1.1. Location map of Hyalite Creek and the Gallatin Valley. Hyalite Creek watershed is highlighted with green shading, the mountain front transition is indicated as the red line, and the Gallatin Valley is shown within the state of Montana (inset) and Upper Missouri Watershed.

CHAPTER TWO

LITERATURE REVIEW

2.1 Water Storage and Baseflow Dynamics in the Intermountain West

This work considers this mountain front transition as a boundary between two distinct process domains (Montgomery 1999). The interconnectivity of surface and groundwater from a mountain catchment across the mountain front transition to an alluvial valley supplies new water – often dominated by snowmelt -- to valley aquifers, driving the downstream return of older aquifer water to valley streams and rivers (Covino & McGlynn 2007). This movement of water through soils, regolith, and bedrock also dictates weathering trajectories that in turn influence the chemistry of groundwater and surface water. In this work, I used geochemical tracers of lithologic source and weathering to explore the movement of water above, through, and below the mountain front transition in Hyalite Canyon and the Gallatin Valley, Montana.

Mountain stream runoff is often modeled solely using surface water, yet there is a strong interaction between surface water and groundwater throughout the reach of a mountain stream (Payn et al. 2009). The gains and losses of water throughout the reach of a stream influence the stream's solute composition in characteristic ways that reflect both water balance and interaction with the substrate through weathering (Payn et al. 2009; Covino & McGlynn 2007; Capell et al. 2011; Yang et al. 2017; Jasechko 2016; Jasechko & Kirchner 2016). Generally, the interaction of water with rock and soil leaves a geochemical fingerprint on the water that potentially allows determination of origin and

flow path of the water. Due to analytical complexity, specialized equipment, and expense, geochemical tools are an underutilized source of information about the nature of base flow along mountainous streams. Mountain stream, soil, and groundwater interconnectivity influence stream discharge, solute composition, water quality, and alluvial-aquifer recharge, yet characterization of these connections, particularly longitudinally along stream channels, has been limited. Changing climate and precipitation patterns will potentially influence snowpack storage and hence late summer flows supplied by groundwater that is recharged by snowmelt at mountain fronts. Ecosystems, agriculture, and municipalities depend on late season flows, making it increasingly important to understand base flow mechanisms and the interaction between surface and groundwater at the mountain front transition between mountain headwater and intermountain basin environments (Yang et al. 2017; Jasechko 2016; Payn et al. 2012; Hoylman et al. 2018; Silverman & Maneta 2016).

2.2 Geochemical Tracers

The geochemical fingerprint of water traces a distinctive signal of weathering and water flow path (Hogan & Blum 2003; Dosseto et al. 2014; Chabaux et al. 2003). As lithology changes across the mountain headwaters to intermountain basin transition, so does the geochemical fingerprint imparted on the water, allowing individual rock units and water residence times to be traced (Barbieri et al. 2005). To examine water flow and storage, I used two geochemical tracers of water/rock and water/soil interaction: strontium isotopes ($^{87}Sr/^{86}Sr$ ratio) and uranium isotopes ($^{234}U/^{238}U$ activity ratio). For these heavy radiogenic isotopes, concentrations tend to be higher in groundwater and

fractionation is limited from near surface processes, making these tracers particularly sensitive to baseflow contributions from distinct lithologies (Paces & Wurster 2014; Drexler et al. 2014).

2.3 Strontium

Strontium has four stable isotopes ^{84}Sr (0.56%), ^{86}Sr (9.87%), ^{87}Sr (7.04%), and ^{88}Sr (82.33%) (Faure & Mensing 2005). The source of isotopic ratio variation is ^{87}Sr, the stable daughter isotope resulting from the beta (β) decay of ^{87}Rb, which has a half-life of 4.9×10^{10} years (Faure & Mensing 2005). The geochemical basis for variations in Sr isotope ratios are differences in the Rb/Sr ratio and the degree of radioactive decay of ^{87}Rb (i.e., age) in the rock or mineral (Capo et al. 1998). The $^{87}Sr/^{86}Sr$ ratio is most commonly evaluated in mixing models because it is conservative (Drexler et al. 2014). The $^{87}Sr/^{86}Sr$ ratio is corrected for natural and instrument fractionation effects during calculation of ratios from measurement values, by normalizing the ratio to known values of the non-radiogenic $^{86}Sr/^{88}Sr$ ratio and reporting values normalized to known standards (Capo et al. 1998).

With environmental and instrumental fractionation accounted for, the corrected $^{87}Sr/^{86}Sr$ ratio retains a unique fingerprint of host lithology, making the $^{87}Sr/^{86}Sr$ ratio a useful tool for examining weathering sequences, dust inputs, and carbonate accumulation in rocks and soils (Capo et al. 1998; Capo & Chadwick 1999; Hart et al. 2004; White et al. 2009; Chadwick et al. 2009; Bullen et al. 1997). In stream solutes, $^{87}Sr/^{86}Sr$ ratios have also been used to trace soil and rock weathering inputs to stream geochemistry (Jacobson

et al. 2002; Jacobson et al. 2003; Horton et al. 1999; Frost & Toner 2004; Négrel et al. 2004). In Hyalite Canyon, younger (Eocene) volcanic and sedimentary rocks with a lower Rb/Sr ratio will likely have a lower $^{87}Sr/^{86}Sr$ ratio than the older Archean gneiss rocks containing a higher Rb/Sr ratio. Literature values from previous studies in the region estimate $^{87}Sr/^{86}Sr$ isotope ratios of ~0.70433-0.70826 for Absaroka volcanics rocks (Feeley & Cosca 2003; Lindsay & Feeley 2003; Hiza 1999), 0.71062 for carbonates (Kharaka et al. 1991), 0.70883 for Madison group limestones (Moore-Nall 2016), and 0.70617-0.78304 (mean 0.73267) for Archean gneiss rock units (Wooden & Mueller 1988).

2.4 Uranium

Uranium has three naturally occurring isotopes: ^{238}U (99.3%), ^{235}U (0.72%), and ^{234}U (0.0055%), all of which are radioactive (Faure & Mensing 2005). While U and U series isotopes are used in a variety of geochemical and geochronological assessments, the $[^{234}U/^{238}U]$ ratio (square brackets indicate activity) provides a measure of water-rock interaction over timescales of thousands to hundreds of thousands of years. The geochemical variation in $[^{234}U/^{238}U]$ ratios is based on ^{234}U as a daughter product of ^{238}U. The decay of ^{238}U to ^{234}U occurs when ^{238}U undergoes α decay (half-life 4.468 billion years) to form ^{234}Th, which rapidly undergoes β decay (half-life 24.1 days) to ^{234}Pa (half-life 1.17 minutes) and subsequently α decay to ^{234}U (half-life 245,500 years). The daughter product ^{234}U is more stable than its rapidly decaying parents, and its half-life determines the timescales addressed by its assessment relative to ^{238}U (Faure & Mensing 2005). Because of the large, energetic α particle emitted, recoil effects from α decay can

damage the crystal lattice surrounding the daughter element, or simply eject the daughter, resulting in the preferential release of ^{234}U during water-rock contact. Due to recoil effects, natural waters typically have a [$^{234}U/^{238}U$] ratio greater than one, with a higher [$^{234}U/^{238}U$] ratio reflecting longer time of water-rock contact, lower water rock ratio, or increased surface area (Bourdon et al. 2003; Chabaux et al. 2003; Dosseto et al. 2008; Depaolo et al. 2006). The degree of preferential weathering of ^{234}U varies as a function of U distribution (in water and rock), surface area and time (Maher, Depaolo, et al. 2006; Depaolo et al. 2012; Suksi et al. 2006)

In addition, the solubility of U is influenced by its redox state. Oxidized U(VI) is largely soluble in aqueous solutions and reduced U(IV) is more commonly found in rocks and precipitates out of solution under reducing conditions. Fractionation effects are small (Brown et al. 2018) and several studies suggest that electrons are ejected during α recoil, resulting in higher $^{235}U/^{238}U$ associated with more oxidized U (Bourdon et al. 2003; Stylo et al. 2015; Andersen et al. 2017; Basu et al. 2015). This tool has been applied to redox active environmental contexts such as roll front deposits (Brown et al. 2016) but is not applied here.

2.5 Mixing Theory

Mixing models can serve to quantify inputs of surface water and groundwater to stream flow using isotope ratios as conservative tracers. Mixing models determine the fraction of a mixture that can be attributed to candidate end members. A two-component mixing model defines a mixture (M) using the concentration (C) and fractional

contribution (*f*) of each end member, in this case two components A and B (Faure & Mensing 2005; Arendt et al. 2015):

$$C_M = C_A f_A + C_B f_B \qquad \text{eq 1}$$

where $f_A + f_B = 1$

When a two-component mixing model is defined by concentration, a linear mixing line between the end members is formed, with fractional contributions evenly distributed along the mixing line (Figure 2.1). When isotopic ratio (R) is considered, the mixing model becomes more complex:

$$R_M = R_A \bullet f_A \bullet \left(\frac{C_A}{C_M}\right) + R_B \bullet f_B \bullet \left(\frac{C_B}{C_M}\right) \qquad \text{eq 2}$$

When isotopic ratios are considered and concentrations differ, the mixing line between endmembers as a function of isotopic character is non-linear (Figure 2.2). Fractional inputs along these mixing curves are not evenly distributed along the mixing curve, but instead are weighted towards the end member with the higher concentration. When two isotopes are considered the isotopic composition of each end member defines its location in x,y space on a dual isotope plot, with the component of higher concentration influencing the isotopic ratio of the mixture more strongly, resulting in a family of hyperbolic mixing curves (Faure & Mensing, 2015; Drexler et. al., 2014). Mixtures of multiple elements with different isotopic ratios, such as U and Sr, can be described using two sets of mixing equations (Drexler et al. 2014). By using isotopic ratios of two elements with somewhat different behavior, we constrain the contributions of variable lithology and substrate weathering to groundwater supplying streamflow.

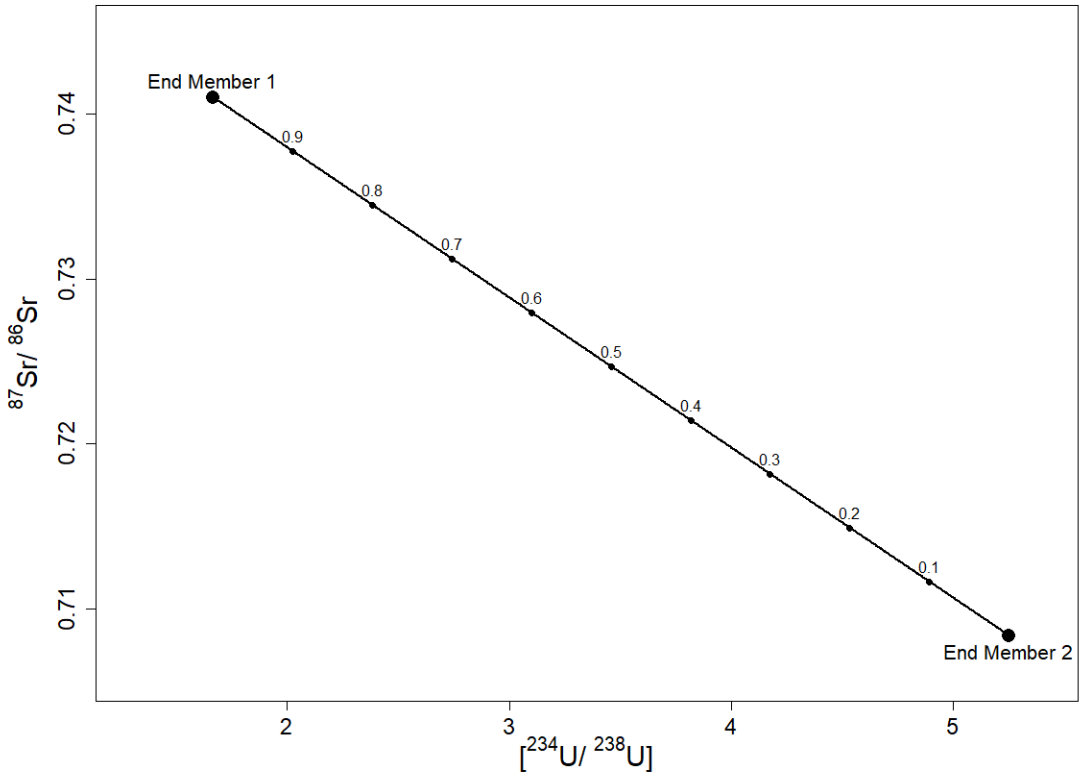

Figure 2.1 Example of linear relationship in two end member mixing model. End members have different isotopic ratios and equal concentrations of U and Sr. Notice fractional inputs are evenly spaced along the line.

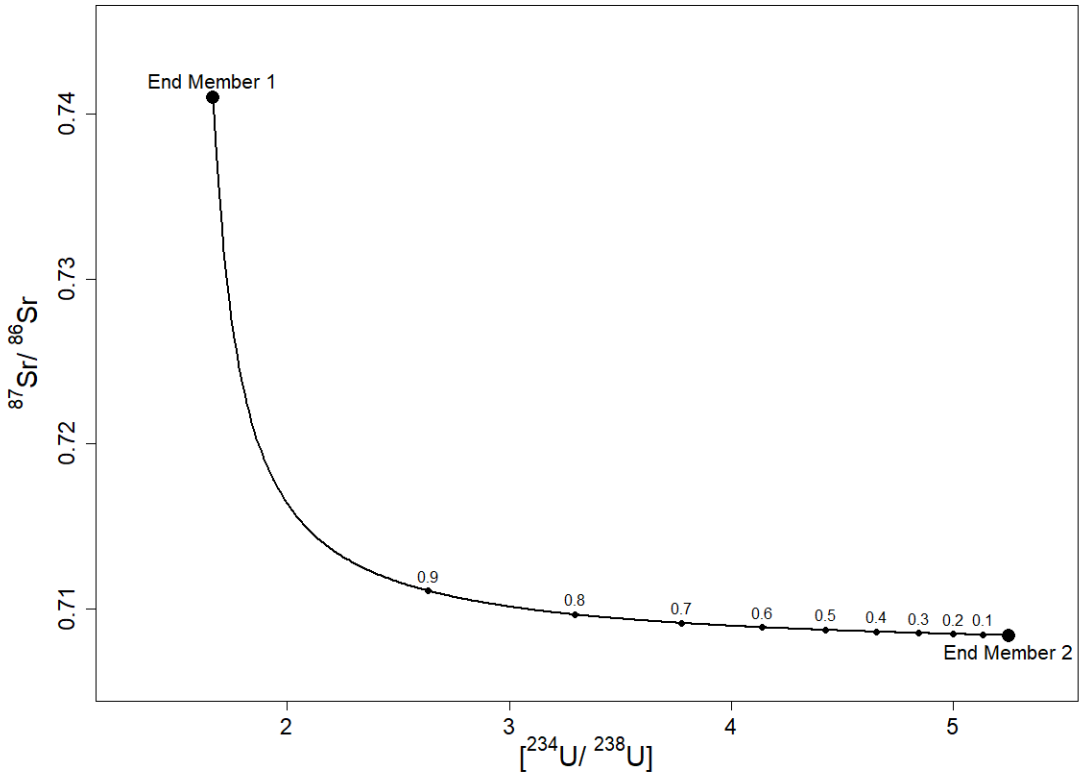

Figure 2.2 Example of curved relationship in a two end member mixing model. Endmembers have different isotopic ratios and different concentrations of U and Sr. Notice the fractional inputs are pushed towards to end member with the higher concentration of one or both components.

CHAPTER THREE

SR AND U ISOTOPES REVEAL THE INFLUENCE OF LITHOLOGIC STRUCTURE ON STREAM-GROUNDWATER INTERACTION ALONG A MOUNTAIN HEADWATER CATCHMENT (HYALITE CANYON, MT)

Contribution of Authors and Co-Authors

Manuscript in Chapter 3

Author: Florence Rita Miller

Contributions: Florence Miller was responsible for developing field sites, sample collection and solute analysis, Sr and U isotope purification, data analysis, and original composition of manuscript.

Co-Author: Dr. Stephanie A. Ewing

Contributions: Dr. Stephanie A. Ewing was responsible for project conceptualization, securing funding, weathering and tracer expertise, Sr and U purification methodologies and analysis, and original manuscript writing and editing.

Co-Author: Dr. Robert A. Payn

Contributions: Dr. Robert A. Payn was responsible for project conceptualization, securing funding, hydrology expertise, methodologies and analysis of monte carlo and mixing optimization model, and manuscript writing and editing.

Author: Dr. James B. Paces

Contributions: Dr. James B. Paces was responsible for project conceptualization, securing funding, U and Sr isotope analysis, mixing model development, and manuscript writing and editing.

Co-Author: Sam Leuthold

Contributions: Sam Leuthold contributed to sample collection and handling for solute analysis, water isotope insight outlined in companion paper, and manuscript editing.

Co-Author: Dr. Stephan Custer

Contributions: Dr. Stephan Custer contributed hydrogeologic expertise, knowledge of local geology and hydrology, compilation of local Sr values and manuscript editing.

Manuscript Information

Florence R. Miller, Stephanie A. Ewing, Robert A. Payn, James B. Paces, Sam Leuthold, Stephan Custer

Water Resources Research

Status of Manuscript:
_X_ Prepared for submission to a peer-reviewed journal
____ Officially submitted to a peer-reviewed journal
____ Accepted by a peer-reviewed journal
____ Published in a peer-reviewed journal

AGU Publications

3.1 Abstract

Changing climate and precipitation patterns are projected to reduce snowpack storage and late summer stream flows in mountain headwaters of the western United States. Ecosystems, agriculture, and municipalities depend on late summer flow in streams supplying water to the mountain front. Therefore, improved understanding of groundwater storage contributions to mountain streams is increasingly important. In this work we use $^{87}Sr/^{86}Sr$ ratios and $^{234}U/^{238}U$ activity ratios ($[^{234}U/^{238}U]$) as indicators of water-rock interaction contributing to runoff and groundwater as well as surface-subsurface hydrologic exchanges along Hyalite Creek, a mountain headwater tributary within the upper Missouri River basin. Main stem and tributary flow was sampled from 2100 to 1690 m elevation over a two-year period from 2016 to 2018, focusing on presumed baseflow conditions in February and August. Stream water in upper Hyalite Creek has low $^{87}Sr/^{86}Sr$ values (0.70846-0.70921), typical of Tertiary volcanic and sedimentary host units, and low $[^{234}U/^{238}U]$ values (1.50–1.72), consistent with more aggressive weathering of U from soils during recharge or short hydrologic flowpaths. In middle Hyalite Creek, $[^{234}U/^{238}U]$ in the main stem increases to 3.20, reflecting inflows of groundwater associated with the Madison Group limestones at 1920 m elevation. Local springs discharging from the Madison Group limestones have $[^{234}U/^{238}U]$ values of 5.23-5.29 and $^{87}Sr/^{86}Sr$ of 0.70835-0.70836 indicating inflows from deeper groundwater sources. In lower Hyalite Creek, progressive increases in $^{87}Sr/^{86}Sr$ values (0.70973-0.71202) and decreases in $[^{234}U/^{238}U]$ (2.12-1.69) suggest inputs of water from the Archean gneiss that forms the mountain front. Groundwater from wells completed in the

gneiss have elevated $^{87}Sr/^{86}Sr$ values of 0.73687-0.74497 and relatively low [$^{234}U/^{238}U$] of 1.28-1.85, consistent with radiogenic Sr developed in Archean-aged rocks and shorter flowpaths, with a possible contribution from weathering of soils or pre-weathered rock fractures. We use these results in mixing models to estimate that over local reaches of ~100 m, inflows from the Madison aquifer contribute ~4% of streamflow during baseflow conditions. Local inflows from Archean gneisses increased $^{87}Sr/^{86}Sr$ values in Hyalite Creek to a degree that varied seasonally, indicating contributions of ~2 to 8%, with higher contributions found in late winter. At the same time, decreased values of [$^{234}U/^{238}U$] in the lower canyon suggest contributions of proximally sourced water distinct from our well water endmember proxy. Our results provide new insight about groundwater contributions to seasonal variation in streamflow within this mountain headwater system.

3.2 Introduction

Mountainous regions of the western United States face impending water management challenges, given the combination of urban growth and water scarcity driven by projected changes in precipitation and snowpack dynamics in mountain environments (Silverman et al. 2013; Knowles et al. 2005). The intermountain west supports both urban and rural communities that rely heavily on mountain headwaters for municipal and agricultural water supplies (Hoylman et al. 2018; Silverman & Maneta 2016). Mountain headwater catchments ultimately supply a majority of the water found in the rivers and aquifers of intermountain basins (Wilson & Guan 2004), where more intensive human land and water use tends to occur. However, the nature and extent of the

influence of groundwater storage on these mountain headwater contributions is generally poorly quantified, leading to uncertainty in estimates of mountain headwater contributions to water-resource availability during low-flow conditions. This study uses geochemical tracers to explore the longitudinal and temporal distribution of groundwater contributions to baseflow conditions in a mountain headwater stream, focusing on a canyon within the upper Missouri and Gallatin River Basins (Figure 3.1). We demonstrate how analyses of weathering products found in stream solute loads provide a useful tool for inferring the distribution of groundwater storage in the watershed. This work is an element of a larger study to understand how the transition in process domains at mountain fronts influences how changes in climate at high elevation will translate to changes in low-flow water supply to intermountain basin communities and ecosystems (Montgomery 1999).

Mountain headwaters are often characterized by steep mountain streams with geomorphologic development fundamentally controlled by lithology, structural features, tectonic regime, fluvial erosion or deposition, and glaciation (Amundson et al. 2015; Dixon et al. 2016). Weathering in high elevation mountain headwater process domains is generally limited by relatively low temperatures and rapid mechanical erosion, compared to intermountain basin process domains. As a result, soils in high elevation mountain headwater catchments are generally thin and less developed in terms of mineral transformation and mass loss to chemical weathering. Furthermore, high relief results in hillslope aspect having a strong influence on the extent of substrate weathering (Hinckley et al. 2014), and topography strongly influences seasonal precipitation and runoff (Jencso

et al. 2009; Emanuel et al. 2014; McGuire et al. 2005; Jencso & McGlynn 2011). Along a mountain headwater valley, stream water solute qualities reflect the exchanges between surface water and groundwater throughout the mountain headwaters (Payn et al. 2009). These concomitant gains and losses of water along a stream result in longitudinal patterns of solute composition reflecting dilution and solute-load inputs characteristic of transport of weathering products (or lack thereof) to the stream (Covino & McGlynn 2007; Capell et al. 2011; Yang et al. 2017; Jasechko 2016; Jasechko & Kirchner 2016). Thus, mountain headwaters are key in controlling both streamflow and water quality. Water emerging at the mountain front provides a fingerprint of lithologies within the mountain catchment delivering it, and patterns in water quality along the stream provide information about the spatial distribution of groundwater sources contributing to stream flow generation.

Stratigraphy, geological structures, geomorphic features, and lithology combine to influence catchment topography, as well as the surface and subsurface dynamics that dictate relative contributions of baseflow to mountain headwater stream systems. Tectonic activity has uplifted most mountain blocks in the western US in response to compressive or extensional movements of the upper crust. Consequently, deformation and faulting provide groundwater conduits or barriers that dictate water flow and storage. In addition, Pleistocene alpine glaciation has dramatically altered higher-elevation valley structure and subsequent flow dynamics (Green et al. 2013), with many features of a glaciated landscape such as meadows and moraines contributing to potential groundwater storage (Gordon et al. 2015; Somers et al. 2016). Understanding stream baseflow

generation mechanisms across varying topography, lithologic groups, and geomorphic features in post-glacial mountainous catchments is required to predict how baseflow in mountain headwater streams may respond to changes in climate drivers.

The study of baseflow generation in mountain headwaters receives less attention than the study of event flow generation, particularly in snowmelt-dominated systems (Soulsby & Tetzlaff 2008; Payn et al. 2012). Most work in mountain headwater watersheds has been focused on topographic controls on event flow contributions to streamflow (Jencso & McGlynn 2011; McGuire et al. 2005; McGlynn & McDonnell 2003). However, changes in the climate and distribution of precipitation demand a better understanding of the mechanisms controlling variation in baseflow, particularly in semi-arid systems where water-resource availability during dry seasons is a major concern (Soulsby & Tetzlaff 2008). A first step to understanding the longer-term storage that serves as a reservoir for baseflow is to identify the location and relative contribution from aquifers that contribute to lower stream flows across a catchment.

Geochemical tracers of baseflow sourced by aquifers of varying size and residence times offer an opportunity to investigate a distinctive signal of groundwater contribution to streamflow. Often these tracers record a signal of both weathering and aquifer path or transit time (Hogan & Blum 2003; Dosseto et al. 2014; Chabaux et al. 2003). Therefore, the geochemical signal imparted on groundwater contributing to baseflow varies with the chemical composition, age, and weathering susceptibility of the aquifer rock or geomorphic units. As lithology changes throughout the reach of a mountain stream and across the mountain front, so does the cumulative geochemical

fingerprint imparted on the water. These fingerprints allow baseflow at the outlet to be traced back to its host rock or sediment and allow longitudinal surveys of water quality at baseflow to reveal the location and relative contribution of discharge from specific aquifers to the stream.

Individual rock and geomorphic units also differ in their potential to host groundwater and produce varying transit times. Some sources for baseflow involve short residence times between recharge and return flow or preferential flow along the soil-bedrock interface (Pierret et al. 2014). Other aquifers have the capacity to store or transmit larger volumes representing groundwater from broader or more distant recharge areas (Barbieri et al. 2005). Our approach was to track geochemical attributes imprinted by weathering variation of different lithologic units to identify groundwater aquifer sources and their contribution to streamflow along a lithologically diverse mountain catchment.

Geochemical tracers used in weathering and water movement studies have included elemental constituents (Roy et al. 1999) as well as isotopic compositions. These tracers are used as indicators of water source or metrics of residence time in soils, groundwater, and streams (Négrel et al. 2004; Chadwick et al. 2009). This study uses $^{87}Sr/^{86}Sr$ and $[^{234}U/^{238}U]$ values (square brackets denote activity ratio) as natural geochemical tracers to investigate the sources and pathways of water contributing to streamflow during baseflow conditions. Over the past two decades, many studies have used strontium (Sr) isotope ratios (primarily $^{87}Sr/^{86}Sr$, but also $^{88}Sr/^{86}Sr$) to examine weathering sequences, dust inputs, and carbonate accumulation in rocks and soils (Capo

et al. 1998; Capo & Chadwick 1999; Hart et al. 2004; White et al. 2009; Chadwick et al. 2009; Bullen et al. 1997). In surface water and groundwater systems, $^{87}Sr/^{86}Sr$ data have been used to trace sources of soil and rock weathering inputs to stream geochemistry (Jacobson et al. 2002; Jacobson et al. 2003; Horton et al. 1999; Frost & Toner 2004). More recently, U-series isotopes, notably [$^{234}U/^{238}U$], have been used to examine processes of water-rock interaction that rely on the balance between recoil effects that increase [$^{234}U/^{238}U$] and bulk U dissolution that decreases [$^{234}U/^{238}U$] (Bourdon et al., 2003; Chabaux et al. 2003; Dosseto et al. 2008; DePaolo et al. 2006). Water/rock interactions with the different lithologies or flowpaths present in the watershed have the potential to leave unique $^{87}Sr/^{86}Sr$ and [$^{234}U/^{238}U$] isotopic signatures that may allow determination of multiple sources, pathways and mixing relations among end members (Paces & Wurster 2014; Drexler et al. 2014). Both U and Sr are readily soluble in oxidizing aqueous systems and their radiogenic isotopes are not affected substantially by mass dependent fractionation in near-surface environments by common processes such as evaporation, transpiration, mineral precipitation, and sorption/desorption processes (Paces & Wurster, 2014). Thus, Sr- and U-isotopes can potentially provide a precise and accurate fingerprint of water sources and hydrologic evolution (Pierret et al. 2014; Roback et al. 2001; Ryu et al. 2009; Drexler et al., 2014). Together, U and Sr isotopic ratios provide a useful means of examining the influence of weathering processes, water sources, and the degree of water-rock interaction on stream geochemistry, using reactive transport modeling and end member mixing analysis approaches (Maher, Depaolo, et al. 2006; Depaolo et al. 2006; Drexler et al., 2014; Paces & Wurster 2014).

Here, we explore the influence of aquifer contributions with varying geochemical weathering products to baseflow generation in a mountain headwater catchment, using Hyalite Creek in southwestern Montana as a case study. Hyalite Creek is a steep, glaciated, mountain headwater stream with a watershed area of approximately 126 km^2, draining into the intermountain basin and associated alluvial aquifer of the Gallatin Valley. We use geochemical tracers to examine water flow and storage dynamics along the main stem of the mountain stream, with a goal of characterizing a spatially explicit map of the influence of aquifers hosted in four diverse lithologic units with distinct isotopic character and the resulting effects on water quality and supply at the watershed outlet. We demonstrate how [$^{234}U/^{238}U$] and $^{87}Sr/^{86}Sr$ values reveal baseflow and storage dynamics across a catchment that includes lithologic units with variable chemical compositions, ages, and degrees of weatherability.

3.3 Methods

3.3.1 Study Area

Hyalite Creek in southwestern Montana traverses a number of bedrock lithologies along its length that allow its use as a case study for assessing contributions of multiple aquifers to baseflow. Hyalite Creek, located in the north-central Gallatin Mountain Range, is a headwater of the Gallatin River (Figure 3.1), supplying water to the Gallatin Valley, an intermountain basin supporting rapidly growing municipalities including Bozeman, Montana. Hyalite Creek is dammed midway up Hyalite Canyon, creating a reservoir that supplies one-third of Bozeman's municipal water supply along with water for irrigation use (DNRC 2014). Flow out of Hyalite Creek at the mountain front has

been diverted as a water source for agricultural irrigation in the Gallatin Valley since 1871 (Kramer 2013). In addition, Hyalite Canyon has an extensive logging history beginning in the 1870s through 1911 (Kramer 2013). Currently, Hyalite Canyon is heavily used for recreation with about 80,000 visitors per month during the peak summer season (Gedeon 2015).

Soils in Hyalite Canyon are thin, reflecting limited chemical weathering due to cold temperatures and rapid mechanical erosion rates. Chemical composition of soils are strongly influenced by the chemical composition of the parent material and mineral reactions facilitated by water movement (N. R. C. S. United States Department of Agriculture 1996). In meadows and open slopes, soils classified as Mollisols have developed with relatively thick, dark A horizons. In forested areas, soils classified as Alfisols and Inceptisols have developed thin A horizons and weak subsurface horizons.

Hyalite Canyon receives an average of 82 cm of precipitation annually (30 year average 1981-2010) (USDA NRCS; Prism Climate Group), with 40% of that falling as snow. At an elevation of 2469 m, the maximum monthly mean temperature is 14°C in July and the minimum monthly mean temperature is -7.7°C in December (Shower Falls SnoTel, USDA NRCS). Vegetation in Hyalite Canyon is primarily evergreen coniferous forest, with dominant species of lodgepole pine (*Pinus contorta*) and subalpine fir (*Abies lasocarpa*) and dispersed populations of Douglas fir (*Pseudotsuga menziessii).*

3.3.2 Sample Site Selection

Sampling sites (Table 3.1) traversed rock units with distinct geochemical character (Figure 3.1, Table 3.2). Sampling sites included surface waters in Hyalite Creek

and five tributaries (HY1 through HY15), a spring and associated spring channel in the bank of Hyalite Creek (HY16 and HY17), a well and associated cistern in Hodgeman Canyon (GW2 and GW3), and a well in the uppermost alluvial fan formed by Hyalite Creek at the mountain front (GW4) (Figure 3.1). Surface waters were sampled during baseflow conditions in February and August 2016-2018, when baseflow was presumed to dominate stream flow generation based on hydrograph levels.

We started with six primary surface water sites along Hyalite Creek in 2016, targeting waters flowing over major lithologic units (HY1 through HY6, labeled sequentially with decreasing elevation). We expanded the number of sites between 2016 and 2018, based on identification of reaches with notable longitudinal changes in chemistry and their potential end member contributors. Ultimately, sample sites included ten main stem locations (in order of decreasing elevation: HY1, HY7, HY9, HY10, HY11, HY4, HY14, HY15, HY5, HY6), five tributaries (HY2, HY3, HY12, HY13, HY8), two springs (HY16, HY17), three wells (GW2, GW3, GW4), and one neighboring stream (Sourdough Creek) in the next major valley to the east (SD1) (Table 3.1, Figure 3.1).

Two sampling locations were co-located at sites with continuous stream gauges along Hyalite Creek. HY7 is co-located with a Montana Department of Natural

Resources and Conservation gauge (DNRC; number 41H 2000) downstream of Hyalite Reservoir, and HY6 is co-located with a U.S. Geological Survey gauge (USGS; number 06050000) located at the mouth of Hyalite Canyon (Table 3.1, Figure 3.1). Hydrographs from these two gauges depict a snowmelt dominated hydrologic regime (Figure 3.2), with flows ranging from 0.18 to 5.34 $m^3 s^{-1}$ at the DNRC gauge (HY7) and from 0.48 to 7.51 $m^3 s^{-1}$ at the USGS gauge (HY6) during the sampling period from 2016 to 2018. Hydrographs show how our sampling events align with the baseflow conditions (Figure 3.2, note the log scale), where August sampling dates reflect low summer flows and February sampling dates reflect low winter flows. On a given sampling date, flow in the main stem of Hyalite Creek increased between sites HY7 and HY6: on 2/19/2016 from 0.34 to 0.55 $m^3 s^{-1}$ (net gain of 0.21 $m^3 s^{-1}$ or a 62% increase), on 8/24/2016 from 1.40 to 1.65 $m^3 s^{-1}$ (net gain of 0.25 $m^3 s^{-1}$ or a 18% increase), and on 8/23/2017 from 1.14 to 1.57 $m^3 s^{-1}$ (net gain of 0.43 $m^3 s^{-1}$ or a 38% increase). There were no gauge data for HY7 during 2/4/2017 sampling due to freezing. Thus, net gains between H7 and HY6 stream discharge increased by similar absolute volumes between February and August, but those gains represent a proportionally larger fraction of stream flow during February due to lower flow conditions in general.

Hyalite Creek traverses a range of lithologic units known to have distinct geochemical character (Table 3.2), from the highest sample site at 3140 m above sea level to the lowest site near the mountain front at an elevation of 1690 m above sea level (Figure 3.1) (Vuke et al. 2007; Berg et al. 1999; Kellogg & Williams 2006; Vuke et al. 2014; Berg et al. 2000). Specific contributions of rock weathering products to Hyalite

Creek water will depend on differential mineral weatherability; however, the general range of $^{87}Sr/^{86}Sr$ values observed for these lithologies is substantial enough to use $^{87}Sr/^{86}Sr$ data to fingerprint water/rock interactions. Uppermost Hyalite Creek (3140-2100 m elevation) is underlain by Eocene-aged andesitic to basaltic rocks of the Washburn Group within the Absaroka Volcanic Supergroup. Sample sites located in the steep glaciated terrain cutting volcanic rocks include Upper Hyalite Creek (HY1) and Emerald Creek tributary (HY2), both located above Hyalite Reservoir (Figure 3.1). These Eocene volcanic rocks cap a sequence of Cretaceous- to Cambrian-aged sedimentary rocks exposed in the middle elevations of Hyalite Canyon (2010 to 1875 m). Lithologies include a succession of shales, limestones, siltstones, and sandstones that become progressively older with decreasing elevation (Figure 3.1). Main stem sites HY7 and HY9 are located at the transition from Tertiary volcanic to Cretaceous sedimentary lithologies downstream of Hyalite Reservoir. Lick Creek (HY3), a tributary that joins the main stem between those two sites, drains Mesozoic siliciclastic sedimentary units including the Cretaceous-aged Thermopolis shale. Mississippian-aged Madison Group limestones are exposed further downstream at elevations of 1925 to1915 m (Kirk, 2002). At an elevation of 1920 m, a spring (HY16) and associated spring channel (HY17) discharge from the Madison aquifer, an important regional karst aquifer known to contribute flow to springs and baseflow in the neighboring Sourdough Canyon (Kirk 2002), as well as to baseflow in Gallatin Canyon and Hyalite Canyon. The main stem of Hyalite Creek crosses Mississippian- to Cambrian-aged sedimentary rock units at elevations of 1910 to 1860 m, and includes sites HY10, HY11, and HY4. Tributaries

Buckskin Creek (HY12), ‘Meadow’ Creek (HY13), and Moser Creek (HY8) drain areas underlain by those same Paleozoic sedimentary rock units, although Moser Creek’s watershed also includes Archean gneisses and Eocene volcanics and ‘Meadow’ Creek is fed by a spring emerging from Eocene volcanics (Figure 3.1). At its lowest elevations (1875 to 1690 m), Hyalite Creek cuts a narrow, unglaciated canyon through Archean quartzofeldspathic gneiss. Main stem sites HY14 and HY15 are located within the transition to gneiss near an elevation of 1875 m. Main stem site HY5 is located at an elevation of 1730 m, and site HY6 is located near the mountain front at an elevation of 1690 m, just downstream of a shear zone within the Archean gneiss (May, 1985). Groundwater present in fractured Archean gneiss was sampled at a cistern and well in the neighboring Hodgeman Canyon (GW2, GW3) at 1690 m elevation. Groundwater from site GW4, a residential well located in the uppermost part of the Hyalite Creek alluvial fan (Figure 3.1), is thought to represent water mountain front recharge from Hyalite Creek supplying the alluvial aquifer in the Gallatin Valley.

Moraines deposited from the most recent Pinedale glaciation period (~30 to 15 ka) are present within the headwaters of Hyalite and Emerald Creeks (HY1, HY2) and extend downstream nearly to Hyalite Creek’s convergence with Lick Creek (HY3) at an elevation of about 1975 m (Weber 1965). Based on these moraines, Pinedale glaciation eroded Absaroka volcanic rocks in the upper reaches of Hyalite Creek through Jurassic-aged sedimentary rocks in the middle elevations of the stream (Figure 3.1). Moraines associated with the older Bull Lake glaciation (~180 to 130 ka) extend further down canyon, from the headwaters of Hyalite and Emerald Creeks (HY1, HY2) to just above

Langohr Campground (HY4) at an elevation of about 1860 m (Weber 1965), passing through Devonian to Cambrian-aged sedimentary rock units between 1975 and 1850 m elevation. The canyon narrows rapidly downstream from the terminus of Bull Lake glaciation through the Archean gneiss.

3.3.3 Water Sampling Procedures and Solute Analysis

Surface water samples were collected using a peristaltic pump (Geotech™ Denver, CO, United States) with platinum-cured Silicon tubing. Samples were filtered at the time of sampling using a 0.45 µm, mid-capacity capsule filter (Geotech™ Denver, CO, United States). In situ temperature, pH, specific electrical conductivity (SC), and dissolved oxygen (DO) were measured at each sampling site using a handheld multimeter (YSI 556 Yellow Springs, OH, USA). Alkalinity was measured in the field using colorimetric titration (Hach™ kit; phenolphthalein/bromethymol blue and H_2SO_4). When conditions allowed, discharge was measured using the area-velocity method, where water velocities were measured using an electromagnetic flow meter (Marsh McBirney / Hach™ Loveland, CO, United States). Comparison of continuous gauge data with measured discharge suggests uncertainty of about 10% between the gauging methods (Table G.5). Wells were sampled by purging three well volumes prior to water collection, employing the same procedures of water filtration, sample collection, alkalinity, and multimeter measurement used to collect surface water samples.

Chemical and isotopic analyses were conducted at Montana State University (MSU) in Bozeman, MT, the Montana Bureau of Mines and Geology (MBMG) in Butte, MT, and the USGS Southwest Isotope Research Laboratory (SWIRL) in Denver, CO.

Major cations and trace metal concentrations were analyzed by Inductively Coupled Plasma - Optical Emission Spectroscopy (ICP-OES; Perkin Elmer™ Waltham, MA, United States) at MBMG and the MSU Environmental Analysis Laboratory, and by inductively coupled plasma mass spectrometry (ICP-MS) at MBMG. Radiogenic isotope ratios $^{87}Sr/^{86}Sr$ and [$^{234}U/^{238}U$] as well as U concentrations were measured by thermal ionization mass spectrometry (TIMS) at SWIRL.

U and Sr isotopic analysis followed procedures described in Ewing et. al. (2015) and Paces & Wurster (2014). Water samples, field blanks, procedural blanks, and standards of known composition were prepared for U and Sr isotopic analysis at the MSU Soil Biogeochemistry laboratory. The amount of sample processed was based on U concentrations, which were much lower than Sr concentrations (Table 3.3). Sample volumes containing ~100 ng U and 0.01 – 0.13 mg Sr were weighed in 500 mL Teflon vials, acidified with 1-2 mL of trace metal grade (TMG) concentrated HNO_3, and spiked with known amounts of highly purified ^{236}U-spike solution to allow determination of U concentration by isotope dilution. Field and procedural blanks were spiked with known amounts of both ^{236}U and ^{84}Sr. Water was completely evaporated from processed samples on a hotplate in an exhausting HEPA-filtered clean hood. The residual solids were dissolved with approximately 5-10 mL of TMG ~7N HNO_3, transferred to 15 mL Teflon vials, and were again evaporated. If dissolved organic carbon (DOC) concentrations were >10 ppm, re-dissolved samples were transferred to pre-cleaned quartz crucibles, evaporated to dryness, and heated to 550°C in a muffle furnace for one hour to remove organic compounds. Combusted residues were dissolved in 10-15 mL of ~7N TMG

HNO_3, transferred to 15 mL Teflon vials and evaporated. Residual solids from evaporated samples were re-dissolved in 0.6 mL of ~7N Optima™-grade HNO_3, transferred to acid-washed 2 mL centrifuge tubes, and centrifuged for 10 minutes at 10,000 rpm. Any solids were returned to the original Teflon vials and refluxed with concentrated, ultrapure HF and HNO_3, were again evaporated, dissolved in 0.6 mL of ~7N Optima™ HNO_3, and combined with the previously dissolved portion. Final solutions thus represent fully dissolved samples. Sr and U salts were separated and purified by standard ion exchange chemistry using AG1-X8 resin for the U fraction and Sr-Spec™ resin for the Sr fraction.

Purified U aliquots were loaded onto the evaporation side of a double rhenium filament assembly and analyzed by TIMS using the USGS SWIRL ThermoFinnigan Triton™ equipped with a single secondary electron multiplier and a retarding potential quadrapole (RPQ) electrostatic filter. Intensities of ^{234}U, ^{235}U, and ^{236}U were measured sequentially in multi-dynamic peak-jumping mode. To correct for instrument bias and drift, the $^{234}U/^{235}U$ values measured for unknowns were normalized by the same factor needed to adjust $^{234}U/^{235}U$ values measured for a NIST U-isotope standard (SRM 4231B) run in the same magazine to the accepted value of 0.007294 (±0.000028). One hundred fourteen analyses of SRM 4321B yielded an average $^{234}U/^{235}U$ value of 0.007303 (0.007292 to 0.007314, 95% confidence interval), which is within error overlap of the NIST certified value. Measured $^{234}U/^{235}U$ atomic ratios were converted to $[^{234}U/^{238}U]$ using decay constants published by Cheng et al. (2013) ($\lambda_{234} = 2.82206 \times 10^{-6}$ yr^{-1}) and Jaffey et al. (1971) ($\lambda_{238} = 1.55125 \times 10^{-10}$ yr^{-1}), assuming that all U has an atomic $^{238}U/^{235}U$ composition of 137.88 (Steiger & Jager 1977). Analytical errors for measured $[^{234}U/^{238}U]$ are given at the

95% confidence level (i.e. twice the standard deviation) and include contributions from within-run counting statistics plus uncertainties propagated from blank, spike, and mass fractionation corrections, as well as external error derived from multiple analyses of the U isotope standard. Replicate analyses of a secondary standard consisting of 69.3-Ma uranium ore from the Schwartzwalder mine expected to be in radioactive secular equilibrium (i.e., $[^{234}U/^{238}U] = 1.000$; (Ludwig et al. 1985)) yielded an average $[^{234}U/^{238}U]$ value of 0.9997±0.0032 (2×standard deviation for 65 analyses). Total process blanks for U were typically 0.01–0.1 ng compared to total U abundances of 5–600 ng (median 85 ng). An in-house water "standard" developed by the USGS Branch of Quality Systems (SRS T-221) was processed multiple times at both MSU and SWIRL to evaluate interlaboratory biases. Results for $[^{234}U/^{238}U]$ are identical within reported analytical uncertainty; however, U concentrations for aliquots processed at MSU are more scattered (±7.7%, 2×SD, N=4) with an average of 1.40±0.11 μg L^{-1}, which is lower than the published most-probable-value of 1.49±0.08.

Purified Sr aliquots were loaded onto single rhenium filaments atop an initial load of tantalum oxide used as an activator and analyzed at the USGS SWIRL by multicollector TIMS using either a ThermoFinnigan Triton™ or an Isotopx Phoenix™. Isotope measurements were made on 5 to 10 volt ^{88}Sr signals using multi-dynamic, triple-jump analytical routines where instrumental mass fractionation was corrected using $^{86}Sr/^{88}Sr$ measured during the same run assuming a value of 0.1194. Replicate analyses of the National Institute of Standards and Technology Sr-isotope standard, SRM 987 (accepted $^{87}Sr/^{86}Sr$ value of 0.710248; (McArthur et al. 2001)) used as a primary standard to normalized instrument bias and drift, yielded mean values of 0.710250 ±0.000007 (±2×SD, N=314)

using the Triton™ and 0.710242±0.000012 (±2×SD, N=15) using the Phoenix™. Measured $^{87}Sr/^{86}Sr$ values for unknown samples were adjusted by the same amount needed to obtain the accepted value for NIST 987 analyzed during the same session. Replicate $^{87}Sr/^{86}Sr$ analyses of the modern-marine carbonate standard, EN-1 (accepted value of 0.7091741±0.0000024, (McArthur et al. 2006)), gave mean values of 0.709174±0.000008 (±2×SD; N=174), and 0.709176±0.000005 (±2×SD, N=5) on respective instruments. Total process blanks for Sr were typically <0.001 µg compared to total Sr abundances of 20–140 µg (median 40 µg). Analytical errors for $^{87}Sr/^{86}Sr$ values are given at 95% confidence levels (~2σ) and include within-run uncertainties and external error based on replicate analyses of standards. Results for $^{87}Sr/^{86}Sr$ measured in SRS T-221 processed at MSU and SWIRL are identical within reported analytical uncertainty.

3.3.4 Isotope Ratio and Elemental Ratio Interpretation

We interpret the Sr isotope ratio to indicate the isotopic character of weathered materials in contact with surface and groundwater, providing information about the mineralogical content and age of that weathered material. Strontium has four stable isotopes ^{84}Sr, ^{86}Sr, ^{87}Sr, and ^{88}Sr, where ^{87}Sr is the beta-decay product of rubidium-87 (^{87}Rb) with a half-life of 48.8 billion years (Faure & Mensing 2005). Differences in $^{87}Sr/^{86}Sr$ in rocks and minerals depend on the Rb/Sr present in the material and its age. Water interacting with solid materials during recharge and flow dissolves some of that Sr and incorporates the $^{87}Sr/^{86}Sr$ ratio present in the lithologic source without significant isotopic fractionation. However, differences in weatherability of individual mineral components with variable Rb/Sr may result in a range in $^{87}Sr/^{86}Sr$ values depending on

any preferential dissolution that takes place (White et al., 2005; Négrel et al. 2004; Pierret et al. 2014; Barbieri et al. 2005).

Ratios of concentrations for geochemically similar elements, such as Ca/Sr, have also been used to investigate hydrologic processes (Banner 1995; Land et al. 2000; Hogan & Blum 2003). Both Sr and Ca are divalent Group 2 alkaline earth metals of similar size, therefore they react similarly allowing Sr to substitute readily for Ca in mineral lattices. During precipitation of carbonate minerals, Ca is preferentially incorporated into the crystal lattice, effectively increasing the Ca/Sr in the solid and decreasing the Ca/Sr in remaining water (White et al. 2005). Consequently, Ca/Sr values along with $^{87}Sr/^{86}Sr$ provide additional context for examining weathering and interaction of substrate and water (Hogan and Blum, 2003).

We interpret the U activity ratios to indicate how the degree of alpha recoil from the U-decay series influences the U activity ratio of the water it comes into contact with in terms of residence time, flowpath length, and exposed rock surface area to volume of water ratio providing information about the extent of water/rock interaction. Uranium has three naturally occurring isotopes ^{238}U, ^{235}U, and ^{234}U, all of which are radioactive (Faure & Mensing 2005). ^{234}U is an intermediate alpha-decay product in the ^{238}U-series decay chain with a half-life of 245,620 years (Cheng et al. 2013). In rocks and minerals older than about 1 Ma, ^{234}U abundances reach a state of radioactive secular equilibrium with ^{238}U, meaning that the growth and decay of ^{234}U become balanced with decay of ^{238}U (half-life of 4.47×10^9 years) such that levels of radioactivity (rates of decay) for both isotopes are equal and the ratio of their activities equals unity (that is, $[^{234}U/^{238}U] = 1.00$;

Bourdon et al., 2003). Radioactive disequilibrium occurs as a consequence of water-rock interaction because the ^{238}U decay process emits an energetic alpha particle, which displaces the short-lived daughter (^{234}Th) due to alpha recoil. ^{234}Th decays rapidly through ^{234}Pa to ^{234}U which may be ejected into interstitial pore space, or remain in lattice sites damaged by the decay process. In either case, ^{234}U becomes more susceptible to leaching relative to ^{238}U resulting in [$^{234}U/^{238}U$] values greater than one in the aqueous phase. The degree of [$^{234}U/^{238}U$] enrichment is a function of U concentration, particle surface area, water/rock ratios, chemical reactivity, and time (Depaolo et al. 2006; Maher et al. 2006). Higher [$^{234}U/^{238}U$] values reflect low water-rock ratios, longer flowpaths allowing more exposure to recoil ^{234}U, or greater mineral surface areas interacting with a given volume of water (Dosseto et al. 2008; Depaolo et al. 2012; Suksi et al. 2006; Chabaux et al. 2003; Bourdon et al. 2003). However, enrichment of [$^{234}U/^{238}U$] is limited by rates of weathering and bulk rock dissolution, which drive [$^{234}U/^{238}U$] back towards unity (Maher et al., 2006).

3.3.5 Data Analysis

We interpreted patterns in stream flow generation from groundwater aquifers along Hyalite Creek first by examining the longitudinal patterns in chemical and isotope characterizations with respect to decreasing elevation with distance downstream. Longitudinal analysis allowed consideration of how geologic structures, geomorphology, and lithology influence the character of stream flow generation and surface-subsurface water interaction (Gardner et al. 2011). This sampling strategy subsequently allowed us

to construct mixing models that quantify fractional inputs of groundwater to reaches of Hyalite Creek where geochemical data indicated notable influence of a given aquifer.

Two mixing analyses were performed to estimate the fraction of stream flow that could be attributed to chemically distinguishable aquifers along Hyalite Canyon. A binary mixture (M) can be calculated from concentrations (C), isotopic ratios (R), and fractional contributions (f) from each of two end members. In this case the two end members are the water at the upstream end of a reach (A) and the water contributed from a given groundwater source along the reach (B) that together constitute the mixture (M) at the downstream end of the reach (Faure & Mensing 2005; Arendt et al. 2015):

$$C_M = C_A f_A + C_B f_B \quad (1)$$

$$R_M = R_A f_A \left(\frac{C_A}{C_M}\right) + R_B f_B \left(\frac{C_B}{C_M}\right) \quad (2)$$

where $f_A + f_B = 1$. Here, we identify hydrologic end members and evaluate mixtures of end members defined by Sr concentration, $^{87}Sr/^{86}Sr$, U concentration, and $[^{234}U/^{238}U]$, so equations 1 and 2 were repeated for Sr and U and solved simultaneously. Isotopes of Sr and U are particularly well suited for unconfounded identification of end members because their ratios are usually not affected by dilution or near-surface physical or chemical processes other than those of interest here (Paces and Wurster, 2014).

Rather than evaluating the entire stream system simultaneously, we used the binary mixing model and Monte Carlo analysis to estimate groundwater inputs to Hyalite Creek over two reaches where groundwater inputs from particular aquifers are likely to yield distinctive geochemistry: (1) groundwater in contact with the Madison Group limestones and (2) groundwater in contact with the Archean gneiss. While there are

numerous tributaries and other small inputs of water to Hyalite Creek, we refined our sampling to capture the two distinct reaches of Hyalite Creek where groundwater inputs from these sources can be quantified without the potentially confounding effects of surface inflow. The upper to middle elevations of Hyalite Creek were characterized as a two end member mixture between the upper (younger) sedimentary and volcanic catchment areas represented by Hyalite Creek below Hyalite Reservoir (i.e., end member A; site HY7, 1962 m) and groundwater input from the Madison aquifer (i.e., end member B; sites HY16 and HY17; 1931-1936 m) to form Hyalite Creek below the Madison inflows (i.e., the resulting mixture, M; site HY10, 1909 m) during August 2017 baseflow conditions. A second two-component end member mixing model uses waters of middle Hyalite Creek below the influence of the Madison (end member A; sites HY14 and HY15; 1854 m) and Archean gneiss derived groundwater sampled in Hodgeman's Canyon (end member B; sites GW2 and GW3), to estimate fractional inputs from the Archean gneiss to lower Hyalite Creek (the mixture, M: site HY5, 1807 m) during both August and February baseflow conditions.

For a given mixing reach and end member definition, we solved equations 1 and 2 simultaneously for U and Sr using a numerical iterative optimization scheme. The optimization goal was to find the combination of f_A (upstream end member) and f_B (groundwater end member) for the mixing model that would have the maximum likelihood of matching the observed concentrations and isotope ratios for both Sr and U at the downstream end of the reach. We used R statistical software and the optim() function from the base R stats package to find the maximum likelihood estimate (i.e.

MLE analysis) based on the quasi-Newton L-BFGS-B algorithm (Appendix E). Likelihood for the MLE was calculated based on the assumption that the residual errors between the modeled mixture values and the observed mixture values were independent and normally distributed (see supplemental material Appendix E). The assumed standard deviations of the residual errors necessary for calculating the likelihood in this fashion were based on estimates of analytical uncertainty of each end member in the overall sample analysis workflow.

We estimated the effect of uncertainty in end member concentrations and isotope ratios on the MLE-inferred composition of a given observed mixture using a Monte Carlo analysis. We characterized uncertainty for each end member using a random variable with a normal distribution estimated from multiple samples characterizing that end member over time and similar sites sampled on the same date. We then generated an ensemble of 5,000 realizations of the MLE-inferred composition for a given observation, where each realization was generated by randomly sampling from the normal distributions defining the uncertainty in the end members and repeating the MLE. Normal distributions truncated at zero were used to characterize uncertainty in end members, such that nonsensical results from physically impossible negative concentrations or isotope ratios in end members were excluded from the ensemble results. The 95% confidence intervals of the ensemble results are reported based on the 2.5 and 97.5 percentiles of the 5,000 iterations.

Equation 2 describes two end member mixing using an isotopic system with distinct compositions in each end member. However, many hydrologic situations are

more complex and involve mixtures of more than two end members. In these situations, the use of a single isotope-system may not be sufficient to discriminate between multiple end members. Recent studies evaluated simple three end member mixing using two independent isotope systems to determine contributions of different hydrologic sources with distinct radiogenic isotope signatures (Paces and Wurster, 2014, Drexler et al., 2014). We follow this general approach in lower Hyalite Canyon, where we consider whether inmixing of Archean gneiss derived water can explain the observed isotopic values.

3.4 Results

3.4.1 U and Sr Concentrations

Concentrations of dissolved Sr and U in the mainstem of Hyalite Creek tend to increase downstream as elevation decreases (Table 3.3, Figure 3.3a). Concentrations of Sr increase from 0.02–0.03 mg L^{-1} in the upper elevations of Hyalite Creek (sites HY1 and HY2) to 0.04–0.05 mg L^{-1} at lower elevations (sites HY5 and HY6). Much of this increase occurs over the reach where the stream bed intersects Mesozoic sedimentary rocks, particularly from sites HY7 to HY10. Further downstream, Hyalite Creek intersects older geologic units including Paleozoic carbonate rocks between sites HY10 and HY4. Sr concentrations in the mainstem remain more-or-less constant between 0.04 to 0.06 mg L^{-1} over this middle reach and into the lower reach, which cuts through Archean gneiss at sites HY14, HY15, HY5, and HY6. Samples from tributary watersheds draining Mesozoic and Paleozoic sedimentary rocks tend to have higher and more variable Sr concentrations (0.08 to 0.16 mg L^{-1}) resulting from more extensive water/rock

interaction with more readily weatherable sedimentary lithologies. Groundwater sampled from wells or springs hosted in the Archean gneiss from Hodgeman's canyon (GW2 and GW3) has Sr concentrations similar to those of the lower reaches of Hyalite Creek (0.05 to 0.06 mg L^{-}). The alluvial aquifer well sample at the mouth of Hyalite Canyon has a higher Sr concentration (0.11 mg L^{-1}) than samples of Hyalite Creek at the mountain front. Overall, Sr concentrations did not vary systematically among sampling dates at any given site.

Concentrations of U followed trends similar to Sr concentrations, and generally increased with distance downstream in the mainstem of Hyalite Creek (Table 3.3, Figure 3.3b). At higher elevation (sites HY1 and HY2), where Hyalite Creek drains Tertiary volcanic rock, U concentrations vary between 0.005 and 0.015 μg L^{-1}. Again, much of the longitudinal increase in concentration occurs in the middle elevations of Hyalite Creek (sites HY7 to HY4) coinciding with the inflow of springs and tributaries having higher and more variable U concentrations (0.017 to 0.713 μg L^{-1}) than the mainstem at a given location (0.023 to 0.242 μg L^{-1}). Samples at a given site collected in February and August have similar U concentrations for the majority of site locations (HY1-HY4, HY7-HY17). Concentrations of U in water increase in mainstem samples from the lower elevations of Hyalite Creek (HY5, HY6) in February (0.544 to 0.791 μg L^{-1}) but not in August (0.121 to 0.170 μg L^{-1}).The gneiss-hosted groundwater from Hodgeman Canyon wells (sites GW2 and GW3) had U concentrations in the range of 0.353 to 0.364 μg L^{-1}, which was near the middle of the range observed in samples from sites HY5 and HY6. The upper

alluvial fan well (GW4) has a U concentration of 0.233 μg L^{-1}, intermediate between those of February and August samples from Hyalite Creek at the mountain front.

3.4.2 Ca/Sr Ratios

Ratios of Ca/Sr along Hyalite Creek follow patterns similar to those observed for Sr and U concentrations (Table 3.3). Values in the mainstem tend to gradually increase with distance downstream from values between 170 and 200 in upper Hyalite Creek (sites HY1 and HY2) to values between 250 and 290 in the lower canyon (HY5 and HY6). Much of this shift occurs over the transition from areas underlain by Tertiary volcanic rock to Mesozoic sediments (sites HY7 and HY9). Values continue to increase in the middle elevations of the mainstem between sites HY10 and HY14, reflecting inputs from Paleozoic carbonate units in this reach. Ca/Sr values remain constant as the mainstem cuts through Archean gneiss (sites HY15, HY5, and HY6), although some seasonal variation between February and August sampling events is notable in lower canyon samples. Tributary samples at middle elevations show greater variability (both higher and lower values). In contrast to mainstem water, Archean gneiss wells (sites GW2 and GW3) have high Ca/Sr ratios of 321 and 467. The well in the alluvial fan aquifer at the mouth of Hyalite Canyon also has a much higher Ca/Sr value (383) than samples of Hyalite Creek water at the mountain front (249–297). Alkalinity follows trends in the Ca/Sr (Table 3.3), with higher values in tributaries draining Mesozoic and Paleozoic sedimentary rock units, and gradually increasing values in mainstem samples downstream of confluences with tributaries draining sedimentary rock units. Across the

sites, variations in Ca/Sr do not follow any systematic temporal patterns between sampling dates.

3.4.3 Sr Isotope Ratios ($^{87}Sr/^{86}Sr$)

Inflections in $^{87}Sr/^{86}Sr$ values along the mainstem of Hyalite Creek also align with transitions in parent bedrock along the valley (Tables 3.2 and 3.3, Figure 3.4). Values for $^{87}Sr/^{86}Sr$ range from 0.70883 to 0.70921 in the upper reaches draining Tertiary volcanic bedrock (sites HY1 and HY2). $^{87}Sr/^{86}Sr$ in mainstem samples decrease to values of 0.70853 to 0.70871 below Hyalite Reservoir (site HY7) through areas draining Mesozoic and Paleozoic marine mudstones, shales, and limestones at intermediate elevations (sites HY9 through HY11). Tributaries and springs along this reach (sites HY3, HY16 and HY17) contribute somewhat lower $^{87}Sr/^{86}Sr$ values ranging from 0.70835 to 0.70859. Tributaries draining sub-basins containing mixtures of Paleozoic sediments (sites HY13 and HY12) and Archean gneiss (site HY8) have elevated $^{87}Sr/^{86}Sr$ values ranging from 0.70893 to 0.71181. Mainstem samples have $^{87}Sr/^{86}Sr$ values that increase marginally through this reach where bedrock transitions from Paleozoic sedimentary rock to Archean gneiss to values of 0.70866 to 0.70885. Unlike Sr concentrations, $^{87}Sr/^{86}Sr$ values showed minimal differences regardless of sample date for a given mainstem or tributary site in upper and middle Hyalite Canyon.

Mainstem samples in the lower reach of Hyalite Creek have $^{87}Sr/^{86}Sr$ values that increase to a range of 0.70973 to 0.71202, reflecting input from water in contact with Archean gneiss (sites HY5 and HY6, Figure 3.4). Groundwater samples from wells in the Archean gneiss (sites GW2 and GW3) have much higher $^{87}Sr/^{86}Sr$ compositions of

0.73687 and 0.74497 (Table 3.3). Values of $^{87}Sr/^{86}Sr$ in mainstem samples from sites in lower Hyalite Canyon (HY5 and HY6) show substantial variation among sample dates, with the highest values observed in February and the lowest values observed in August (overall range of 0.709734 to 0.711415). Furthermore, $^{87}Sr/^{86}Sr$ values in samples of mainstem water at the canyon mouth (site HY6) were consistently higher than water sampled upstream (site HY5) during each sampling campaign. Values of $^{87}Sr/^{86}Sr$ in August streamflow at HY6 were much lower than that measured in the June 2017 sample of groundwater from the alluvial fan near the mouth of the canyon (site GW4; values of (0.710067–0.709977 versus 0.71221, respectively). However, $^{87}Sr/^{86}Sr$ values for streamflow at HY6 in February 2016 and 2017 (0.712017 and 0.711124) were similar to GW4 groundwater in June 2017.

3.4.4 Uranium Activity Ratios ($[^{234}U/^{238}U]$)

Samples of Hyalite Creek headwaters (sites HY1 and HY2) as well as water from immediately below Hyalite Reservoir (HY7) have relatively low and uniform $[^{234}U/^{238}U]$ values ranging from 1.59 to 1.72 (Table 3.3, Figure 3.5). In contrast, water discharging from the Madison aquifer at sites HY16 and HY17 have the highest $[^{234}U/^{238}U]$ values of 5.23 and 5.29. Mainstem samples throughout intermediate elevations where Hyalite Creek traverses Madison aquifer rocks (sites HY10 and HY11) and immediately downstream (sites HY4, HY14, HY15) have $[^{234}U/^{238}U]$ that increase to values between 2.94 and 3.20. Tributaries draining sedimentary rocks in tributary watersheds along the same reach (sites HY3, HY12, HY13, and HY8) show a wide range of $[^{234}U/^{238}U]$ values from 1.50 to 2.69.

Mainstem samples of lower Hyalite Creek (sites HY5 and HY6) have distinctly lower [$^{234}U/^{238}U$] values (1.69 to 2.13) relative to those at intermediate elevations, reflecting a progressive decrease as Hyalite Creek cuts through Archean gneiss. Values of [$^{234}U/^{238}U$] in lower Hyalite Creek are similar to those in groundwater sampled from wells drilled in Archean gneiss (GW2 and GW3; 1.85 and 1.49). Differences in [$^{234}U/^{238}U$] at a given site are only apparent at sites HY4, HY5, and HY6. February samples from site HY4 displayed higher [$^{234}U/^{238}U$] values than August samples, while February samples from sites HY5 and HY6 displayed lower [$^{234}U/^{238}U$] values compared to August samples. Values of [$^{234}U/^{238}U$] in lower Hyalite Creek are also comparable to those in groundwater sampled from alluvium along the mountain front near the mouth of Hyalite Canyon (GW4; 1.78).

3.4.5 Estimates of Fractional Groundwater Contributions

Variations in isotopic ratios across the full sample set were evaluated in $^{87}Sr/^{86}Sr$ vs. [$^{234}U/^{238}U$] space as a three end member mixture defined by end members representing compositions derived from Archean gneiss, Madison Group limestones, and Absaroka volcanics (Figure 3.6). Progression of Hyalite Creek Sr and U isotopic ratios within the curved space defined by the three end member isotopic ratio mixing model provides a graphic perspective on the cumulative influence of aquifers with distance downstream. Two end member mixtures of concentration (equation 1) will result in points that define a linear relationship between end member compositions. The derivation of the mixing model for an isotopic ratio (equation 2) results in the end member with the higher concentration more effectively influencing the isotopic ratio of

the mixture. If concentrations are not equal in the end members, this nonlinearity results in a hyperbolic mixing curve with non-equal spacings of fractional contributions when isotopic ratios are plotted (Faure & Mensing, 2015). Mixing end members are represented by (1) average values for samples from Hyalite Creek passing over mainly Absoroka volcanics above the influence of Madison Group limestones (HY7), characterized by low $^{87}Sr/^{86}Sr$ and $[^{234}U/^{238}U]$ values; (2) Madison aquifer spring water (HY16, HY17), characterized by low $^{87}Sr/^{86}Sr$ and high $[^{234}U/^{238}U]$; and (3) well water drawn from Archean gneiss (GW2, GW3), characterized by high $^{87}Sr/^{86}Sr$ and low $[^{234}U/^{238}U]$. We used these end member values to create the mixing web shown in Figure 3.6.

As seen in Figure 3.6, streamflow in the upper reaches of Hyalite Creek derives its Sr and U from interactions with Eocene Absaroka volcanic rocks resulting in $^{87}Sr/^{86}Sr$ and $[^{234}U/^{238}U]$ compositions that plot in the lower left corner of the mixing web. Moving downstream, the isotopic composition of streamflow moves away from the Eocene volcanic end member along a binary mixing curve defined by Eocene volcanic and Madison aquifer end members (the lower boundary of the mixing web). Because these two lithologies have similar $^{87}Sr/^{86}Sr$ compositions, most of the compositional evolution is involves a progressive increase in $[^{234}U/^{238}U]$ values with relatively constant $^{87}Sr/^{86}Sr$ values. Based on this progression in the three end member mixing model, groundwater from the Madison Group limestones end member contributes up to about 5% of the water mass in the middle reaches of the Hyalite Creek mainstem.

Once the mainstem passes into Archean gneiss bedrock, increasing $^{87}Sr/^{86}Sr$ values and decreasing $[^{234}U/^{238}U]$ values indicate that groundwater contributions from the

Archean gneiss influence the lower reaches. Groundwater in Archean gneiss has [$^{234}U/^{238}U$] compositions similar to water associated with Eocene volcanic rock, but much more radiogenic Sr values (higher $^{87}Sr/^{86}Sr$). As a result, compositions of mainstem water progressively evolve away from the binary mixing curve that is the lower boundary of the mixing web in Figure 3.6, into three end member space towards the Archean gneiss end member in both February and August samples, moving closer to the mixing curve defined by Eocene volcanics and Archean gneiss (left boundary of mixing web) in February during the lowest overall flows in Hyalite Creek. Based on the three end member mixing model, streamflow at the mouth of Hyalite Canyon (HY6) contains up to 6% of the water mass discharging from the Archean bedrock with very little signature left from Madison sources based on low [$^{234}U/^{238}U$] values in these samples.

Mixing relations were also evaluated using a Monte Carlo uncertainty analysis of optimized mixing models, providing perspective on the degree to which groundwater aquifers are likely contributing to Hyalite Creek at two locations along the canyon and during two seasons (Figure 3.7 and D.1, Table C.1). Groundwater contributions from the Madison Group limestones (HY16, HY17) contribute water with [$^{234}U/^{238}U$] values of 5.21 to 5.29 and $^{87}Sr/^{86}Sr$ values of 0.70835 to 0.70836, increasing the [$^{234}U/^{238}U$] values in Hyalite Creek mainstem from 1.62 at HY7 to 2.96 at the downstream site HY10 and decreasing $^{87}Sr/^{86}Sr$ values from 0.70870 to 0.70860. Based on the ensemble of mixing optimizations for net gains over the reach from HY7 to site HY10 (Figures 3.7a and D.1a), we estimate that the Madison Group limestones aquifers draining to this reach contributed approximately 3.7% of the streamflow at site HY10 in Hyalite Creek during

baseflow conditions in August 2017 (reported as the median of the ensemble with a 95% confidence interval of 0.3% to 8.7%).

Contributions from the Archean gneiss aquifer were modeled during baseflow conditions in August 2017 and February 2017 (Figure 3.7b and c and D.1b and c respectively). For the August 2017 model, sites HY14 and HY15 are assumed to represent the end member at the upstream end of the mixing reach, with higher [$^{234}U/^{238}U$] values (2.94 to 3.05) and lower $^{87}Sr/^{86}Sr$ values (0.70874 to 0.70885) relative to the downstream end of the mixing reach at site HY5. Isotopic ratios for the Archean aquifer end member estimated from wells GW2 and GW3 have [$^{234}U/^{238}U$] values of 1.49 to 1.85 and $^{87}Sr/^{86}Sr$ values of 0.73687 to 0.74497. Mixing of mainstem flow with groundwater or runoff inputs over the reach resulted in downstream isotopic ratios (at HY5) of 2.13 for [$^{234}U/^{238}U$] and 0.70973 for $^{87}Sr/^{86}Sr$. The ensemble of mixing optimizations in the reach defined by sites HY14/15 to site HY5, suggest that the Archean aquifers draining to this reach contributed approximately 10.9% of the streamflow at site HY5 during baseflow conditions in August 2017 (reported as the median of ensemble with 95% confidence interval of 7.4% to 16.2%, Figures 3.7b and D.1b). However, the ensemble does not explicitly capture the mixture represented by the downstream site (HY5), indicating that the mixture is not well represented by the end members.

For the February 2017 model, the sample from middle Hyalite Creek at site HY4 (below the influx of the aquifer in the Madison Group limestones and above the Archean gneiss) was used as the upstream end member, because sites HY14 and HY15 were not

sampled on that date. HY4 has a higher [$^{234}U/^{238}U$] value (3.01) and lower $^{87}Sr/^{86}Sr$ value (0.70868) consistent with Madison influence. The same Archean gneiss groundwater samples GW2 and GW3 were used as the groundwater influx end member in the February 2017 model. As simulated in August, the influence of Archean gneiss groundwater would decrease the [$^{234}U/^{238}U$] value and increase the $^{87}Sr/^{86}Sr$ value of Hyalite Creek, generally consistent with the observed reduced [$^{234}U/^{238}U$] value of 1.75 and the increased $^{87}Sr/^{86}Sr$ value of 0.71112 at site HY6. We therefore model HY6 as a mixture between (1) waters of middle Hyalite Creek (HY4), and (2) water derived from the Archean gneiss as represented by GW2 and GW3 (Figure 3.7c). Using these values in our mixing optimization, we estimate that fracture flow from the Archean gneiss contributes a median of 24.2% (95% confidence interval 14.3% to 37.5%, Figures 3.7c and D.1c) of streamflow to lower Hyalite Creek (HY6) during February baseflow conditions. However, the model again fails to explicitly capture the observed mixture value.

Using the same Monte Carlo realization and optimization model we also evaluated the Sr isotopic values alone as an indicator of Archean gneiss influence, based on the sensitivity of this tracer to the Archean endmember. Using only Sr isotopic ratio, we estimate that a range of 1.6% to 4.1% (reported as a 95% confidence interval with a median of 2.4%) of water in lower Hyalite Creek can be attributed to inflows from the Archean gneiss during baseflow conditions in August and 4.9% to 14.6% (reported as a 95% confidence interval with a median of 8.4%) of water can be attributed to Archean gneiss inflows in February (simulations not shown).

Absolute fluxes of water relative to measured discharge at the downstream gauge sites can also be estimated from mixing model results. Given the percentage estimates calculated in the preceding paragraphs, additions to mainstem streamflow from Archean sources are estimated at 0.17 $m^3 s^{-1}$, or 11% of the total 1.57 $m^3 s^{-1}$ measured at site HY6 in August 2017. A similar influx of 0.14 $m^3 s^{-1}$ is estimated for February 2017 data (24% of 0.60 $m^3 s^{-1}$). Additions to streamflow from Madison sources in the middle reaches of Hyalite Creek are estimated at 0.04 $m^3 s^{-1}$, or 3.7% of the total 1.14 $m^3 s^{-1}$ measured at site HY7 in August 2017.

3.5 Discussion

Longitudinal surveys of the character of Ca, Sr, and U dissolved in stream and ground waters provide a multifaceted means of assessing groundwater contributions to streamflow along Hyalite Canyon. Data in this study track the compositional evolution of streamflow caused by contributions from groundwater or tributary flow that reflect weathering of soils and rocks of varying lithology, allowing useful hydrologic inferences for local streamflow generation longitudinally throughout the reach of Hyalite Creek. Elemental concentrations are characteristic of matrix materials in soils and aquifers that contribute to baseflow, although values are also affected by dilution by meteoric precipitation, concentration by evaporation, removal of water by transpiration, and other near-surface physical and chemical processes. In contrast, isotopes of Sr and U remain largely unaffected by those same processes making them useful tracers of water sources and flow processes. Sr isotope ratios dissolved in water reflect the composition of soils and aquifer rock, weatherability of different constituents, and geologic age of those

solids. Uranium isotope ratios also reflect the weatherability of solids, but are more diagnostic of the extent and duration of water/rock interactions. We use these multifaceted tracers to offer perspective on the nature of hydrologic storage and stream baseflow generation along this mountain headwater canyon.

3.5.1 Values for $^{87}Sr/^{86}Sr$ in Regional Rocks and Waters

Previous studies have compiled $^{87}Sr/^{86}Sr$ values for several rock units and streams in the region (Table 3.2). Values for $^{87}Sr/^{86}Sr$ from previous work provide constraints on how rock age and Rb/Sr ratio in bedrocks of the Hyalite Watershed are likely to manifest in the $^{87}Sr/^{86}Sr$ values observed in Hyalite Creek.

Tertiary (Eocene) Absaroka volcanic rocks similar to those present in Hyalite Canyon (Smedes & Prostka 1972)are dominated by mafic to intermediate compositions with relatively low Rb/Sr and measured $^{87}Sr/^{86}Sr$ values ranging from 0.70433-0.70826 (Feeley & Cosca 2003; Lindsay & Feeley 2003; Hiza 1999). Values for $^{87}Sr/^{86}Sr$ ranging from 0.7072 to 0.7078 were reported for Eocene Absoroka volcanics east of the Hyalite area (Hiza 1999). Waters draining Eocean-aged Absaroka Volcanics in the nearby Clark's Fork of the Yellowstone drainage have $^{87}Sr/^{86}Sr$ values in the range of ~0.704 to 0.705 (Horton et al. 1999; exact values not provided).

Paleozoic aged carbonate sedimentary rocks in the greater Yellowstone National Park region have an average $^{87}Sr/^{86}Sr$ value of 0.71062 (Kharaka et al. 1991) and thermal water and associated travertine deposits at Mammoth Hot Springs have $^{87}Sr/^{86}Sr$ values of 0.7103 to 0.7111 (Leeman et al. 1977). The average $^{87}Sr/^{86}Sr$ value for Madison Group limestones in the Pryor Mountains was given as 0.708834 (Moore-Nall 2016) and

Madison rocks and waters had a range of 0.70873 to 0.70926 in the Big Horn Basin of Wyoming (Frost and Toner, 2004).

In contrast, much older Archean granites and gneisses, including those in the neighboring Beartooth Mountains, exhibit a wide range of present-day $^{87}Sr/^{86}Sr$, reflecting highly variable Rb/Sr ratios within mineral phases comprising the rock, and long time periods over which ^{87}Sr grew in. Measured $^{87}Sr/^{86}Sr$ values for a variety of Archean-age rock types from the eastern and southern Beartooth Mountains range from 0.70617 to 10.7 with a median of 0.76177 (N=84; (Wooden & Mueller 1988; Montgomery & Lytwyn 1984)). Water draining Precambrian granitic gneiss in the Clark's Fork basin yielded $^{87}Sr/^{86}Sr$ values of ~0.721 to 0.732 (Horton et al., 1999; precision as reported).

Although rock analysis was not undertaken as part of this study, published data corroborate assumptions made about the $^{87}Sr/^{86}Sr$ compositions in primary rock types present in Hyalite Canyon (Table 3.2), acknowledging that differential mineral weatherability may explain some differences in waters as compared to source rocks. Eocene to Archean rocks are all assumed to have $[^{234}U/^{238}U]$ close to secular equilibrium (equal to 1.00) regardless of lithology, although readily soluble secondary phases within soils in the region may somewhat higher values (typically less than about 1.6; Sharp et al., 2003).

3.5.2 Origins of Headwater Compositions

Streamflow generated in high elevation glacial basins forming the headwaters of Hyalite and Emerald Creeks are derived exclusively through water/rock reaction with

Eocene volcanic rocks. Sr and U concentrations, Ca/Sr ratio, and alkalinity were low in higher elevation waters draining the Abasaroka volcanics, likely due to igneous rocks that are less calcareous and more resistant to weathering, as well as colder temperatures that are less conducive to chemical weathering.

Values of $^{87}Sr/^{86}Sr$ in water draining Tertiary volcanic rocks in the upper reaches of Hyalite Creek (sites HY1 and HY2) are somewhat higher than values reported for whole rock digestions in the literature. This is likely a consequence of volcanic rocks in the Gallatin Range being part of the older Washburn Group (Smedes & Prostka 1972), which tend to have higher $^{87}Sr/^{86}Sr$ values (median of 0.70725, Lindsay and Feely, 2003; 0.7072–0.7078, Hiza, 1999) than younger rocks in the Absaroka Supergroup. Magmas associated with early eruptions in the volcanic field may have assimilated crustal components with elevated $^{87}Sr/^{86}Sr$ values before chambers and conduits become well established. In addition, leaching of rock and soil by water will preferentially extract Sr from the most weatherable minerals, which are not likely to have remained in equilibrium with the bulk rock over the ~50 million years since formation. Water may preferentially leach phases with elevated Rb/Sr resulting in groundwater or runoff with higher $^{87}Sr/^{86}Sr$ values. Regardless of cause, the similarity of $^{87}Sr/^{86}Sr$ values for streamflow samples draining two separate volcanic-rock headwater basins (upper Hyalite Creek, HY1, and Emerald Creek, HY2; Figure 3.1) indicates that streamflow interacting with Absaroka rocks is well characterized with a mean value of 0.70889 (±0.00008 2×standard deviation [SD] for N=7 excluding 1 outlier). Lower $[^{234}U/^{238}U]$ values in the steeper subcatchments in upper Hyalite Creek (HY1) and in the Emerald Creek tributary (HY2), suggest more

aggressive weathering of U from soils during recharge or relatively rapid communication of meteoric water (Figure 3.5).

3.5.3 Baseflow Contributions from Tributaries and Aquifers Draining Sedimentary Rocks

Concentrations of Sr and U, Ca/Sr ratio, and alkalinity generally increased in the middle elevations of Hyalite Creek (above 1800 m), consistent with baseflow contributions from relatively solute-rich groundwater in sedimentary bedrock that ultimately drain to Hyalite Creek via tributaries or subsurface flow (Figure 3.3). Relative to baseflow derived from Absaroka volcanics, downstream tributaries draining aquifers in more weatherable limestones and shales are likely to contribute higher ion concentrations, or ion loads that are disproportionate to their contribution to flow (Horton et al. 1999; Jacobson et al. 2002; Jacobson et al. 2003). More specifically, tributaries draining aquifers in sedimentary bedrock are more likely to contain secondary carbonates or other Ca-rich secondary phases with elevated Ca/Sr values. Consequently, inputs to streamflow along the intermediate elevations of Hyalite Creek likely contribute substantial ion loading to Hyalite Creek.

The middle reaches of Hyalite Creek drain an area dominated by Mesozoic and Paleozoic sedimentary rocks. Mainstem samples (sites HY7, HY9, HY10 and HY11) show a distinct decrease in $^{87}Sr/^{86}Sr$ values (mean value of 0.70862 ±0.00013 2×SD for N= 7) interpreted to reflect addition of Sr from marine sources. Streamflow from a tributary draining mostly Mesozoic clastic sediments (Lick Creek site HY3) and groundwater discharging from the Madison aquifer (sites HY16 and HY17) have lower $^{87}Sr/^{86}Sr$ values (mean $^{87}Sr/^{86}Sr$ values of 0.70849 and 0.70835, respectively) than those

in mainstem flow at the same elevation (Figure 3.4). This relation is consistent with addition of Sr from marine sources, which had primary $^{87}Sr/^{86}Sr$ between 0.7068 and 0.7082 through most of the Mesozoic and Paleozoic Eras. In contrast, tributary streamflow draining a small sub-basin of volcanic rock in this reach ('Meadow' Creek; site HY13) has a higher $^{87}Sr/^{86}Sr$ value of 0.70893, similar to values draining volcanic rocks in headwater areas.

Contributions to Hyalite Creek streamflow from groundwater discharging from Madison Group limestones is evident from the notable increases in $[^{234}U/^{238}U]$ values along Hyalite Creek (Figure 3.5). Springs issuing from the Madison Group limestones (HY16 and HY17) have elevated $[^{234}U/^{238}U]$ values consistent with water that has had more extensive contact time with matrix materials allowing greater incorporation of recoil ^{234}U from aquifer-rock surfaces. The large changes in $[^{234}U/^{238}U]$ values observed in mainstem samples from sites HY10 and HY11 are coupled with only small changes in U concentration and discharge, consistent with inflows having similar U concentrations but substantial enrichment in ^{234}U. Elevated $[^{234}U/^{238}U]$ values are present in mainstem samples well downstream from the contact with the Madison Group limestones, suggesting the possibility of continued influx from related karst aquifers, or at least reflecting the conservative nature of uranyl complexes in the dissolved load. Decreasing values of $^{87}Sr/^{86}Sr$ in mainstem samples below Hyalite Reservoir through this reach may be derived as a consequence of either tributary additions or gains from aquifer discharge. However, the large increase in $[^{234}U/^{238}U]$ values is interpreted to be diagnostic of groundwater influxes from laterally continuous aquifers such as karst developed in

Madison Group limestones. Equally elevated [$^{234}U/^{238}U$] values are not observed in surface flow from tributaries in the same reach (sites HY13, HY12, and HY8), although values are higher than those in tributary flow above Madison outcrop (HY3) and may indicate a contribution from Madison Group limestone aquifers or other well-travelled groundwater as well.

Mixing models suggest that approximately 4% of water in Hyalite Creek downstream of sites HY16 and HY17 can be attributed to groundwater from the Madison Group limestones, flowing into the reach via subsurface flowpaths, with a range of 0.3% to 8.7% of late summer inflows between elevations of 1962 m and 1909 m (site HY7 to HY10) (Figures 3.7a and D.1a). This observation is consistent with the previous Masters thesis work of Kirk (2002), who made direct observations of discharge changes across this inflow. While the generation of baseflow from aquifers in the Madison Group limestones is modest in terms of percent of stream flow in this reach, [$^{234}U/^{238}U$] values provide a sensitive indicator of baseflow source within these important regional limestone aquifers in Hyalite Creek.

3.5.4 Contribution from Archean Gneiss Fracture Flow

Baseflow generation from groundwater moving through fractures in Archean gneiss is evident from progressive increases in $^{87}Sr/^{86}Sr$ values and decreases in [$^{234}U/^{238}U$] values with distance downstream in the lower elevations of Hyalite Canyon. These isotopic changes are consistent with evolution of mainstem water towards values observed in wells completed in the Archean gneiss bedrock.

The most obvious indicator of water influxes from gneissic terrain are $^{87}Sr/^{86}Sr$ values, which are highly elevated in groundwater pumped from wells GW2 and GW3. The $^{87}Sr/^{86}Sr$ values of mainstem samples never approach values close to those compositions. Nevertheless, samples with the highest $^{87}Sr/^{86}Sr$ values are interpreted to have incorporated the greatest baseflow contribution from the gneiss source. Although baseflow gains increase progressively with decreasing elevation (Figure 3.4) reflecting cumulative contributions from tributaries or groundwater discharge, compositions at the two sites closest to the canyon mouth (HY5 and HY6) show large variations of $^{87}Sr/^{86}Sr$ that depend on date of sample collection. For both sites, samples collected in February 2016 and 2017 have substantially larger $^{87}Sr/^{86}Sr$ values than samples collected in August 2016 and 2017 (Figure 3.4, Table 3.3). Those data indicate that baseflow gains were proportionally greater during winter than during summer. The same pattern is observed for U concentrations (Figure 3.3b), although February samples have U concentrations that are higher than those measured in GW2 and GW3 well water. Values of $[^{234}U/^{238}U]$ also show systematic differences between February and August samples (Figure 3.5) that are consistent with greater contributions from rapid flow through gneiss in winter. Concentrations of Sr and values of Ca/Sr do not show similar seasonal differences.

The largest apparent influxes of water from gneiss sources, as well as the greatest variability in $^{87}Sr/^{86}Sr$ values, are incorporated into mainstem flow downstream from site HY15 at elevations between 1729 and 1707 m (Figure 3.4). A shear zone cutting bedrock just below 1729 m (May 1985) may represent a zone where groundwater fracture flow is focused preferentially. If baseflow gains are derived from groundwater discharging from

fractured gneiss, [$^{234}U/^{238}U$] values suggest a very different type of water/rock interaction compared to flow in aquifers hosted by Madison Group limestone. Low [$^{234}U/^{238}U$] values imply relatively short-range connectivity such that preferential incorporation of recoil ^{234}U generated along fracture surfaces is not sufficient to increase [$^{234}U/^{238}U$] beyond values obtained during infiltration through soils.

Streamflow contributions from groundwater seepage through fractured gneiss may help explain the larger contributions of gneiss-derived water in lower Hyalite Canyon samples in February relative to August. Periods of winter snowmelt on slopes above Hyalite Creek likely enhance local piston-flow through Archean gneiss bedrock at lower elevations. Additionally, stream gains between gauge stations at sites HY7 and HY6 were larger in February 2016 compared to August 2016 and 2017 low-flow conditions (no upstream data in February 2017, although measured discharge suggests similar gains; Figure 3.2), while total discharge was much lower in February compared to August (Figure 3.2). These observations indicate that local stream gains in lower reaches of Hyalite Creek constitute a larger proportion of streamflow during February compared to August. Similar seasonal differences in local streamflow gains were not observed at other sampling sites based on point measures of discharge (Table G.5), in part due to lack of precision in area-velocity measures, but also suggesting the process may be enhanced at lower elevations where late winter snowmelt episodes are likely to produce greater inputs of water. Seasonal variation in the lower canyon isotopic values can be seen in Figures 3.4 and 3.5, suggesting a higher fractional input (but similar absolute volume) of

groundwater derived from fracture flow in the Archean gneiss during winter as compared to late summer.

Using our two-component model combining U and Sr isotopic values in August baseflow conditions, we estimate that somewhere between 7.4% and 16.2% of water in Hyalite Creek downstream of the Archean gneiss fracture flow (HY5) can be attributed aquifers in contact with Archean gneiss (Figures 3.7b and D.1b). During February baseflow conditions, we estimate that somewhere between 14.3% to 37.5% of water in Hyalite Creek downstream of the Archean gneiss fracture flow (HY6) can be attributed to groundwater inputs form the Archean gneiss (Figures 3.7c and D.1c). However, visual examination of Figure 3.7 (b,c) suggests that the estimated contributions are erroneously high, because the mixing lines do not intersect the points we have defined as the mixture.

The Archean gneiss end member (GW2, GW3) was given a large uncertainty in construction of the two-component mixing model to determine fractional contribution of fracture flow through the Archean gneiss, in order to account for well samples possibly differing in chemical composition from fracture flow contributions to Hyalite Creek. Despite this large uncertainty, the Monte Carlo mixing realizations and optimized mixing fractions between the middle reaches of Hyalite Creek (HY4, HY14, HY15) and the Archean gneiss (GW2, GW3) fail to capture the measured lower Hyalite Creek mixture (HY5,HY6) (Figure 3.7 b and c). This observation has two possible explanations: first, there may be inflows from an additional end member that we have not accounted for in this model; second, [$^{234}U/^{238}U$] values of Archean derived water may be lower (and U concentrations may be higher) in the actual inflows to Hyalite Creek in lower Hyalite

Canyon. An additional end member would need to have a lower $^{87}Sr/^{86}Sr$ and [$^{234}U/^{238}U$] composition, somewhat similar to volcanics and sedimentary rocks found in the upper reaches of Hyalite Creek. Return of water derived from such rock units could be delivered by water movement through glacial till throughout the middle reaches of Hyalite Canyon, but this explanation appears physically unlikely given the arrangement of rocks in the lower canyon (Figure 3.1). However, sedimentary units are exposed at similar elevations in the next major canyon to the west (South Cottonwood, Figure 3.1); moreover, higher U concentrations and intermediate $^{87}Sr/^{86}Sr$ composition in February lower canyon samples are reasonably consistent with contributions sedimentary tributaries in the middle canyon (Figures 3.3, 3.4, 3.6). Thus we conclude that an additional subsurface sedimentary contribution cannot be ruled out.

If we assume no additional end member, and given uncertainty about the character of Archean waters directly contributing to lower Hyalite, we can adopt a more conservative approach. Using Sr isotopic values alone because they are a sensitive indicator of Archean gneiss influence, we estimate that a range of 1.6% to 4.1% of water in lower Hyalite Creek can be attributed to inflows from the Archean gneiss during baseflow conditions in August and 4.9% to 14.6% of water can be attributed to Archean gneiss inflows in February. Despite uncertainty, this contribution to baseflow suggests that proximal fracture flow is a previously underappreciated hydrologic pathway likely to influence the quality and quantity of surface water being delivered to the mountain front. This pathway was not evident in solute concentration data or Ca/Sr ratios. Further

research is needed to explicitly characterize these inflows, which are likely to be highly sensitive to changing climate conditions.

3.6 Conclusions

Groundwater contributions to stream flow are important when considering weathering trajectories, water storage and water quality in watersheds fed by mountain headwater streams. Groundwater contributions to baseflow vary seasonally, not just in terms of proportional influence, but also in terms of the flow paths and water-rock interactions driving their chemical character. This study shows that natural geochemical tracers have the potential to provide valuable information about groundwater sources, storage potential, and baseflow generation. We used $^{87}Sr/^{86}Sr$ and $[^{234}U/^{238}U]$ values as sensitive indicators of distinct groundwater inflows in a lithologically diverse catchment. In particular, radiogenic isotopic ratios provide information about groundwater sources that are less likely to be influenced by near-surface physical and chemical processes, such as dilution or evaporation that can strongly affect other constituents. Sampling longitudinally along the length of a stream further allows a spatially explicit perspective on where groundwater sources occur in the catchment that would likely have been overlooked if assessed at coarser scales or only at the watershed outlet. Longitudinal sampling allowed application of mixing models that used combinations of tracer concentrations and isotope ratios to quantify the fractional contributions from groundwater sources. Using these models, we estimate that groundwater contribution from the Madison aquifers represents about 4% of streamflow in the middle reaches of Hyalite Creek. Mixing models also indicate that groundwater discharging from fractured

Archean gneiss supplies up to ~2% of local streamflow during an August baseflow period and ~8% of local streamflow during a February baseflow period, contributions that have been underappreciated in the past. Thus this research elucidates groundwater contributions to streamflow along Hyalite Canyon, an important water resource for agricultural and metropolitan uses in the Gallatin Valley. As urban areas in intermountain basins expand at the same time that snowpack storage is predicated to decrease due to changes in future climate patterns, understanding the mechanisms of groundwater storage, residence time, and contributions in mountain stream systems is becoming increasingly important.

3.7 Acknowledgements

We thank the funding sources for this project including USGS National Institute of Water Resources Competitive Grants Program, the Nielsen Fellowship from the Department of Land Resources and Environmental Sciences at MSU (LRES), and the Montana Agricultural Experiment Station (MAES). We are grateful to Dale White and the US Forest Service, Custer-Gallatin National Forest for permission to conduct this research in Hyalite Canyon. We also thank Erika Sturn, whose Master's work laid the groundwork for this project. We are grateful for field assistance from Ethan Wologo, Joe Capella and Simon Fordyce; laboratory analysis at MBMG by Jackie Timmer and Ashley Huft, and at the LRES Environmental Analytical Laboratory by Dr. Jane Klassen and Dr. Christine Gobrogge. Cliff and Joan Montagne kindly provided access to their home well in Hodgeman's Canyon.

Table 3.1 Hyalite Creek sample descriptions, elevations, and locations.

Site ID	Location	Elevation (m)	Latitude	Longitude
HY1	Hyalite Creek above reservoir	2087	45.452	-110.959
HY2	Emerald Creek	2063	45.475	-110.954
HY7	Hyalite Creek below reservoir at DNRC gauge 41H 2000	1962	45.501	-110.986
HY3	Lick Creek	1960	45.505	-110.988
HY9	Hyalite Creek below Lick Creek confluence	1941	45.506	-110.993
HY16	Madison Group limestone spring channel	1936	45.508	-110.998
HY17	Madison Group limestone spring seep	1931	45.509	-110.997
HY10	Middle Hyalite Creek	1909	45.517	-111.007
HY11	Hyalite Creek at Langohr Logging Road	1882	45.527	-111.013
HY13	Unnamed creek in terminal glacial moraine meadow	1898	45.524	-111.017
HY12	Buckskin Creek	1889	45.530	-111.013
HY4	Hyalite Creek at Langohr Campground	1861	45.535	-111.017
HY8	Moser Creek	1871	45.537	-111.016
HY14	Hyalite Creek below Moser Creek	1854	45.539	-111.020
HY15	Hyalite Creek above Practice Rock	1729	45.554	-111.062
HY5	Hyalite Creek at Practice Rock	1707	45.542	-111.034
HY6	Hyalite Creek at USGS gage 06050000	1690	45.563	-111.072
SD1	Sourdough Creek	1926	45.524	-110.926
GW2	Hodgeman Canyon - gneiss spring	1704	45.585	-111.067
GW3	Hodgeman Canyon - gneiss well	1692	45.586	-111.067
GW4	Hyalite Creek alluvial fan well	1641	45.583	-111.091

Table 3.2 Select values for $^{87}Sr/^{86}Sr$ in bedrocks or groundwaters salient to this work.

Unit Description	Sample Type	$^{87}Sr/^{86}Sr$	Source
Absaroka Volcanic rock units (WY)	Rock	0.70433 - 0.70826	Feeley & Cosca, 2003; Lindsay & Feeley, 2003
Absaroka Volcanics (MT and WY)	Rock	0.70543	Hiza, 1999
Carbonates (average, Yellowstone National Park)	Rock	0.71062	Khraka et al., 1991
Madison Limestone Formation (Bighorn Basin, MT)	Rock	0.70883	Moore-Nall, 2016
Madison Paleokarst (Bighorn Basin, WY)	Rock	0.70875	Frost & Toner, 2004
Madison limestone (Bighorn Basin, WY)	Rock	0.70809	Frost & Toner, 2004
Archean age granitics (Beartooth Mountains, MT)	Rock	0.70617 - 0.78304 (mean 0.73267)	Wooden & Mueller, 1988
Streams draining Eocean Absaroka volcanics (Clark's Fork, WY/MT)	Water	0.704 - 0.705	Horton et al., 1999
Streams draining paleozoic sedimentary units (Clark's Fork, WY/MT)	Water	0.704 - 0.708	Horton et al., 1999
Streams draining precambrian granitic gneiss units (Clark's Fork, WY/MT)	Water	0.721 - 0.732	Horton et al., 1999

Table 3.3 Concentrations of Ca, Sr, U and alkalinity, along with $^{87}Sr/^{86}Sr$ and [$^{234}U/^{238}U$] for individual water samples.

Site ID	Description	Sample Date	Ca (mg L^{-1}) MDL*: 0.0060	Sr (mg L^{-1}) MDL*: 0.0066	U (ug L^{-1})	±2σ	Ca/Sr	$^{87}Sr/^{86}Sr$	±2σ	[$^{234}U/^{238}U$]#	±2σ	Alkalinity mg ($CaCO_3$ L^{-1})
HY1	Hyalite Creek above reservoir	2/19/2016	3.07	0.02	0.005	0.0001	176	0.708832	0.000009	1.722	0.022	
		8/25/2016	3.75	0.02	0.014	0.0001	188	0.708853	0.000010	1.695	0.013	18
		2/4/2017	3.79		0.015	0.0002		0.708898	0.000009	1.642	0.012	15
		8/23/2017	3.78	0.02	0.005	0.0000	179	0.709214	0.000010	1.616	0.025	
HY2	Emerald Creek	2/19/2016	4.60	0.03	0.014	0.0001	172	0.708900	0.000009	1.629	0.006	
		8/25/2016	5.67	0.03	0.012	0.0001	186	0.708904	0.000009	1.691	0.012	29
		2/4/2017	5.87	0.03	0.012	0.0001	196	0.708900	0.000009	1.645	0.006	24
		8/23/2017	5.56	0.03	0.011	0.0001	178	0.708953	0.000009	1.671	0.010	28
HY7	Hyalite Creek below reservoir at DNRC gauge 41H 2000	2/4/2017	9.33	0.04	0.242	0.0024	249	0.708712	0.000010	1.591	0.006	35
		8/23/2017	7.00	0.03	0.023	0.0002	231	0.708701	0.000009	1.621	0.007	12
HY3	Lick Creek	2/19/2016	21.65	0.08	0.536	0.0054	277	0.708458	0.000010	1.570	0.004	
		8/25/2016	44.60	0.14	0.203	0.0020	321	0.708473	0.000010	1.506	0.006	190
		2/4/2017	34.50	0.11	0.160	0.0016	314	0.708589	0.000009	1.497	0.004	123
		8/23/2017	47.00	0.15	0.713	0.0071	313	0.708455	0.000010	1.499	0.005	235
HY9	Hyalite Creek below Lick Creek	8/23/2017	8.52	0.04	0.039	0.0004	243	0.708590	0.000009	1.598	0.007	45
		12/14/2017	11.8	0.05	0.080	0.0008	259	0.708532	0.000009	2.121	0.006	
HY16	Madison Group limestone spring channel	12/14/2017	31.0	0.13	0.424	0.0042	233	0.708352	0.000009	5.226	0.017	
HY17	Madison Group limestone spring seep	12/14/2017	26.9	0.12	0.038	0.0004	222	0.708349	0.000009	5.285	0.013	
		1/29/2018	33.7	0.15	0.382	0.0038	228			5.282	0.032	
		3/27/2018	32.9	0.15	0.372	0.0037	224	0.708357	0.000011	5.215	0.015	
HY10	Middle Hyalite Creek	8/23/2017	11.00	0.04	0.079	0.0008	259	0.708602	0.000010	2.958	0.010	46
		12/14/2017	14.5	0.05	0.114	0.0011	277	0.708574	0.000009	2.957	0.016	
HY11	Hyalite Creek at Langohr Logging Road	8/23/2017	11.00	0.04	0.085	0.0009	259	0.708609	0.000009	2.966	0.008	49

HY13	Unnamed creek in glacial meadow	8/24/2017	14.60	0.08	0.017	0.0002	192	0.708927	0.000009	1.961	0.058	88
HY12	Buckskin Creek	8/23/2017	68.60	0.14	0.592	0.0059	504	0.711457	0.000009	2.695	0.228	212
HY4	Hyalite Creek at Langohr Campground	2/19/2016	13.52	0.05	0.164	0.0016	261	0.708679	0.000009	3.195	0.009	
		8/25/2016	12.50	0.05	0.069	0.0007	277	0.708661	0.000009	2.977	0.011	37
		2/4/2017	17.60	0.06	0.186	0.0019	301	0.708679	0.000010	3.100	0.010	52
		8/23/2017	11.40	0.04	0.088	0.0009	268	0.708789	0.000009	2.983	0.022	28
HY8	Moser Creek	2/4/2017	37.10	0.14	0.596	0.0060	275	0.711434	0.000010	2.236	0.006	106
		8/23/2017	47.10	0.16	0.542	0.0054	294	0.711809	0.000009	2.241	0.008	167
HY14	Hyalite Creek below Moser Creek	8/24/2017	11.60	0.04	0.077	0.0008	267	0.708736	0.000009	3.047	0.012	45
HY15	Hyalite Creek above Practice Rock	8/24/2017	11.60	0.04	0.083	0.0008	270	0.708847	0.000009	2.944	0.013	73
HY5	Hyalite Creek at Practice Rock	2/19/2016	9.86	0.04	0.554	0.0055	246	0.711415	0.000010	1.788	0.005	
		8/25/2016	12.60	0.05	0.170	0.0017	278	0.709791	0.000009	2.086	0.006	43
		8/24/2017	11.90	0.04	0.152	0.0015	272	0.709734	0.000009	2.128	0.008	79
HY6	Hyalite Creek at USGS gage 06050000	2/19/2016	10.05	0.04	0.638	0.0064	249	0.712017	0.000010	1.691	0.005	
		8/25/2016	12.70	0.05	0.121	0.0012	270	0.710067	0.000010	1.966	0.005	
		2/4/2017	14.40	0.05	0.791	0.0079	287	0.711124	0.000009	1.747	0.004	52
		8/24/2017	11.80	0.04			274	0.709977	0.000009			61
SD1	Sourdough Creek	12/13/2017	6.86	0.04	0.024	0.0002	181	0.708617	0.000009	2.047	0.018	
GW2	Gneiss spring	5/18/2017	15.30	0.05	0.353	0.0035	321	0.736865	0.000010	1.849	0.084	37
GW3	Gneiss well	5/18/2017	27.00	0.06	0.364	0.0036	467	0.744966	0.000010	1.489	0.022	146
GW4	Hyalite Creek alluvial fan well	6/20/2017	42.90	0.11	0.233	0.0023	383	0.712214	0.000010	1.784	0.006	139

* Minimum detection limit (MDL)
# Square brackets denote activity ratios

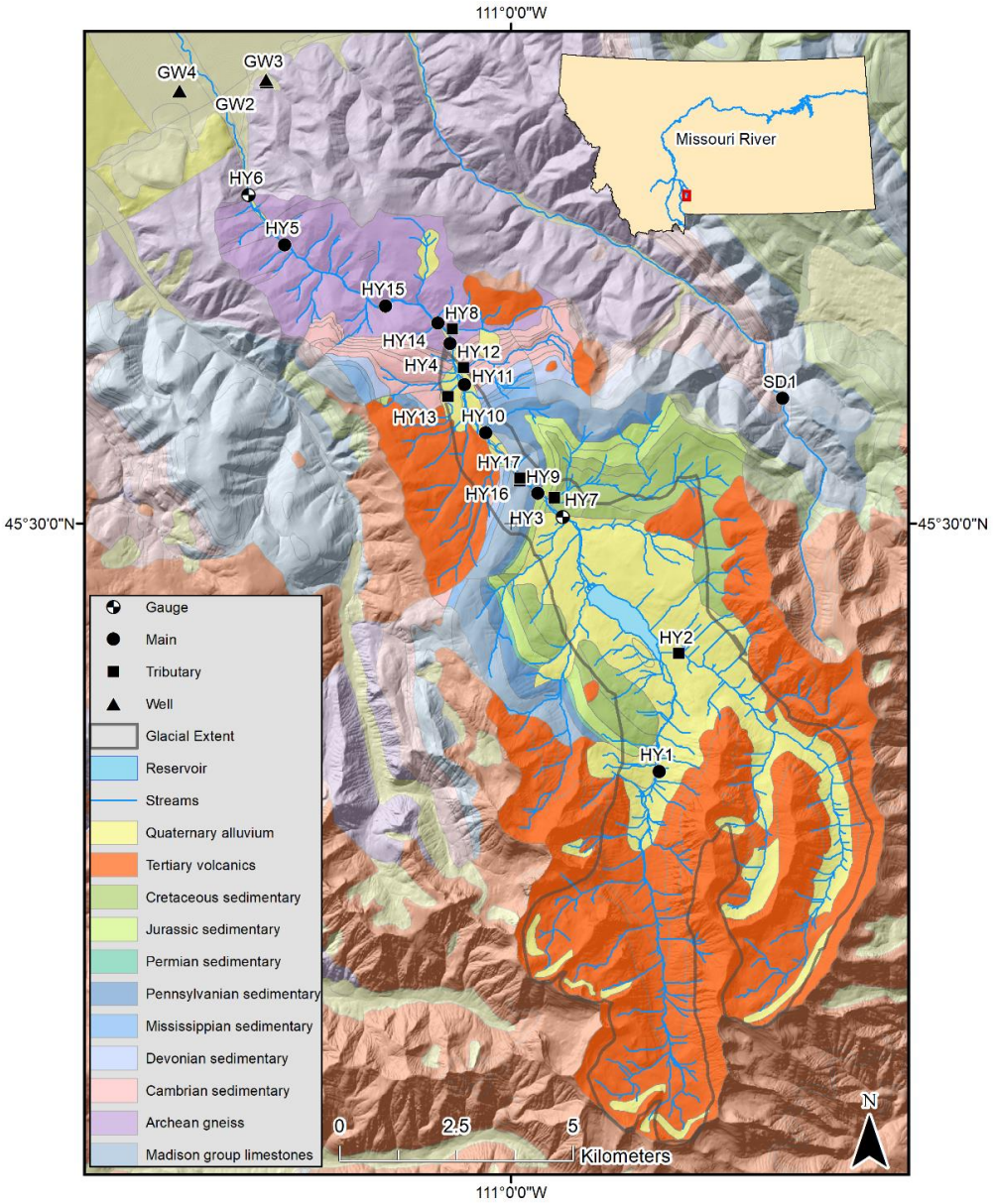

Figure 3.1 Geologic map of study area showing sample sites and gauge locations in Hyalite Canyon. Locations are numbered as specified in Table 3.1 for sites in Hyalite Creek, its tributaries and a well at the canyon outlet (HY1-HY17, GW4); in Hodgeman Canyon (GW2, GW3); and in Sourdough Canyon (SD1). Glacial extent represents extrapolation of moraines thought to reflect Pinedale (~30 to 15 ka) and Bull Lake (~180 to 130 ka) glaciations per Weber (1965). Major lithologic units include the Eocene age Absaroka volcanics (red) and associated tills (yellow) highest elevations, Cretaceous to Cambrian age sedimentary units (greens and blues) at intermediate elevations, and Archean age gneiss along the mountain front (purple) at lowest elevations. The Hyalite Creek watershed is shown in brighter colors. The inset of the state of Montana shows the study area in red, with the Missouri River and its three tributaries in blue (from West to East: Jefferson, Madison, and Gallatin Rivers).

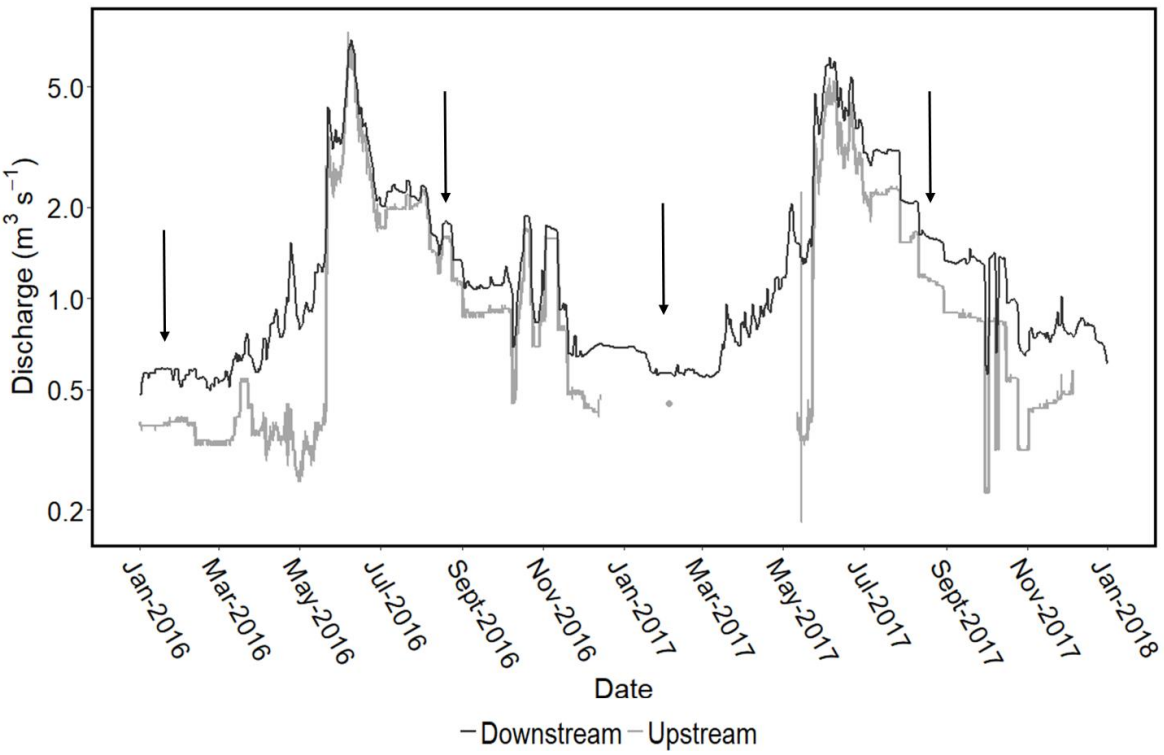

Figure 3.2 Hyalite Creek discharge on a logarithmic scale. Measurements from 1/1/2016 to 1/1/2018 at the DNRC stream gauge (site HY7; hourly discharge measurements; light gray) and at the USGS stream gauge (site HY6; daily mean discharge; dark gray). Gray dot indicates measured discharge (area-velocity method) taken during 2/4/2017 sampling at site HY7 while gauge was unable to record measurements due to ice. Arrows indicate sample dates targeting baseflow conditions in February (2016-2017) and August (2016-2017). Gauge locations shown on Figure 3.1 (U.S. Geological Survey, 2018, Montana DNRC, 2018).

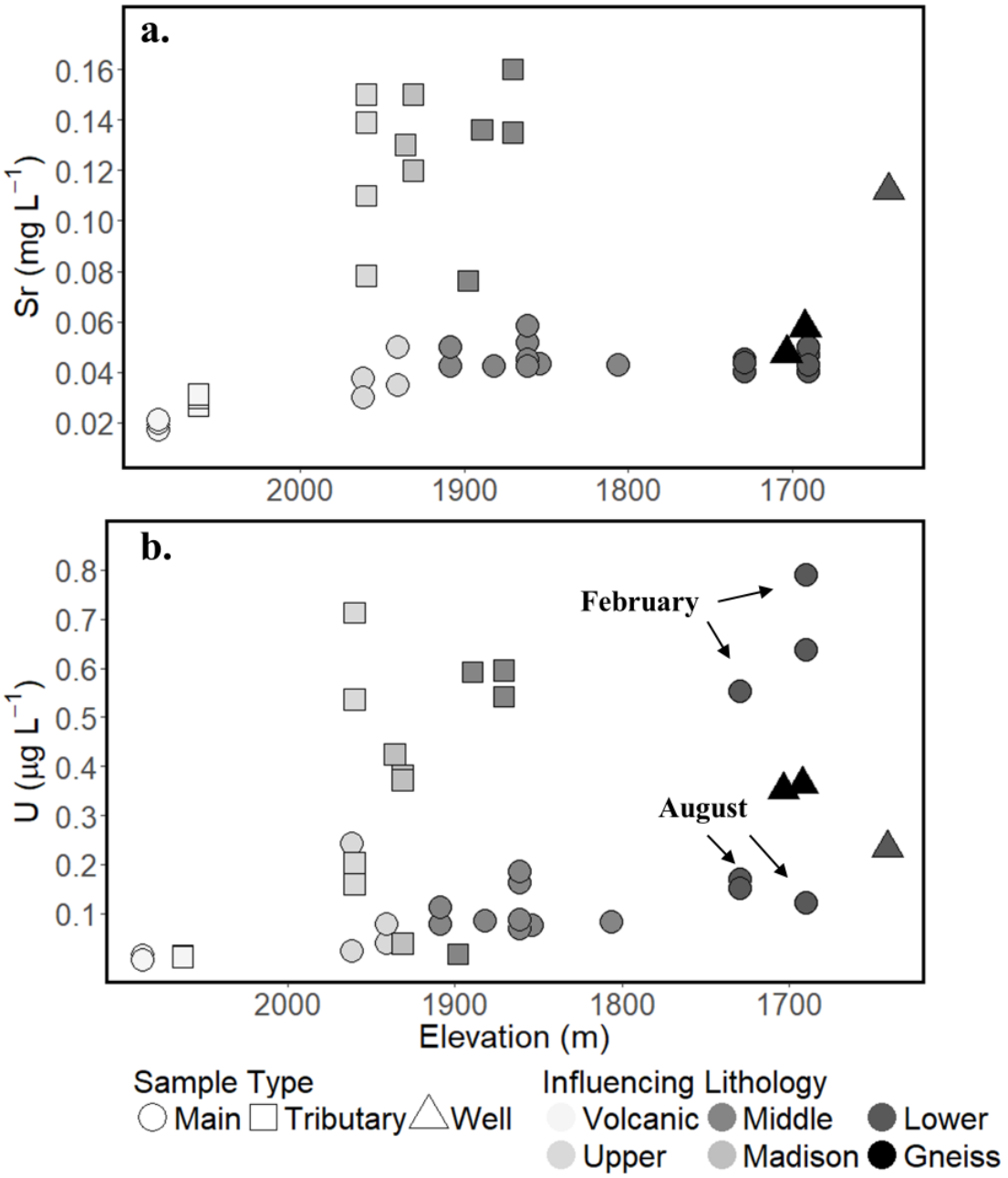

Figure 3.3 Strontium and uranium concentrations in water samples plotted against elevation in Hyalite Canyon. Sr concentrations (a) and U concentrations (b) were measured in water samples collected from the main stem of Hyalite Creek (circles), its tributaries (squares), and nearby wells (triangles). Site locations are shown in Figure 3.1. Greyscale shades indicate hosting rock unit or stream reach.

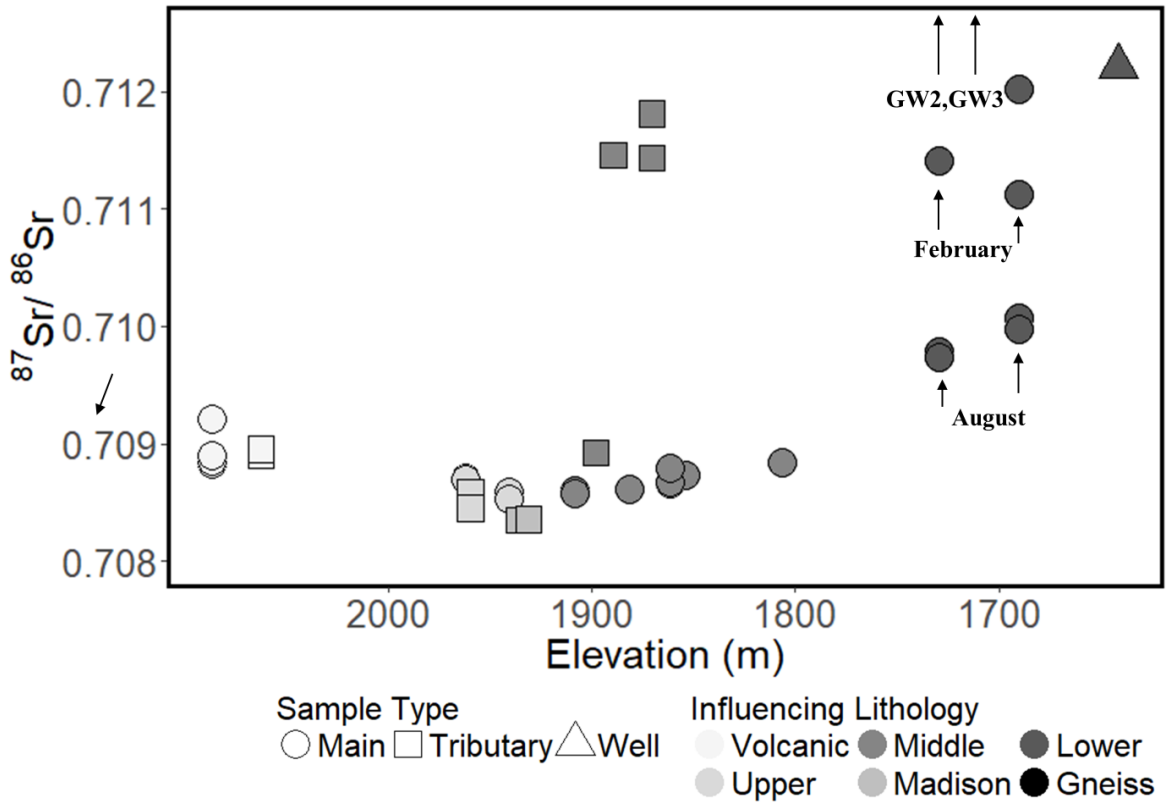

Figure 3.4 $^{87}Sr/^{86}Sr$ ratios in water samples plotted against elevation in Hyalite Canyon. Symbol shapes distinguish samples collected from the mainstem of Hyalite Creek (circles), its tributaries (squares), and nearby wells (triangles). Site locations are shown in Figure 3.1. Greyscale shades indicate hosting rock unit or stream reach. Archean gneiss groundwater samples from Hodgeman Canyon (GW2, GW3) have high values that are off scale here; see Table 3.2.

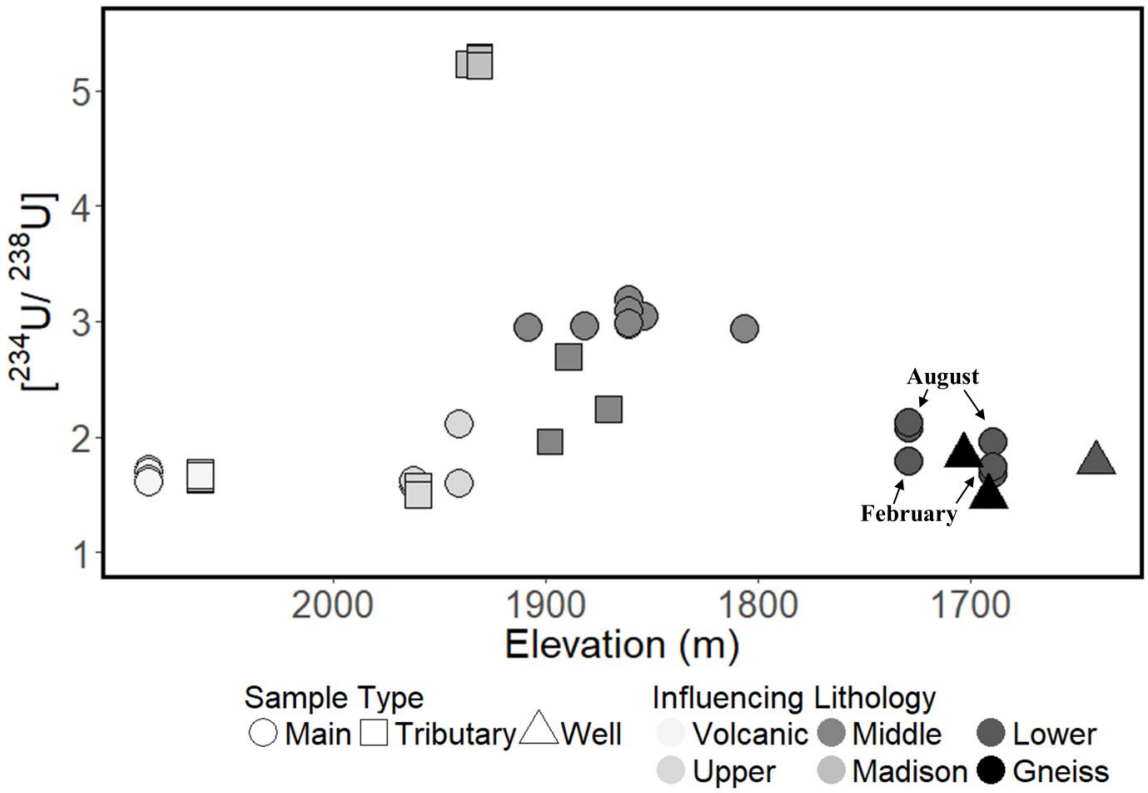

Figure 3.2 [$^{234}U/^{238}U$] values in water samples plotted against elevation in Hyalite Canyon. Symbol shapes distinguish samples collected from the mainstem of Hyalite Creek (circles), its tributaries (squares), and nearby wells (triangles). Site locations are shown in Figure 3.1. Greyscale shades indicate hosting rock unit or stream reach.

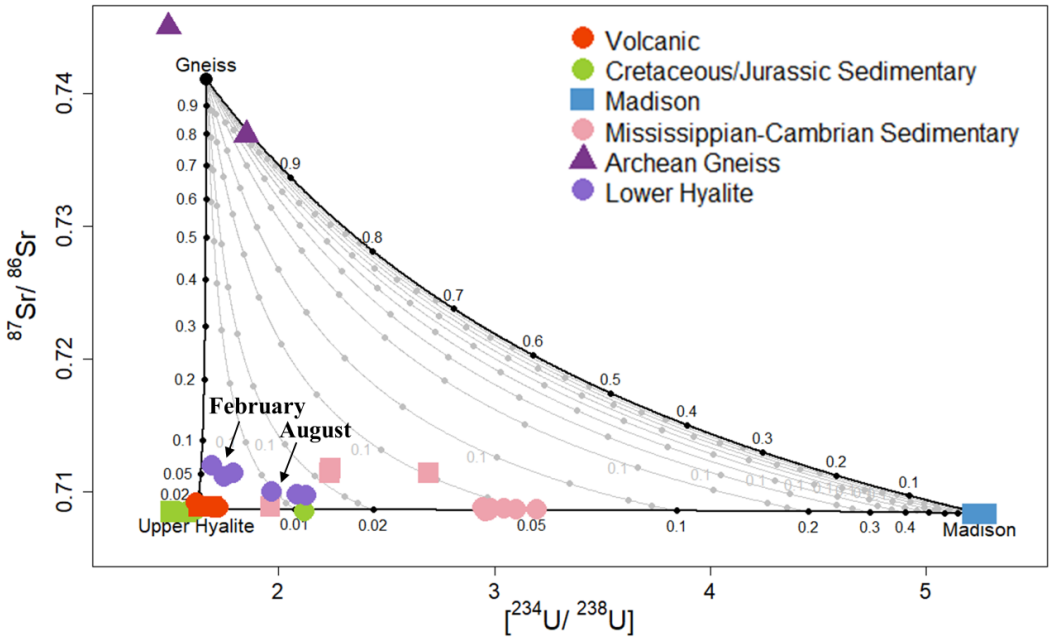

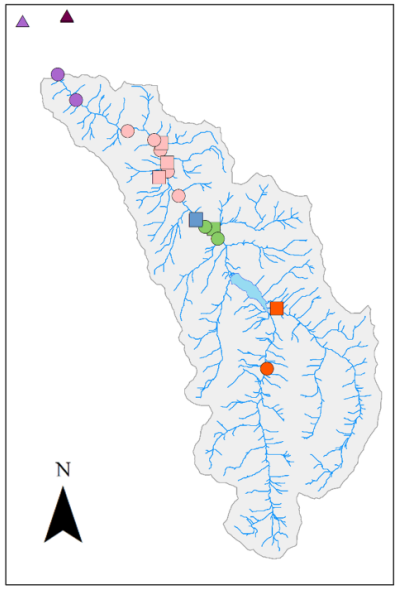

Mixing End-Member Compositions

End member	*Sr (mg L^{-1})*	*$^{87}Sr/^{86}Sr$*	*U (µg L^{-1})*	*$[^{234}U/^{238}U]$*
Upper Hyalite	*0.0304*	*0.708701*	*0.028*	*1.621*
Madison Springs	*0.137*	*0.708343*	*0.393*	*5.252*
Archean Gneiss Groundwater	*0.053*	*0.740866*	*0.359*	*1.669*

Figure 3.6 Three end member mixing model, observed data, and location map of Hyalite Creek. Model defines waters as a mixture of volcanic/sedimentary derived waters in the upper reaches of Hyalite Creek (red and green, HY1, HY2, HY3, HY7, HY9), groundwater inputs from the Madison Group limestones (blue, springs at HY16, HY17) to form middle Hyalite Creek water composition (pink, HY10, HY11, HY12, HY13, HY4, HY14, HY15), that ultimately mixes with fracture flow from the Archean gneiss (dark purple, well samples GW2, GW3) to form the Hyalite Creek mixture at its lower elevations (purple, HY5, HY6). Symbol shapes distinguish samples collected from the mainstem of Hyalite Creek (circles), its tributaries (squares), and nearby wells (triangles). Numbered site locations are shown in Figure 3.1.

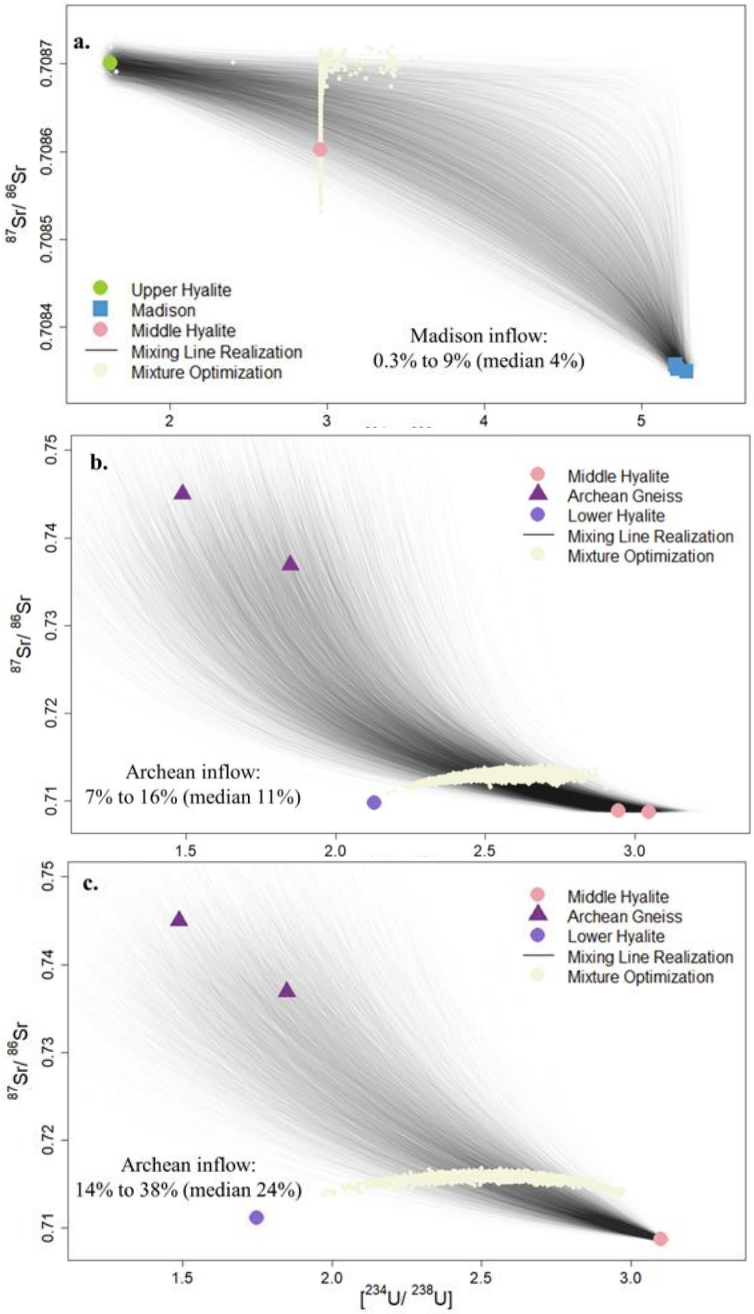

Figure 3.7 Monte Carlo ensembles of two end member mixing models and resulting estimates of fractional groundwater inflows to Hyalite Creek. Inflows are estimated for discreet segments of Hyalite Creek from: (a) the Madison group limestone aquifer at 1920 m elevation in August 2017; (c) the Archean gneiss aquifer in lower Hyalite Canyon in August 2017; and (e) the Archean gneiss aquifer in February 2017. Each semi-transparent black line represents a single realization of a two end member mixing model based on a random sampling from the estimated uncertainty in each of two end members. Overlap of the semi-transparent lines results in darker areas that represent the more probabilistically likely regions of the potential mixing space if the endmembers and uncertainties are accurate. Beige circles represent realizations of each optimized fraction of aquifer contribution corresponding to each mixing line realization. Fractional contributions density plots are summarized in Figure D.1.

CHAPTER FOUR

SR AND U ISOTOPES REVEAL MIXING PATTERNS OF GROUNDWATER AND SURFACE WATER INFLUENCED BY HUMAN MANAGEMENT IN AN INTERMOUNTAIN BASIN (GALLATIN VALLEY, MT)

Contribution of Authors and Co-Authors

Manuscript in Chapter 4

Author: Florence Rita Miller

Contributions: Florence Miller was responsible for sample collection and analysis, Sr and U isotope purification preparation, data analysis, and original composition of manuscript.

Co-Author: Dr. Stephanie A. Ewing

Contributions: Dr. Stephanie A. Ewing was responsible for project conceptualization, securing funding, weathering and tracer expertise, Sr and U purification methodologies and analysis, and original manuscript writing and editing.

Co-Author: Dr. Robert A. Payn

Contributions: Dr. Robert A. Payn was responsible for project conceptualization, securing funding, hydrology expertise, gauge analysis, and manuscript writing and editing.

Co-Author: Sam Leuthold

Contributions: Sam Leuthold contributed to sample collection and analysis, data analysis, water isotope insight outlined in companion paper, and manuscript editing.

Co-Author: Dr. Stephan Custer

Contributions: Dr. Stephan Custer contributed hydrogeologic expertise, knowledge of local geology and hydrology, compilation of local Sr values and manuscript editing.

Co-Author: Tom Michalek

Contributions: Tom Michalek contributed to well sample collection, local hydrologic expertise, coordination of ICP analysis, and manuscript writing and editing.

Co-Author: Dr. James B. Paces

Contributions: Dr. James B. was responsible for project conceptualization, securing funding, U and Sr isotope analysis, and manuscript writing and editing.

Manuscript Information

Florence R. Miller, Stephanie A. Ewing, Robert Payn, Sam Leuthold, Stephan Custer, Tom Michalek, James B. Paces

Journal of Hydrology

Status of Manuscript:
_X_ Prepared for submission to a peer-reviewed journal
____ Officially submitted to a peer-reviewed journal
____ Accepted by a peer-reviewed journal
____ Published in a peer-reviewed journal

Elsevier

4.1 Abstract

A repeated landscape pattern in the inter-mountain west is convergent mountain headwater catchments that supply stream water to divergent flow systems within intermountain basins. The character and flux of water across this process-domain transition is subject to future changes in both mountain headwater precipitation and snowpack dynamics, as well as agricultural and urban land use in rapidly developing intermountain basins. Here we evaluate how interaction between groundwater and surface water transforms water quality across such a transition in the Gallatin River Watershed of southwest Montana, using natural geochemical tracers ($^{87}Sr/^{86}Sr$, Ca/Sr, and $^{234}U/^{238}U$), as well as solute loads. We present data for surface water, groundwater, and soil samples collected between 2016 and 2018, at locations ranging from the Gallatin Range mountain front to the outlet of the Gallatin River Watershed at Logan, Montana. Geochemistry at sampling sites demonstrate variation in Ca/Sr, $^{87}Sr/^{86}Sr$, and $^{234}U/^{238}U$ values resulting from diverse lithologic composition in mountain catchments, as determined by convergent flow discharging at the mountain front. In the intermountain basin surface water, $^{87}Sr/^{86}Sr$ values became similar to those of soil carbonate while [$^{234}U/^{238}U$] reached more intermediate values, suggesting the mixing of surface, soil, and groundwater. Both streamflow and groundwater within the basin tend to have higher concentrations of Sr and alkalinity along with higher Ca/Sr and $^{87}Sr/^{86}Sr$ values that are similar to values in pedogenic carbonates. These patterns are interpreted as evidence that water movement through soils has a strong influence on the solute composition of the water in the valley. Additionally, increased dispersal of water used for agriculture and

domestic use in the Gallatin Valley results in increased infiltration of water through soils and greater amounts of anthropogenic loading of NO_3^- and Cl^- in surface and groundwaters. Our work demonstrates the utility of geochemical tracers for understanding hydrologic and anthropogenic controls on water quality and quantity at the mountain front to intermountain basin transition. Geochemistry across the intermountain basin suggests the influence of valley aquifer recharge, infiltration through soils, and agricultural and municipal redistribution.

4.2 Introduction

Many urban and agricultural areas in the inter-mountain west are characterized by steep, mountain headwater streams generated by groundwater flowing through rapidly weathering substrate and draining into depositional intermountain basins (Figure 4.1a). As a stream passes from a mountain headwater catchment to an intermountain basin, it traverses the mountain front, which marks a distinct hydrologic discontinuity between these two geomorphological process domains (Montgomery 1999). Here we evaluate geochemical indicators to examine the transition in hydrology, weathering processes, and anthropogenic solute loading that occurs in the intermountain basin of the Gallatin Valley near Bozeman, MT.

Mountain headwaters host steep mountain streams that are fundamentally controlled by geologic structures, lithology, and geomorphological landforms (Covino & McGlynn 2007; Capell et al. 2011; Yang et al. 2017; Jasechko 2016; Jasechko & Kirchner 2016). The mountain headwaters process domain is dominated by convergent

flow, that is derived from a combination of snowmelt runoff, flow through hillslope soils, deeper groundwater flow, and stream-subsurface exchange with near-stream (riparian) groundwater. Groundwater in the headwater catchment carries the geochemical signal of weathering derived primarily from infiltration through thin, undeveloped mountain soils followed by flow through fractured rock or karst aquifer systems. Important aspects further influencing that signal may include glacial deposits, disturbances such as wildfires, and human alteration of the physical landscape by logging and other activities. At the mountain front, stream water composition ultimately reflects the cumulative distribution of surface water and groundwater interactions typical of the mountain headwater process domain (Payn et al. 2009; Covino & McGlynn 2007; Jasechko 2016; Jasechko & Kirchner 2016; Capell et al. 2011).

Immediately downstream of the mountain front transition, hydrologic structure of the intermountain basin is characterized by a prevalence of divergent flow paths that recharge aquifers of the intermountain basin (Figure 4.1a). Recharge of the basin aquifer also occurs as deep percolation of soil water resulting fromasufficient infiltration of precipitation to overcome capillary storage and evapotranspirative demand. At lower elevations in the basin, both surface and subsurface hydrologic flow networks transition back to convergence, resulting in springs, wetlands, and groundwater contributions that make up baseflow generation to streams and rivers closer to the watershed outlet (Covino & McGlynn 2007). In the Gallatin Valley, human alteration transforms infiltration recharge by irrigation practices and water distribution through an extensive canal systems. The chemical composition of infiltration recharge is influenced by solute

loading, through agricultural and home lawn amendments, as well as septic systems (Burow et al. 2010; Sigler et al. 2018; Ross et al. 2015). As a result, intermountain basin aquifers reflect the contribution of the mountain headwaters, the interaction of divergent flow with aquifer materials, and the enhanced infiltration resulting from redistribution of water and physical alteration of soils for agricultural and municipal purposes. Additionally, water movement through soils may capture solutes developed during weathering cycles that result in accumulations of clay or carbonate with pedogenesis (Martin & Moore 2008; Dosseto et al. 2014; Liu et al. 2016).

Here we use U and Sr isotope compositions, coupled with solute chemistry, to trace weathering, mixing, and solute loading processes in groundwater, streams, and rivers across the headwater-basin transition from the Gallatin Mountains to the Gallatin Valley in southwest Montana. Elemental concentrations and isotope ratios can provide a measure of source and residence time in hydrologic and weathering studies (Roy et al. 1999; Négrel et al. 2004; Chadwick et al. 2009). In this work we use $^{87}Sr/^{86}Sr$ ratios and [$^{234}U/^{238}U$] activity ratios, in addition to elemental concentrations, to examine the influence of weathering processes, water sources, and interactions between surface water and groundwater flowing downgradient from the mountain headwaters to the intermountain basin (Paces & Wurster 2014; Drexler et al. 2014). The $^{87}Sr/^{86}Sr$ ratio has been used to link soil and rock weathering to stream chemistries (Horton et al. 1999; Jacobson et al. 2003; Jacobson et al. 2002). In rocks and soils, $^{87}Sr/^{86}Sr$ ratios have been used to examine weathering sequences, dust inputs, and carbonate accumulation (Capo et al. 1998; Capo & Chadwick 1999; Hart et al. 2004; White et al. 2009; Chadwick et al.

2009; Bullen et al. 1997). In streams and groundwater, $^{87}Sr/^{86}Sr$ ratios have been used to trace sources of soil and rock weathering inputs to stream geochemistry (Jacobson et al. 2002; Jacobson et al. 2003; Horton et al. 1999; Frost & Toner 2004). Unlike $^{87}Sr/^{86}Sr$ that directly reflects the isotopic composition of Sr inherent in host rocks, [$^{234}U/^{238}U$] compositions depend more on the degree and nature of water-rock interaction based on the effects of recoil during alpha decay (Bourdon et al. 2003; Chabaux et al. 2003; Dosseto et al. 2008; DePaolo et al. 2006).

Using a combination of gauge data, water geochemistry, and soil geochemistry we examine changes in hydrologic processes traversing the mountain headwater to intermountain basin transition. Specifically, solute concentrations and isotopic ratios of surface water, groundwater, and soils explore how watershed transitions from divergent to convergent flow networks are driven by exchanges between surface water and groundwater. Our results provide insight into the influence of major transitions in geomorphological process domains on the flow and chemical loading typical of the Missouri River or other intermountain landscapes.

4.3 Methods

4.3.1 Study Area Description

The Gallatin Valley is predominantly agricultural, but is undergoing rapid urban development, hosting a population of 46,596 in the city of Bozeman and 107,810 in Gallatin County (July 1, 2017 population estimate; United States Census Bureau, 2018). The mean annual temperature for the city of Bozeman is 6°C, ranging from monthly

average low of -11°C in December to monthly average high 28°C in July (30-year normal 1981-2010; U.S. ClimateData 2018) .The mean annual precipitation in Bozeman, MT is 41.22 cm (30 year normal 1981-2010; U.S. ClimateData 2018), although this is known to vary between the drier west side of the valley and the wetter east side flanking the Bridger Mountains. The dominant land use in the Gallatin Valley is irrigated agriculture; however, 204,100 ac of agricultural land has been replaced with housing developments as population has increased from 1982 to 2012 (Kendy 2001; U.S. Department of Agriculture 2015).

Surface geology in the Gallatin Valley is generally classified as Quaternary and older alluvium and eolian deposits overlying Tertiary age deposits (Vuke et al. 2014) (Figure 4.1b). Archean gneiss constituting the geologic basement is exposed at lower elevations along the Gallatin Range mountain front. Gneiss is overlain by sedimentary deposits of Cretaceous to Cambrian age at the middle elevations of the mountain range, with a 'cap' of Eocene age andesitic to basaltic volcanic rocks constituting the upper elevations of the mountain range (Hackett et al. 1960) (Figure 4.1b). These lithologies characterize both the Bridger Range to the north and the Gallatin Range to the south that both contribute to the Gallatin River watershed.

Soil samples from the Gallatin Valley were from profiles developed in alluvially reworked loess over alluvium ((United States Department of Agriculture 1996; Figure 4.1b). Post Farm soils were mapped as the Amsterdam-Quagle silt loam complex formed on stream terraces with a parent material of loess and silty calcareous loess and a drainage class of well drained. The Amsterdam-Quagle complex is classified as Typic

Haplustolls (60%) and Typic Calciustolls (30%), indicating variable degrees of calcium carbonate accumulation. Both Lutz and Ellis Farm soils were mapped as the Blackdog silt loam, classified as Typic Argiustolls and formed on stream terraces with a calcareous loess parent material and a drainage class of well-drained (United States Department of Agriculture 1996). Soils are developed on the surface of landforms mapped as Quaternary (Lutz and Post Farms) and Quaternary-Tertiary (Ellis Farm) alluvial fans (Figure 4.1b). All three sites are managed for agriculture, either for cereal production systems (Lutz and Post Farms) or rangeland (Ellis Farm) hosting temperate grassland species including bluebunch wheatgrass (*Pseudoroegneria spicata*) and Idaho fescue (*Festuca idahoensis*).

4.3.2 Sampling Site Selection

Surface water and groundwater samples were collected from Hyalite Canyon (representing the mountain headwaters) over a period of two years, with detailed results described in Miller et al. (in review). Surface water, groundwater, and soil samples were collected in the Gallatin Valley and Hyalite Canyon (Table 4.1b). A total of 17 surface water sites were sampled in Hyalite Creek and its tributaries (HY1-HY17) to longitudinally capture changes in lithology and topography. Ten surface water sites were sampled in the Gallatin Valley from both the east fork and the main stem of the Gallatin River as well as tributaries (GV1-GV10), to examine how surface water chemical composition changed with tributary convergence and water movement downgradient in the Gallatin Valley. Nine groundwater sites (wells) were sampled ranging from the Gallatin Range mountain front to the lower Gallatin Valley (GW1-GW9). Three soil sites

from three different farms in the Gallatin Valley (Ellis, Lutz, and Post Farms) representative of deep loess deposition on Tertiary and Quaternary surfaces. Surface waters were sampled in February, May, and August of 2016 and 2017. Wells were sampled one to two times between May 2017 and April 2018. Soils were sampled in June of 2017.

4.3.3 Streamflow

Four stream gauges are located in the study area. In Hyalite Creek there is a U.S. Geological Survey (USGS) gauge (number 06050000, Hyalite Creek near Bozeman, MT) located at the mouth of Hyalite Canyon (site HY6 in this study). Two stream gauges are located on the main stem of the Gallatin River in the Gallatin Valley; one USGS gauge (number 06043500, Gallatin River at Gallatin Gateway) located at the mountain front (site GV3) and one USGS gauge (number 06052500, Gallatin River at Logan) located below the convergence with the East Gallatin River (site GV7). An additional USGS gauge (number 06048650, East Gallatin River) is located on the East Gallatin River (site GV6). Discharge data from all gauges were downloaded from the USGS National Water Information System website (Figure 4.2). Daily mean discharges during the period of sampling are provided, and mean daily discharges are compared to assess the average behavior of the watershed over the periods of record for the gauges. Most of the river flow at Logan (GV7) is expected to be composed of flows at Gallatin Gateway (GV3), Hyalite Creek (HY6), and the East Gallatin (GV6), so the sum of daily flows at GV3, HY6, and GV6 was calculated for comparison with the measured flow at GV7 (Figure 4.2).

4.3.4 Sampling Procedures

Surface water samples were collected using a peristaltic pump (Geotech™ Denver, CO, United States) with platinum-cured Silicon tubing. Samples were filtered at the time of sampling using a 0.45 µm, mid-capacity capsule filter (Geotech™ Denver, CO, United States). In situ temperature, pH, specific electrical conductivity (SC), and dissolved oxygen (DO) were measured at each sampling site using a handheld multimeter (YSI 556 Yellow Springs, OH, USA). Alkalinity was measured in the field using colorimetric titration (Hach™ kit; phenolphthalein/bromethymol blue and H_2SO_4). When conditions allowed, discharge was measured using the area-velocity method, where water velocities were measured using an electromagnetic flow meter (Marsh McBirney / Hach™ Loveland, CO, United States). Comparison of continuous gauge data with measured discharge suggests uncertainty of about 10% between the gauging methods. Wells were sampled by purging three well volumes prior to water collection employing the same procedures of water filtration, sample collection, alkalinity, and multimeter measurement used to collect surface water samples. Soil samples were taken with a Giddings soil-coring machine with a 2.1-inch coring tube, from a depth of 0-120 cm, and separated into 15 cm depth intervals for processing and analysis.

4.3.5 Water Geochemical Analysis

Chemical and isotopic analyses were conducted at Montana State University (MSU) in Bozeman, MT, the Montana Bureau of Mines and Geology (MBMG) in Butte, MT, and the USGS Southwest Isotope Research Laboratory (SWIRL) at the Denver Federal Center in Denver, CO. Major anions were analyzed by ion chromatography

(Dionex™) at the MSU Environmental Analytical Laboratory. Major cations and trace metal concentrations were analyzed by Inductively Coupled Plasma - Optical Emission Spectroscopy (ICP-OES; Perkin Elmer™ Waltham, MA, United States) at MBMG and the MSU Environmental Analysis Laboratory, and by inductively coupled plasma mass spectrometry (ICP-MS) at MBMG. Radiogenic isotope ratios $^{87}Sr/^{86}Sr$ and [$^{234}U/^{238}U$] (where square brackets denote activity ratios), as well as U concentrations by isotope dilution with ^{236}U, were measured by thermal ionization mass spectrometry (TIMS) at SWIRL.

4.3.6 Soil Acetic Acid Extractions

Soil samples were dried at 50° degrees C until they displayed no mass change with time, sieved to less than 2 mm using a barrel sieve, and milled overnight on a roller mill at MSU. Soils were analyzed for total carbon percentage (%TC) at the MSU Environmental Analytical Laboratory by combustion (Costech ESC 4010 CHNSO Analyzer). Sr isotopic composition of pedogenic carbonate in the soils was analyzed by acetic acid extraction. Two replicates of 1g of soil from each depth increment of 45–60, 60–75, 75–90, and 90–105 cm were processed separately to extract labile fractions using two sequentially applied aliquots of 20 mL of 1N optima grade acetic acid. The soil-acid aliquots were mixed in 50 centrifuge tubes on a hotdog roller for 20 minutes. Tubes were centrifuged for 10 minutes at 10,000 rpm, the supernatant extract was transferred to a separate tube, and a second aliquot of 20 mL 1N optima acetic acid was added to the soil pellet and rolled for 20 minutes. The second extract was added to the original extract

yielding a total of 40 mL for each soil depth increment extract. Extracts were then dried down and resuspended in 7N trace metal grade HNO_3 for Sr isotopic analysis.

4.3.7 Geochemical Tracers: U and Sr Isotope Analysis

U and Sr isotopic analysis followed procedures described in Ewing et al. (2015) and Paces & Wurster (2014). Water samples, field blanks, procedural blanks, and standards of known composition were prepared for U and Sr isotopic analysis at the MSU Soil Biogeochemistry laboratory. The amount of sample processed was based on U concentrations, which were much lower than Sr concentrations (Table 3.2). Sample volumes containing ~100 ng U and 0.01 – 0.13 mg Sr were weighed in 500-mL Teflon vials, acidified with 1-2 mL of trace metal grade (TMG) concentrated HNO_3, and spiked with known amounts of highly purified ^{236}U-spike solution to allow determination of U concentration by isotope dilution. Field and procedural blanks were spiked with known amounts of both ^{236}U and ^{84}Sr. Water was completely evaporated from processed samples on a hotplate in an exhausting HEPA-filtered clean hood. The residual solids were dissolved with approximately 5-10 mL of TMG ~7N HNO_3, transferred to 15 mL Teflon vials, and were again evaporated. If dissolved organic carbon (DOC) concentrations were >10 ppm, re-dissolved samples were transferred to pre-cleaned quartz crucibles, evaporated to dryness, and heated to 550°C in a muffle furnace for one hour to remove organic compounds. Combusted residues were dissolved in 10-15 mL of ~7N TMG HNO_3, transferred to 15 mL Teflon vials and evaporated. Residual solids from evaporated samples were re-dissolved in 0.6 mL of ~7N Optima™-grade HNO_3, transferred to acid-washed 2 mL centrifuge tubes, and centrifuged for 10 minutes at

10,000 rpm. Any solids were returned to the original Teflon vials and refluxed with concentrated, ultrapure HF and HNO_3, were again evaporated, dissolved in 0.6 mL of ~7N Optima™ HNO_3, and combined with the previously dissolved portion. Final solutions thus represent fully dissolved samples. Sr and U salts were separated and purified by standard ion exchange chemistry using AG1-X8 resin for the U fraction and Sr-Spec™ resin for the Sr fraction.

Purified U aliquots were loaded onto the evaporation side of a double rhenium filament assembly and analyzed by TIMS using the USGS SWIRL ThermoFinnigan Triton™ equipped with a single secondary electron multiplier and a retarding potential quadrapole (RPQ) electrostatic filter. Intensities of ^{234}U, ^{235}U, and ^{236}U were measured sequentially in multi-dynamic peak-jumping mode. To correct for instrument bias and drift, the $^{234}U/^{235}U$ values measured for unknowns were normalized by the same factor needed to adjust $^{234}U/^{235}U$ values measured for a NIST U-isotope standard (SRM 4231B) run in the same magazine to the accepted value of 0.007294 (±0.000028). One hundred fourteen analyses of SRM 4321B yielded an average $^{234}U/^{235}U$ value of 0.007303 (0.007292 to 0.007314, 95% confidence interval), which is within error overlap of the NIST certified value. Measured $^{234}U/^{235}U$ atomic ratios were converted to $[^{234}U/^{238}U]$ using decay constants published by Cheng et al. (2013) ($\lambda_{234} = 2.82206 \times 10^{-6}$ yr^{-1}) and Jaffey et al. (1971) ($\lambda_{238} = 1.55125 \times 10^{-10}$ yr^{-1}), assuming that all U has an atomic $^{238}U/^{235}U$ composition of 137.88 (Steiger & Jager 1977). Analytical errors for measured $[^{234}U/^{238}U]$ are given at the 95% confidence level (i.e. twice the standard deviation) and include contributions from within-run counting statistics plus uncertainties propagated from blank, spike, and mass

fractionation corrections, as well as external error derived from multiple analyses of the U isotope standard. Replicate analyses of a secondary standard consisting of 69.3-Ma uranium ore from the Schwartzwalder mine expected to be in radioactive secular equilibrium (i.e., $[^{234}U/^{238}U] = 1.000$; Ludwig et al. 1985) yielded an average $[^{234}U/^{238}U]$ value of 0.9997±0.0032 (2×standard deviation for 65 analyses). Total process blanks for U were typically 0.01–0.1 ng compared to total U abundances of 5–600 ng (median 85 ng). An in-house water "standard" developed by the USGS Branch of Quality Systems (SRS T-221) was processed multiple times at both MSU and SWIRL to evaluate interlaboratory biases. Results for $[^{234}U/^{238}U]$ are identical within reported analytical uncertainty; however, U concentrations for aliquots processed at MSU are more scattered (±7.7%, 2×SD, N=4) with an average of 1.40±0.11 µg L^{-1}, which is lower than the published most-probable-value of 1.49±0.08.

Purified Sr aliquots were loaded onto single rhenium filaments atop an initial load of tantalum oxide used as an activator and analyzed at the USGS SWIRL by multicollector TIMS using either a ThermoFinnigan Triton™ or an Isotopx Phoenix™. Isotope measurements were made on 5 to 10 volt ^{88}Sr signals using multi-dynamic, triple-jump analytical routines where instrumental mass fractionation was corrected using $^{86}Sr/^{88}Sr$ measured during the same run assuming a value of 0.1194. Replicate analyses of the National Institute of Standards and Technology Sr-isotope standard, SRM 987 (accepted $^{87}Sr/^{86}Sr$ value of 0.710248; McArthur et al. 2001) used as a primary standard to normalized instrument bias and drift, yielded mean values of 0.710250 ±0.000007 (±2×SD, N=314) using the Triton™ and 0.710242±0.000012 (±2×SD, N=15) using the

Phoenix™. Measured $^{87}Sr/^{86}Sr$ values for unknown samples were adjusted by the same amount needed to obtain the accepted value for NIST 987 analyzed during the same session. Replicate $^{87}Sr/^{86}Sr$ analyses of the modern-marine carbonate standard, EN-1 (accepted value of 0.7091741±0.0000024, McArthur et al. 2006), gave mean values of 0.709174±0.000008 (±2×SD; N=174), and 0.709176±0.000005 (±2×SD, N=5) on respective instruments. Total process blanks for Sr were typically <0.001 µg compared to total Sr abundances of 20–140 µg (median 40 µg). Analytical errors for $^{87}Sr/^{86}Sr$ values are given at 95% confidence levels (~2σ) and include within-run uncertainties and external error based on replicate analyses of standards. Results for $^{87}Sr/^{86}Sr$ measured in SRS T-221 processed at MSU and SWIRL are identical within reported analytical uncertainty.

4.4 Results

4.4.1 River Gauge Discharge

Discharge from the four gauges in the Gallatin Valley depict a snowmelt dominated system, with lower flow conditions generally occurring during late summer through late winter (Figure 4.2). The mean daily hydrograph peaks in June for the Gallatin River (sites GV3, gauge elevation: 1,575 m, drainage area: 2,121 km^2 and GV7, gauge elevation: 1,246 m, drainage area: 4,633 km^2) and Hyalite Creek (site HY6, gauge elevation: 1,688 m, drainage area: 126 km^2) which drain higher elevation watersheds of the Gallatin and Madison mountain ranges. The mean daily hydrograph peaks in May for the East Gallatin River (GV6), which drains the lower elevation region of the watershed including the Bridger mountain range (gauge elevation: 1,409 m, drainage area: 585 km^2)

(U.S. Geological Survey, 2018). Irrigation canals are opened in late June resulting in a notable extraction divergence between the GV3 and GV7 hydrographs from late June to late August, during which the Gallatin River discharge at the watershed outlet (GV7) is lower than the Gallatin River discharge at the mountain front (GV3). We approximate this difference in discharge associated with extraction in terms of a water balance defining the net loss of water from this reach of the Gallatin River, where:

Water loss = (consumptive irrigation use + groundwater recharge from ditch leakage) + groundwater recharge from streams - streamflow generation from local groundwater discharge – East Gallatin River contributions

The gross loss of water from the Gallatin River between GV3 and GV7 can be quantified by the sum of consumptive irrigation use, recharge of groundwater from leaking irrigation ditches, and recharge of groundwater from streams. The gross gain of water to the Gallatin River between GV3 and GV7 can be quantified by the sum of local streamflow generation by groundwater discharge from the valley aquifer and the contribution of surface flow from the East Gallatin River. The aggregate volume of net water loss (sum of gross gains and losses) represents consumptive water use in the valley, and timing of the recovery from this net loss in the autumn may be influenced by delayed movement of water through the valley aquifer (Figure 4.2).

4.4.2 Alkalinity, Strontium, Ca/Sr, and $^{87}Sr/^{86}Sr$

Alkalinity tended to increase with decreasing elevation from Hyalite Creek through the Gallatin Valley (Table 4.2, Figure 4.3). In the mountain headwaters of Hyalite Creek (HY1, HY2) alkalinity ranged from 15 to 38 mg $CaCO_3$ L^{-1}. Some

sedimentary derived tributaries in the mountain headwaters of Hyalite Creek had high alkalinity (123 to 235 mg $CaCO_3$ L^{-1}), as reflected by a gradual increase in alkalinity of the main stem of Hyalite Creek (HY6) to a range of 52 to 61 mg $CaCO_3$ L^{-1}. In the Gallatin Valley, alkalinity increased with decreasing elevation from a range of 49 to 131 mg $CaCO_3$ L^{-1} at the mountain front (GV1-GV3) to a range of 143 to 214 mg $CaCO_3^{-1}$ at GV7. Alkalinity was highest (432 mg $CaCO_3$ L^{-1}) in groundwater samples from a shallow (static water level 17 m) valley well (GW5). Seasonally, alkalinity was highest during August sampling campaigns and lowest during the May sampling campaign.

Like alkalinity, Sr concentrations tended to increase with decreasing elevation from Hyalite Creek through the Gallatin Valley (Table 4.2, Figure 4.4). Concentrations of Sr ranged from 0.02 to 0.03 mg L^{-1} in the mountain headwaters of Hyalite Creek (HY1, HY2), with some sedimentary derived tributaries in Hyalite Canyon delivering higher concentrations of Sr, up to 0.16 mg L^{-1}; accordingly below these inflows we observed a gradual increase in Sr concentration of the main stem of Hyalite Creek (HY6) to a maximum ranging from 0.04 to 0.05 mg L^{-1}. In the Gallatin Valley, Sr concentration increased from a range of 0.04 to 0.07 mg L^{-1} at the mountain front (GV1-GV3) and further increased moving through the Gallatin Valley to a range of 0.07 to 0.21 mg L^{-1} at GV7. In the Hyalite Canyon surface waters, Sr concentrations were lowest in May runoff samples, except for sites influenced by Archean gneiss aquifers (HY5, HY6) ,which had the highest Sr concentrations in May runoff samples. In Gallatin Valley surface waters and wells, all Sr concentrations were lowest in May and highest during August and

February, suggesting baseflow conditions synchronous with the mountain headwaters domain (Miller et al., in review).

Values of Ca/Sr varied with diverse lithology, particularly near the mountain front (Table 4.2, Figure 4.5). Hyalite Creek (HY1-HY17) had variable Ca/Sr ratios ranging from 172 to 504, Cottonwood Creek (GV2) had high Ca/Sr ratios ranging from 445 to 552, and the mountain headwaters of the Gallatin River (GV3) had a lower range of Ca/Sr ratios, 139 to 182. As water moves through the Gallatin Valley, mountain front water sources mix, resulting in Ca/Sr ratios that range from 155 to 245 at the downstream end of the valley (GV7). Ca/Sr ratio showed some seasonal variation, but did not exhibit systematic seasonal trends.

Similar to the Ca/Sr ratio, the $^{87}Sr/^{86}Sr$ ratio varies with lithology, but with clearer distinction among rock units (Table 4.2, Figure 4.6). The mountain headwater stream Hyalite Creek (HY1 – HY17) has varying $^{87}Sr/^{86}Sr$ values with lithology (0.70835 – 0.71202). At the mountain front, wells completed in Archean gneiss at the mountain front (GW2, GW3, GW6, GW7) have the highest $^{87}Sr/^{86}Sr$ isotope ratios ranging from 0.73686 to 0.74497. Contributions from these groundwaters increase $^{87}Sr/^{86}Sr$ ratios in stream water, which increase from 0.70883 to 0.70921 at the highest elevations in Hyalite Creek (HY1, HY2) to 0.71057 to 0.71245 in Hyalite Creek at the mountain front (GV1) (Miller et al., in review). Other streams at the mountain front have varying $^{87}Sr/^{86}Sr$ values, with $^{87}Sr/^{86}Sr$ values in Cottonwood Creek (GV2) ranging from 0.71339 to 0.71568 and the $^{87}Sr/^{86}Sr$ values in the Gallatin River near the mountain front (GV3) ranging from to 0.71077 to 0.71098. The $^{87}Sr/^{86}Sr$ ratios approached values consistent with local soil

carbonate $^{87}Sr/^{86}Sr$ values moving down valley, ranging from 0.71120 to 0.71182 at the lowest elevation site (GV7).

Acetic acid extracts from the three loess-derived soils in the Gallatin Valley also had intermediate $^{87}Sr/^{86}Sr$ ratios, ranging from 0.70981 to 0.71160 (Table 4.3, Figure 4.7). The Ellis Farm soil, formed on an older Quaternary-Tertiary alluvial fan surface, had higher total carbon content (sum of 279,000 kg C ha^{-1} over 14 to 105 cm depth interval) than Lutz or Post Farm soils (sums of 205,000 and 200,000 kg C ha^{-1} respectively over same depth interval), assumed to be primarily carbonate-C at these depths. The older Ellis Farm soil had $^{87}Sr/^{86}Sr$ values ranging from 0.70981 to 0.71010 and had a total carbon weighted average $^{87}Sr/^{86}Sr$ ratio of 0.71002 over a depth interval of 45 to 105 cm. The Post and Lutz Farm soils, formed on the younger Quaternary alluvial fan surfaces, had higher $^{87}Sr/^{86}Sr$ values than Ellis Farm (0.71119 to 0.71149 at Lutz Farm and 0.71095 to 0.71160 at Post Farm), and had higher total carbon weighted $^{87}Sr/^{86}Sr$ averages of 0.71128 and 0.71122, respectively, over the same depth interval.

4.4.2 Uranium and [$^{234}U/^{238}U$]

U concentrations tended to increase with a decrease in elevation from the mountain headwaters to the intermountain basin process domain. U concentrations increased from a range of 0.01 to 0.02 µg L^{-1} at the highest elevations in Hyalite Creek (HY1, HY2) to a range of 0.19 to 1.09 µg L^{-1} at the mountain front (GV1-GV3), and further increased to a range of 0.86 to 2.34 µg L^{-1} with decrease in elevation through the Gallatin Valley (GV7) (Table 4.2, Figure 4.8). Seasonally, U concentrations were highest

in February low flow conditions and lowest in May runoff conditions across the mountain headwaters and intermountain basin.

Values of [$^{234}U/^{238}U$] for surface waters varied with the degree of groundwater influence, with greatest variation of [$^{234}U/^{238}U$] values occurring within the mountain headwaters reach of Hyalite Creek, where main stem sites ranged from 1.50 to 3.20 (Table 4.2, Figure 4.9). Streams exiting the mountain front (GV1-GV3) had [$^{234}U/^{238}U$] values ranging from 1.61 to 2.54. Wells in the Gallatin Valley (GW1-GW9) exhibited a somewhat broader range of [$^{234}U/^{238}U$] values than Gallatin Valley surface waters, ranging from 1.28 to 2.73. Lower [$^{234}U/^{238}U$] values ranging from 1.84 to 1.93 were observed at the most down-valley site, GV7. Overall, [$^{234}U/^{238}U$] values were lower during May runoff conditions than during February and August.

4.4.3 Nitrate and Chloride

Concentrations of nitrate and chloride ions tended to increase with decrease in elevation from the mountain front through the intermountain basin (Table 4.2, Figures 4.10-4.12). Concentrations of NO_3^- generally increased from a concentrations up to 0.07 mg NO_3^--N L^{-1} in Hyalite Canyon, to concentrations up to 0.14 mg NO_3^--N L^{-1} at the mountain front (GV1-GV3), to concentrations ranging from 0.15 to 0.65 mg NO_3^--N L^{-1} at the lowest elevation sampled in the Gallatin Valley (GV7). Concentrations of Cl^- followed similar trends, from a range of 0.07 to 0.20 mg L^{-1} at the highest elevations in Hyalite Creek (HY1 and HY2), to a range of 0.15 to 2.05 mg L^{-1} at the mountain front (GV1-GV3), and a range of 2.43 to 7.89 mg L^{-1} at the lowest elevation site in the Gallatin Valley (GV7). High NO_3^- (8.20 mg NO_3^--N L^{-1}) and Cl^- (46.37 mg L^{-1}) concentrations

were found in a shallow mid-valley well (GW5) (Figures 4.10 and 4.11). Seasonally, across all process domains, concentrations of NO_3^- varied inconsistently between May runoff and February and August low flow conditions. At the highest elevations of Hyalite Creek (HY1, HY2), NO_3^- concentrations were higher in February (range of 0.02 -0.05 mg NO_3^--N L^{-1}) than in August low flow conditions (all values below instrument detection limit) (Figure 4.10). At lower elevations in Hyalite Creek (HY7-HY6) NO_3^- concentrations were higher in August (range of 0.01 to 0.07 mg NO_3^--N L^{-1}) than in February low flow conditions (range of 0.01 to 0.04 mg NO_3^--N L^{-1}). In the Gallatin Valley intermountain basin rivers (GV7), NO_3^- concentrations were higher in February (range of 0.57 to 0.65 mg NO_3^--N L^{-1}) than in August low flow conditions (range of 0.27 to 0.30 mg NO_3^--N L^{-1}). In the mountain headwaters of Hyalite Creek Cl^- concentrations were highest in May and lowest in August (0.07 to 0.31 mg L^{-1}). In the Gallatin Valley, higher concentrations of Cl^- were observed during August and February low flow conditions than in May runoff conditions with higher Cl^- concentrations observed in August as compared to February low flow conditions (range of 0.15 to 14.12 mg L^{-1}) (Figure 4.11). Across locations and seasons in the Gallatin Valley, concentrations of NO_3^- and Cl^- increased together (R^2 = 0.8031, Figure 4.12).

4.5 Discussion

4.5.1 Mixing of Surface Waters, Groundwater, and Soil Water

In the mountain headwaters and at the mountain front, both $^{87}Sr/^{86}Sr$ and Ca/Sr ratios in streamflow varied with lithologic source while [$^{234}U/^{238}U$] ratios varied with extent of water/rock interaction (Miller et al. in review). With decrease in elevation from

the mountain front in the Gallatin Valley, surface water values became less variable among sites at similar elevations, suggesting consistent mixing of sources. Variation in $^{87}Sr/^{86}Sr$ values for surface water and groundwater at the mountain front reflect variable lithologic sources and water-rock interaction upgradient (e.g., fracture flow through older rocks supplying $^{87}Sr/^{86}Sr$ of 0.73687 – 0.74497); however $^{87}Sr/^{86}Sr$ values showed less variation among sites not in the immediate vicinity of the mountain front, suggesting water mixing and water flow through soils and aquifer material with intermediate $^{87}Sr/^{86}Sr$ values. Values for $^{87}Sr/^{86}Sr$ appear relatively uniform in water samples from both the Gallatin and East Gallatin River and nearby wells, before the East Gallatin and Gallatin converge, indicating strong groundwater surface water exchange (Figure 4.6). The overall rise in surface water $^{87}Sr/^{86}Sr$ at the mountain front (Figure 4.6a) suggests the influence of Archean gneiss fracture flow, which is characterized by high $^{87}Sr/^{86}Sr$. The overall rise in surface water $^{87}Sr/^{86}Sr$ moving downgradient in the Gallatin valley suggests the influence of water flow through calcareous loess derived soils, characterized by $^{87}Sr/^{86}Sr$ values similar to those found in Gallatin Valley soil and groundwater samples.

Ca/Sr ratio also spoke to variable lithologic source, mostly with respect to water interaction with carbonate rocks and secondary carbonate in soils. In the mountain headwaters, streams water interaction with a variety of lithologic sources including volcanics, carbonates, and gneisses, resulted in a wide range of Ca/Sr ratios (172 to 504). At the mountain front, Ca/Sr ratios ranged from 139 to 528, reflecting the diverse lithologies with which water interacted among differing mountain headwaters.

Groundwaters also had a large range of Ca/Sr ratios (193 to 467), with higher values at sites GW2 and GW3 (321, 467) possibly indicating interaction with secondary carbonate in gneiss (White et al. 2005). Higher values at sites GW1, GW4, GW5 (383, 399, 447) were possibly due to water interaction with secondary carbonates from soils (White et al. 1996). The wide range of Ca/Sr ratios at the mountain front narrowed to a range of 155 to 245 near the outlet of the Gallatin River Watershed (GV7), suggesting that stream flow generation at the lower elevations was coming from a mixed reservoir of waters with variable contact with carbonates.

Observed [$^{234}U/^{238}U$] ratios were most variable in Hyalite Canyon (1.50 to 5.29) due to the influence and mixing of event flow and older groundwater contributions (Miller et al. in review). Mountain front surface and groundwaters had less variable [$^{234}U/^{238}U$] values (1.28 to 2.54). In the intermountain basin these values converged to lower, more uniform values of 1.84 – 1.93 at the Gallatin River at Logan (GV7) (Figure 4.9). Variation in [$^{234}U/^{238}U$] values in streams at the mountain front suggest the variable influence of surface water, shallow soil water and groundwater interaction on the composition of mountain streams. The mountain front wells (GW2-GW4, GW6, GW7) had low [$^{234}U/^{238}U$] values (1.30 to 1.85), suggesting a mixture of low values in snowmelt and runoff water moving rapidly through fracture flow at the mountain front. Moving down valley, wells showed [$^{234}U/^{238}U$] values consistent with a range of groundwater, soil water, and runoff mixtures (1.35 to 2.73), converging on low values suggestive of limited influence by deep groundwater and thus potentially indicating water movement

through soils as well as relatively rapid movement of aquifer water through the valley alluvium.

4.5.2 Weathering of Primary and Secondary Carbonates in Soils

Changes in soil $^{87}Sr/^{86}Sr$ composition, coupled with increasing total carbon content, can indicate greater carbonate accumulation and therefore longer weathering duration (Jacobson et al. 2002). The Ellis Farm soil, formed on an older Quaternary-Tertiary fan surface, had higher total carbon content (279,000 kg ha^{-1}) than Lutz or Post Farm soils (205,000 and 200,000 kg ha^{-1} respectively) that formed on younger Quaternary fan surfaces. In addition, the older Ellis Farm soil (formed on Quaternary-Tertiary fan surface with calcareous loess parent material) had lower $^{87}Sr/^{86}Sr$ (0.70981 - 0.71010), resulting in lower carbonate weighted $^{87}Sr/^{86}Sr$ averages (0.71002) (Figure 4.8). The greater accumulation of pedogenic carbonate on these older surfaces could result in a greater contribution of carbonate components from older soils to water in valley aquifers, but higher groundwater $^{87}Sr/^{86}Sr$ values with decreasing elevation (0.711435 to 0.721694 at valley wells GW1, GW5, GW8, GW9) seem to contradict this expectation. On the Post and Lutz Farm soils, developed on younger Quaternary fan surfaces derived from calcareous loess, $^{87}Sr/^{86}Sr$ ratios are higher (0.71095 – 0.71160) and more consistent with groundwater values, and carbonate accumulation is lower (200,000 and 205,000 kg C ha^{-1}), with a higher weighted $^{87}Sr/^{86}Sr$ averages (0.71122 and 0.71128). This could indicate that the weathering of reworked silts favored more radiogenic components on younger fan surfaces, with lower carbonate accumulation possibly resulting in better communication with the aquifer through recharge.

4.5.3 Infiltration through Soils

Mountain front recharge delivers surface and groundwater inputs with compositions that reflect water-rock interactions in the mountain headwaters (Miller et al., in review). Moving downgradient in the intermountain basin, solute loads are modified, imprinting the weathering signal of water-rock interactions, water infiltration through soils, and lateral flow through aquifer substrates as indicated by increased concentrations of Sr and alkalinity, and evolution of Ca/Sr and $^{87}Sr/^{86}Sr$ ratios moving down valley (Maher, DePaolo, et al. 2006; Frost & Toner 2004). Further increases in alkalinity and Sr concentrations in both surface and groundwater as it moves downgradient through the Gallatin Valley could reflect leaching of secondary carbonates from soils and/or dissolution of calcareous aquifer materials (Maher, DePaolo, et al. 2006; Négrel et al. 2004; Bullen et al. 1997). Leaky irrigation canals that disperse river water across Gallatin Valley farms may enhance leaching of soil carbonate. Surface and groundwaters from headwater and mountain front sites exhibit a larger range of $^{87}Sr/^{86}Sr$ values (0.70835 to 0.74497) compared to the more limited range of intermediate $^{87}Sr/^{86}Sr$ values (0.71120 to 0.71183) in water at the lower end of the Gallatin Valley. Comparable compositions of $^{87}Sr/^{86}Sr$ in water samples from various sites in the valley likely corresponds to the widespread presence soils with intermediate $^{87}Sr/^{86}Sr$ values (0.70981 to 0.71160). The evolution of Sr isotopes from mountain-front input across the valley is interpreted as evidence for infiltration through calcareous soils that contributes to the geochemistry and water balance of the valley aquifer and rivers. This interpretation is consistent with the strikingly low [$^{234}U/^{238}U$] values in the lower valley waters (Figure 4.9).

Contributions of soil components through substrate weathering are enhanced by leaky irrigation canals facilitating increased infiltration through soils in the intermountain basin. Infiltration through soils delivers a characteristic biogeochemical signal of soil carbonate weathering. The more intermediate Ca/Sr and $^{87}Sr/^{86}Sr$ also may be strongly influenced by physical modification of soils associated with agricultural or urban development that allow increased effective infiltration. The net losses apparent along the Gallatin River (Figure 4.2) indicate a substantial combination of consumptive irrigation use, recharge of the aquifer through flood irrigation or leaky ditches, and recharge of the aquifer through the river bed. The effect of recharge from irrigation infrastructure on the chemistry of the valley aquifer enhances the biogeochemical signal of soil carbonate on surface and groundwater, and provides a pathway for introducing anthropogenic and agricultural contaminants.

4.5.4 Anthropogenic Influence

Concentrations of $NO3^-$ and Cl^- measured in Gallatin Valley samples speak the coupling of human and natural systems in the intermountain basins. Anions can readily identify agricultural and anthropogenic sources of contamination, and can offer insight into how biologic, agricultural, and anthropogenic controls influenced fluctuations in concentrations (Sigler et al. 2018). Overall, anion concentrations increase as surface water and groundwater move downgradient in the Gallatin Valley reflecting additions of water soluble components from altered water flow, application of fertilizers, leakage of canal water from unlined ditches, leaching of septic fields, and other human inputs that influence the hydrologic system in the intermountain basin (Sigler et al. 2018; Scanlon et

al. 2005; Böhlke et al. 2007; Kelley et al. 2017; Williams et al. 2015; Bohlke & Denver 1995). The positive correlation of NO_3^- and Cl^- concentrations is particularly diagnostic of source from septic systems (Burow et al. 2010). This is further supported by higher NO_3^- and Cl^- concentrations observed in groundwater pumped from shallow valley wells (grey triangles in Figure 4.12). The steady increase in anion concentration moving downgradient in the Gallatin Valley suggests water picking up increasing anthropogenic contamination as it infiltrates through soils and returns to stream water and groundwater.

4.5.5 Seasonality: Runoff Dilution and Influence of Irrigation

Concentrations of dissolved constituents (Alkalinity, Sr, U, NO_3^-, and Cl^-) show seasonal trends with higher values during baseflow conditions (February and August) and lower values during runoff conditions (May) (Figures 4.3, 4.4, 4.8, 4.10, 4.11). Thus, the dissolved ion load present in water at any time reflects a balance between baseflow generation and surface flow dilution. This balance also is apparent in the lower [$^{234}U/^{238}U$] values in mountain front surface and groundwater samples collected in May, which are interpreted to represent mixing of stored groundwater that had preferentially incorporated recoil ^{234}U, with runoff water or infiltration, that has not developed higher [$^{234}U/^{238}U$] values (Böhlke et al. 2007). Further down valley, we observed less seasonal variation in [$^{234}U/^{238}U$], indicating more effective mixing and ultimately averaging of constituent water from multiple sources, consistent with our conceptual model (Figure 4.1a).

In the headwaters of Hyalite Creek, seasonally variable NO_3^- concentrations likely reflect a combination of several processes including (1) N processing in soils and

connection to streams during late winter that results in increased stream NO_3^-; (2) plant uptake during mid-summer that results in decreased stream NO_3; and (3) anthropogenic contamination of lower canyon waters during low flow conditions in August resulting in increased stream NO_3 in areas of high recreational use (Leuthold et al. in review). Agriculture influences such as crop rotation and irrigation likely also impart seasonal control of anion concentrations in the Gallatin Valley. Crop uptake of NO_3^- during the growing season may result in higher NO_3^- concentrations in February samples as compared to August (Sigler et al. 2018), due to influence of soil solutes on shallow, more rapidly moving water in the valley aquifer. Concentrations of alkalinity, Sr, and Cl^- are highest during August, suggesting that limited plant uptake, summer irrigation, leaky canals, and agricultural and municipal irrigation practices contribute to effectively moving more water through the soil. These sources have the potential to pick up stronger signals from weathering of secondary carbonate as well as incorporating anthropogenic influences from both septic and agricultural fields.

4.6 Conclusions

A better understanding of the coupling between mountain front water recharge and supply to surface water and groundwater systems in intermountain basins is important for better predicting water quality and availability in areas of the western US experiencing shifts towards increasing aridity and urban development. Work presented in this study builds on results obtained for a longitudinal examination of streamflow generation in a mountain headwater system that showed Ca/Sr, $^{87}Sr/^{86}Sr$, and [$^{234}U/^{238}U$] data could be used to identify distinct influxes across a lithologically diverse terrain. As

discharge of this mountain front water enters the intermountain basin, geochemical trends across the valley suggest three key processes affecting water evolution. First, moderation of Ca/Sr, $^{87}Sr/^{86}Sr$, and [$^{234}U/^{238}U$] to more intermediate values indicate a gradual homogenization of water as it moves down gradient in the Gallatin Valley. Second, higher concentrations of Sr, U, and alkalinity, higher Ca/Sr ratios, and evolution of $^{87}Sr/^{86}Sr$ in water that are consistent with values determined in local soil carbonates suggest that infiltration through valley soils and mobilization of secondary carbonate components has a marked effect on the geochemical composition of the water. Finally, the increased water movement through soil in the Gallatin Valley facilitated the distributive process of irrigation and domestic water use increases anthropogenic contamination of cations and anions in surface and groundwaters. The presence of an extensive canal and associated irrigation system in the Gallatin Valley creates seepage and return flow that increase water infiltration through soil and shallow aquifers, magnifying the influence of fertilizers, septic systems, and anthropogenic activity. We propose that these patterns are typical of flow systems across mountain-basin transitions in the intermountain west, where water originating from mountain headwaters carries a distinct geochemical signature of water-rock interaction. At the mountain front, this water recharges valley aquifers that with distance down-valley are influenced by infiltration through soils, transforming both the quality and quantity of surface water and groundwater as a function of agricultural practices, municipal redistribution, density of septic systems and mobilization of secondary weathering products from soils and deeper substrate weathering environments.

4.7 Acknowledgments

We thank the funding sources for this project including USGS National Institute of Water Resources Competitive Grants Program, the Nielsen Fellowship from the Department of Land Resources and Environmental Sciences at MSU (LRES), and the Montana Agricultural Experiment Station (MAES). We are grateful to Dale White and the US Forest Service, Custer-Gallatin National Forest for permission to conduct this research in Hyalite Canyon. We also thank Erika Sturn, whose Master's work laid the groundwork for this project. We are grateful for field assistance from Ethan Wologo, Joe Capella and Simon Fordyce; laboratory analysis at MBMG by Jackie Timmer and Ashley Huft, and at the LRES Environmental Analytical Laboratory by Dr. Jane Klassen and Dr. Christine Gobrogge. Cliff and Joan Montagne, Jane Klassen, Eric Haferman, Dean Fraley, and Julie and Pete Geddes kindly provided access to their home wells.

Table 4.1. Sample locations and elevations for Hyalite Creek and the Gallatin Valley.

Site ID	Sample Type	Location	Elevation (m)	Latitude	Longitude
HY1	Surface Water	Hyalite Creek above reservoir	2087	45.452	-110.959
HY2	Surface Water	Emerald Creek	2063	45.475	-110.954
HY7	Surface Water	Hyalite Creek below reservoir at DNRC gauge 41H 2000	1962	45.501	-110.986
HY3	Surface Water	Lick Creek	1960	45.505	-110.988
HY9	Surface Water	Hyalite Creek below Lick Creek	1941	45.506	-110.993
HY16	Surface Water	Madison limestone spring channel	1936	45.508	-110.998
HY17	Surface Water	Madison limestone spring seep	1931	45.509	-110.997
HY10	Surface Water	Middle Hyalite Creek	1909	45.517	-111.007
HY11	Surface Water	Hyalite Creek at Langohr Logging Road	1882	45.527	-111.013
HY13	Surface Water	Unnamed creek in terminal glacial moraine meadow	1898	45.524	-111.017
HY12	Surface Water	Buckskin Creek	1889	45.530	-111.013
HY4	Surface Water	Hyalite Creek at Langohr's Campground	1861	45.535	-111.017
HY8	Surface Water	Moser Creek	1871	45.537	-111.016
HY14	Surface Water	Hyalite Creek below Moser Creek	1854	45.539	-111.020
HY15	Surface Water	Hyalite Creek above Practice Rock	1729	45.554	-111.062
HY5	Surface Water	Hyalite Creek at Practice Rock	1807	45.542	-111.034
HY6	Surface Water	Hyalite Creek at USGS gauge 06050000	1690	45.563	-111.072
SD1	Surface Water	Sourdough Creek	1926	45.524	-110.926
GV1	Surface Water	Hyalite/Middle Creek at S. 19th	1618	45.453	-110.958
GV2	Surface Water	S. Cottonwood Creek	1596	45.577	-111.145
GV3	Surface Water	Gallatin River at USGS gauge 06043500	1580	45.510	-111.259
GV4	Surface Water	Gallatin River at Axtell Bridge	1473	45.624	-111.211
GV5	Surface Water	Hyalite/Middle Creek at Monforton School Rd.	1428	45.686	-111.169
GV6	Surface Water	E. Gallatin River at USGS gauge 06048650	1405	45.726	-111.066

GV9	Surface Water	E. Gallatin River at Belgrade	1321	45.838	-111.160
GV10	Surface Water	E. Gallatin River at Dry Creek Rd.	1296	45.874	-111.233
GV8	Surface Water	Gallatin River at Manhattan	1294	45.859	-111.229
GV7	Surface Water	Gallatin River at USGS gauge 06052500	1246	45.886	-111.441
GW2	Groundwater	Hodgman Canyon - gneiss spring	1704	45.585	-111.067
GW3	Groundwater	Hodgman Canyon - gneiss well	1692	45.586	-111.067
GW4	Groundwater	Hyalite Creek alluvial fan well	1641	45.583	-111.091
GW7	Groundwater	Mystic Heights subdivision well #2	1630	45.594	-111.046
GW6	Groundwater	Mystic Heights subdivision well #3	1622	45.596	-111.046
GW5	Groundwater	Hitching Post subdivision well	1543	45.631	-111.028
GW1	Groundwater	Bozeman Trail Rd. well	1517	46.661	-111.000
GW8	Groundwater	MBMG Monitoring well GWIC ID: 266832	1303	45.846	-111.264
GW9	Groundwater	MBMG Monitoring well GWIC ID: 266803	1288	45.875	-111.265
EF	Soil	Ellis Farm soil sample	1522	45.657	-111.974
PF	Soil	Post Farm soil sample	1465	45.673	-111.151
LF	Soil	Lutz Farm soil sample	1414	45.818	-111.052

Table 4.2. Chemical data including concentrations anions, alkalinity, Sr, Ca, as well as Ca/Sr, $^{87}Sr/^{86}Sr$, and [$^{234}U/^{238}U$] ratios.

Site ID	Description	Sample Date	NO_3^- (mg N L^{-1})	±2σ	Cl^- (mg L^{-1})	±2σ	Alkalinity (mg $CaCO_3$ L^{-1})	Ca (mg L^{-1}) MDL: 0.0060	Sr (mg L^{-1}) MDL: 0.0066	U (µg L^{-1})	±2σ	Ca/Sr	$^{87}Sr/^{86}Sr$	±2σ	[$^{234}U/^{238}U$]	±2σ
HY1	Hyalite Creek above reservoir	2/19/2016	0.05	0.002	0.13	0.013		3.07	0.02	0.01	0.0001	176	0.70883	0.00001	1.722	0.022
		5/18/2016	0.01	0.001	0.13	0.013	9	4.21	0.02	0.01	0.0002	185	0.70872	0.00001	1.604	0.013
		8/25/2016			0.07	0.007	18	3.75	0.02	0.01	0.0001	188	0.70885	0.00001	1.695	0.013
		2/4/2017	0.05	0.002	0.14	0.007	15	3.79		0.02	0.0002		0.70890	0.00001	1.642	0.012
		5/16/2017	0.01	0.001	0.20	0.010	22	3.90	0.02			182				
		8/23/2017			0.11	0.023		3.78	0.02	0.00	0.0000	179	0.70921	0.00001	1.616	0.025
HY2	Emerald Creek	2/19/2016	0.02	0.001	0.18	0.018		4.60	0.03	0.01	0.0001	172	0.70890	0.00001	1.629	0.006
		5/18/2016	0.01	0.001	0.17	0.017	15	4.92	0.03	0.02	0.0003	175	0.70901	0.00001	1.643	0.010
		8/25/2016			0.13	0.013	29	5.67	0.03	0.01	0.0001	186	0.70890	0.00001	1.691	0.012
		2/4/2017	0.03	0.002	0.20	0.010	24	5.87	0.03	0.01	0.0001	196	0.70890	0.00001	1.645	0.006
		5/16/2017	0.03	0.001	0.22	0.011	11	4.59	0.03			177				
		8/23/2017			0.14	0.029	28	5.56	0.03	0.01	0.0001	178	0.70895	0.00001	1.671	0.010
HY7	Hyalite Creek below reservoir at DNRC gauge 41H 2000	2/4/2017	0.01	0.000	0.21	0.011	35	9.33	0.04	0.24	0.0024	249	0.70871	0.00001	1.591	0.006
		5/16/2017	0.01	0.000	0.26	0.013	24	8.56	0.03			247				
		8/23/2017	0.05	0.010	0.12	0.025	12	7.00	0.03	0.02	0.0002	231	0.70870	0.00001	1.621	0.007
HY3	Lick Creek	2/19/2016	0.01	0.001	0.27	0.014		21.65	0.08	0.54	0.0054	277	0.70846	0.00001	1.570	0.004
		5/18/2016	0.01	0.001	0.16	0.016	57	17.50	0.06			314	0.70857	0.00001	0.000	0.000
		8/25/2016			0.28	0.014	190	44.60	0.14	0.20	0.0020	321	0.70847	0.00001	1.506	0.006
		2/4/2017	0.01	0.000	0.29	0.014	123	34.50	0.11	0.16	0.0016	314	0.70859	0.00001	1.497	0.004
		5/16/2017			0.20	0.010	39	15.50	0.05			307				
		8/23/2017			0.24	0.048	235	47.00	0.15	0.71	0.0071	313	0.70846	0.00001	1.499	0.005
HY9	Hyalite Creek below Lick Creek	8/23/2017	0.06	0.012	0.15	0.031	45	8.52	0.04	0.04	0.0004	243	0.70859	0.00001	1.598	0.007
HY16	Madison limestone spring channel	12/14/2017	0.00	0.010	0.19	0.038				0.08	0.0008		0.70853	0.00001	2.121	0.006
HY17	Madison limestone spring seep	12/14/2017	0.09	0.019	0.34	0.067				0.42	0.0042		0.70835	0.00001	5.226	0.017
		12/14/2017	0.11	0.022	0.33	0.065				0.04	0.0004		0.70835	0.00001	5.285	0.013
		1/29/2018								0.38	0.0038				5.282	0.032
		3/27/2018								0.37	0.0037		0.70836	0.00001	5.215	0.015
HY10	Middle Hyalite Creek	8/23/2017	0.06	0.012	0.16	0.033	46	11.00	0.04	0.08	0.0008	259	0.70860	0.00001	2.958	0.010
		12/14/2017			0.19	0.038				0.11	0.0011		0.70857	0.00001	2.957	0.016
HY11	Hyalite Creek at Langohr Logging Road	8/23/2017	0.05	0.011	0.16	0.032	49	11.00	0.04	0.09	0.0009	259	0.70861	0.00001	2.966	0.008
HY13	Unnamed creek in glacial meadow	8/24/2017	0.03	0.006	0.29	0.059	88	14.60	0.08	0.02	0.0002	192	0.70893	0.00001	1.961	0.058
HY12	Buckskin Creek	8/23/2017	0.01	0.010	0.30	0.059	212	68.60	0.14	0.59	0.0059	504	0.71146	0.00001	2.695	0.228
HY4	Hyalite Creek at Langohr's Campground	2/19/2016	0.01	0.001	0.20	0.020		13.52	0.05	0.16	0.0016	261	0.70868	0.00001	3.195	0.009

		5/18/2016			0.20	0.020	98	23.70	0.08	0.21	0.0040	302	0.70881	0.00001	2.367	0.035
		8/25/2016	0.07	0.004	0.14	0.014	37	12.50	0.05	0.07	0.0007	277	0.70866	0.00001	2.977	0.011
		2/4/2017	0.02	0.001	0.24	0.012	52	17.60	0.06	0.19	0.0019	301	0.70868	0.00001	3.100	0.010
		5/16/2017			0.25	0.013	39	16.20	0.06			268				
		8/23/2017	0.04	0.008	0.16	0.031	28	11.40	0.04	0.09	0.0009	268	0.70879	0.00001	2.983	0.022
HY8	Moser Creek	2/4/2017	0.01	0.001	0.34	0.017	106	37.10	0.14	0.60	0.0060	275	0.71143	0.00001	2.236	0.006
		5/16/2017			0.18	0.009	51	16.50	0.06			254				
		8/23/2017			0.31	0.062	167	47.10	0.16	0.54	0.0054	294	0.71181	0.00001	2.241	0.008
HY14	Hyalite Creek below Moser Creek	8/24/2017	0.07	0.014	0.18	0.037	45	11.60	0.04	0.08	0.0008	267	0.70874	0.00001	3.047	0.012
HY15	Hyalite Creek above Practice Rock	8/24/2017	0.06	0.011	0.15	0.031	73	11.60	0.04	0.08	0.0008	270	0.70885	0.00001	2.944	0.013
HY5	Hyalite Creek at Practice Rock	2/19/2016	0.02	0.001	0.22	0.022		9.86	0.04	0.55	0.0055	246	0.71141	0.00001	1.788	0.005
		5/18/2016			0.20	0.020	78	21.60	0.07	0.46	0.0090	304	0.71246	0.00001	1.666	0.006
		8/25/2016	0.07	0.004	0.14	0.014	43	12.60	0.05	0.17	0.0017	278	0.70979	0.00001	2.086	0.006
		5/16/2017	0.00	0.000	0.26	0.013	54	16.60	0.06			281				
		8/24/2017	0.03	0.005	0.19	0.038	79	11.90	0.04	0.15	0.0015	272	0.70973	0.00001	2.128	0.008
HY6	Hyalite Creek at USGS gage 06050000	2/19/2016	0.02	0.001	0.23	0.023		10.05	0.04	0.64	0.0064	249	0.71202	0.00001	1.691	0.005
		5/18/2016			0.21	0.021	82	22.00	0.07	0.56	0.0110	313	0.71295	0.00001	1.578	0.005
		8/25/2016	0.07	0.003	0.16	0.016		12.70	0.05	0.12	0.0012	270	0.71007	0.00001	1.966	0.005
		5/16/2017			0.24	0.012	68	15.40	0.06			278				
		2/4/2017	0.04	0.002	0.24	0.012	52	14.40	0.05	0.79	0.0079	287	0.71112	0.00001	1.747	0.004
		8/24/2017	0.01	0.010	0.15	0.030	61	11.80	0.04			274	0.70998	0.00001		
SD1	Sourdough Creek	12/13/2017	0.03	0.006	0.16	0.033				0.02	0.0002		0.70862	0.00001	2.047	0.018
GV1	Hyalite/Middle Creek at S. 19th	2/26/2016	0.06	0.003	0.25	0.012		15.57	0.06	0.63	0.0063	278	0.71214	0.00001	1.672	0.004
		5/6/2016	0.01	0.001	0.23	0.023	73	20.20	0.06	0.50	0.0050	312	0.71245	0.00001	1.614	0.004
		8/25/2016	0.07	0.004	0.15	0.015	49	11.50	0.05	0.19	0.0019	246	0.71057	0.00001	1.804	0.005
		2/5/2017	0.04	0.002	0.26	0.013	49	17.70	0.06	0.51	0.0051	289	0.71157	0.00001	1.697	0.005
		5/17/2017			0.24	0.012	70	18.40	0.06			297				
		8/25/2017	0.01	0.010	0.18	0.036	60	12.50	0.04	0.24	0.0024	282	0.71131	0.00001	2.046	0.007
GV2	S. Cottonwood Creek	2/26/2016	0.06	0.003	0.51	0.026		17.91	0.04	0.56	0.0056	508	0.71403	0.00001	2.534	0.007
		5/6/2016	0.14	0.007	0.34	0.017	92	22.30	0.05	0.30	0.0030	482	0.71568	0.00001	2.144	0.006
		8/25/2016			0.58	0.029	151	24.90	0.06	0.20	0.0020	445	0.71339	0.00001	2.362	0.006
		2/5/2017	0.07	0.004	0.49	0.024	115	28.70	0.05	0.45	0.0045	528	0.71417	0.00001	2.543	0.008
		5/17/2017	0.07	0.004	0.33	0.017	99	17.60	0.04			460				
		8/25/2017			0.30	0.059	143	37.80	0.07	0.41	0.0041	552	0.71373	0.00001	2.432	0.022
GV3	Gallatin River at USGS gauge 06043500	2/26/2016	0.03	0.002	2.05	0.103		27.21	0.18	0.87	0.0087	152	0.00000	0.00000	2.052	0.005
		5/6/2016	0.05	0.002	0.92	0.046	87	19.90	0.11	0.48	0.0048	178	0.71077	0.00001	1.742	0.005
		8/26/2016			1.36	0.068	112	27.50	0.20	0.24	0.0024	139	0.71090	0.00001	2.067	0.005

		2/5/2017	0.07	0.003	1.64	0.082	90	38.30	0.23	1.09	0.0109	167	0.71098	0.00001	2.038	0.008
		5/17/2017	0.04	0.002	0.96	0.048		18.90	0.10			182				
		8/25/2017	0.00	0.010	1.34	0.268	131	37.30	0.22	0.64	0.0064	169	0.71085	0.00001	2.057	0.005
GV4	Gallatin River at Axtell Bridge	5/6/2016	0.05	0.002	0.96	0.048	78	21.10	0.12	0.50	0.0050	176	0.71077	0.00001	1.765	0.005
		8/26/2016	0.01	0.001	1.45	0.072	104	25.20	0.18	0.28	0.0028	142	0.71103	0.00001	2.035	0.006
		2/5/2017	0.06	0.003	1.66	0.083	89	37.90	0.22	1.22	0.0122	176	0.71117	0.00001	2.033	0.006
		5/17/2017	0.04	0.002	0.99	0.049	100	21.80	0.11			191				
		8/25/2017	0.01	0.010	1.47	0.294	118	38.60	0.22	0.70	0.0070	176	0.71094	0.00001	2.035	0.006
GV5	Hyalite/Middle Creek at Monforton School Rd.	2/26/2016			0.77	0.039		13.32	0.05	0.66	0.0066	271	0.71171	0.00001	1.658	0.004
		5/6/2016	0.18	0.009	1.73	0.086	131	26.70	0.10	1.13	0.0113	269	0.71219	0.00001	1.711	0.005
		8/26/2016	0.06	0.003	1.84	0.092	146	26.90	0.16	1.10	0.0110	164	0.71146	0.00001	1.879	0.005
		5/17/2017	0.09	0.005	1.03	0.052	88	20.00	0.07			297				
		8/25/2017			2.59	0.519	174	44.80	0.20	1.08	0.0108	224	0.71147	0.00001	1.812	0.005
GV6	E. Gallatin River at USGS gauge 06048650	2/26/2016	0.31	0.015	13.73	1.373		29.72	0.13	1.96	0.0196	232	0.71005	0.00001	1.859	0.005
		5/6/2016	0.06	0.003	3.56	0.178	153	26.90	0.10	0.70	0.0070	271	0.70899	0.00001	1.767	0.005
		8/26/2016	0.08	0.004	9.32	0.932	185	28.00	0.14	0.28	0.0028	194	0.71034	0.00001	1.896	0.005
		5/17/2017	0.12	0.006	4.73	0.236	143	17.10	0.07			247				
		8/25/2017	0.09	0.018	7.28	1.455	214	52.40	0.21	1.24	0.0124	254	0.71027	0.00001	1.861	0.005
GV9	E. Gallatin River at Belgrade	8/31/2017	0.54	0.108	14.12	2.824	220	56.10	0.20	1.59	0.0159	276	0.71132	0.00001	1.857	0.005
GV10	E. Gallatin River at Dry Creek Rd.	8/31/2017	0.67	0.134	9.72	1.943	205	54.00	0.20	1.65	0.0165	271	0.71202	0.00001	1.909	0.005
GV8	Gallatin River at Manhattan	8/25/2017	0.00	0.010	1.89	0.378	132	40.50	0.22	0.80	0.0080	187	0.71144	0.00001	1.901	0.006
GV7	Gallatin River at USGS gauge 06052500	2/26/2016	0.57	0.057	6.26	0.313		23.25	0.13	1.96	0.0196	184	0.71177	0.00001	1.905	0.005
		5/6/2016	0.15	0.008	2.70	0.135	115	28.60	0.14	0.86	0.0086	203	0.71120	0.00001	1.840	0.005
		8/26/2016	0.27	0.013	6.69	0.669	167	23.40	0.15	2.11	0.0211	155	0.71183	0.00001	1.911	0.005
		2/5/2017	0.65	0.065	4.79	0.239	154	50.00	0.20	2.34	0.0234	245	0.71176	0.00001	1.925	0.006
		5/17/2017	0.15	0.007	2.43	0.122	105	27.10	0.13			217				
		8/25/2017	0.30	0.059	7.89	1.578	207	48.60	0.23	1.99	0.0199	213	0.71175	0.00001	1.900	0.005
GW2	Gneiss spring	5/18/2017	0.07	0.003	0.59	0.030	37	15.30	0.05	0.35	0.0035	321	0.73687	0.00001	1.849	0.084
GW3	Gneiss well	5/18/2017	0.11	0.005	0.76	0.038	146	27.00	0.06	0.36	0.0036	467	0.74497	0.00001	1.489	0.022
GW4	Hyalite Creek alluvial fan well	6/20/2017	2.25	0.113	9.39	0.469	139	42.90	0.11	0.23	0.0023	383	0.71221	0.00001	1.784	0.006
GW7	Mystic Heights subdivision well #2	6/22/2017	1.67	0.083	4.10	0.205	154	22.00	0.11	0.92	0.0092	204	0.73865	0.00001	1.279	0.004
GW6	Mystic Heights subdivision well #3	6/22/2017	1.65	0.082	4.09	0.204	117	21.30	0.11	0.90	0.0090	199	0.73856	0.00002	1.275	0.005
GW5	Hitching Post subdivision well	6/22/2017	8.20	0.410	46.37	4.637	432	72.60	0.18	4.61	0.0461	399	0.72169	0.00002	1.351	0.004
GW1	Bozeman Trail Rd. well	6/22/2017	2.85	0.143	21.18	1.059	242	68.00	0.15	2.39	0.0239	447	0.71193	0.00001	2.734	0.007
GW8	MBMG Monitoring well GWIC ID: 266832	7/20/2017	0.58	0.115	2.12	0.424	159	50.30	0.26	1.42	0.0142	193	0.71144	0.00001	2.135	0.005
GW9	MBMG Monitoring well GWIC ID: 266803	7/20/2017	0.02	0.010	6.27	1.254	367	98.20	0.50	3.18	0.0318	195	0.71185	0.00001	1.847	0.005

Table 4.3. Soil bulk density, total carbon (TC) % and kg/ha, and $^{87}Sr/^{86}Sr$ isotope ratios for select depth increments.

Farm	Depth increment (cm)	Rep.	Bulk Density (kg/m3)	TC (%)	±2σ	TC (kg/ha)	$^{87}Sr/^{86}Sr$	±2σ
Ellis Farm	45-60	1	1526	1.44	0.07	33044	0.70981	0.000011
Ellis Farm	45-60	2	1526	1.45	0.07	33082	0.70981	0.000011
Ellis Farm	60-75	1	1513	3.40	0.17	77148	0.70996	0.000010
Ellis Farm	60-75	2	1513	3.02	0.15	68564	0.70995	0.000019
Ellis Farm	60-75	2	1513	3.02	0.15	68564	0.70996	0.000019
Ellis Farm	75-90	2	1409	4.75	0.24	100502	0.71008	0.000011
Ellis Farm	90-105	1	1381	3.28	0.16	67896	0.71008	0.000010
Ellis Farm	90-105	2	1381	3.72	0.19	76995	0.71010	0.000010
Lutz Farm	45-60	1	1554	2.88	0.14	67125	0.71120	0.000013
Lutz Farm	45-60	1	1554	2.88	0.14	67125	0.71120	0.000013
Lutz Farm	45-60	2	1554	2.94	0.15	68519	0.71120	0.000011
Lutz Farm	60-75	1	1450	2.41	0.12	52517	0.71132	0.000010
Lutz Farm	60-75	2	1450	2.48	0.12	53924	0.71130	0.000010
Lutz Farm	75-90	1	1359	1.80	0.09	36683	0.71146	0.000009
Lutz Farm	75-90	2	1359	1.94	0.10	39616	0.71149	0.000011
Lutz Farm	90-105	1	1711	1.74	0.09	44712	0.71119	0.000012
Lutz Farm	90-105	2	1711	1.83	0.09	47068	0.71123	0.000010
Post Farm	45-60	1	1118	2.52	0.13	42232	0.71104	0.000011
Post Farm	45-60	2	1118	2.60	0.13	43559	0.71104	0.000018
Post Farm	45-60	2	1118	2.60	0.13	43559	0.71105	0.000018
Post Farm	60-75	1	1325	2.89	0.14	57356	0.71095	0.000009
Post Farm	60-75	2	1325	3.05	0.15	60682	0.71097	0.000011
Post Farm	75-90	1	1183	2.54	0.13	45153	0.71128	0.000010
Post Farm	75-90	2	1183	2.83	0.14	50285	0.71131	0.000011
Post Farm	90-105	1	1315	2.46	0.12	48580	0.71159	0.000010
Post Farm	90-105	2	1315	2.63	0.13	51917	0.71160	0.000010

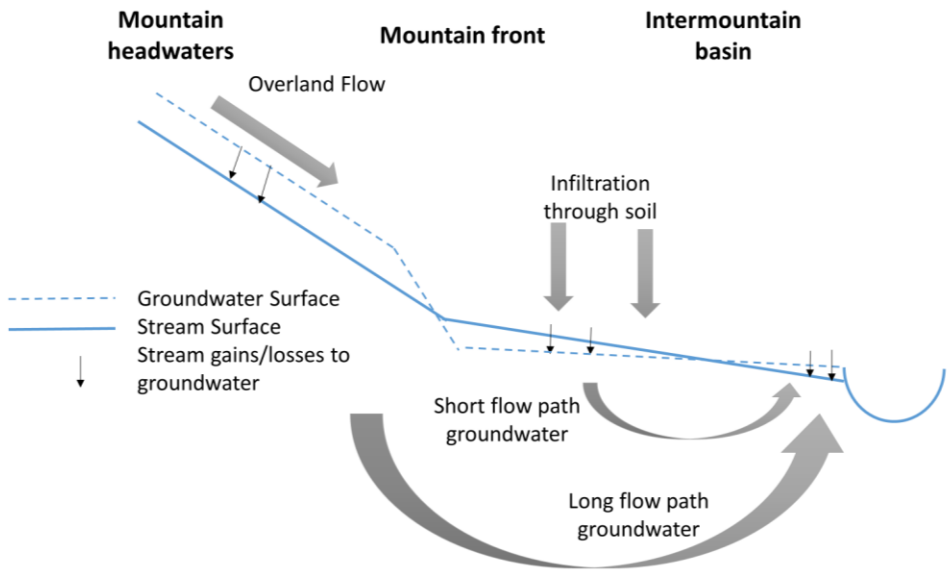

Figure 4.1a. Cartoon of water flow moving from the mountain headwaters to intermountain basin. The mountain headwaters process domain is characterized by convergent flow to the stream; with runoff, flow through soils and deeper groundwater contributing to stream flow. The mountain front is characterized by divergent flow that recharges aquifers in the intermountain basin. Water infiltration through soil contributes to shallow groundwater sources. Downgradient in the intermountain basin the flow system returns to convergent flow with stream water, and shallow and deeper groundwater inflows contributing to stream flow.

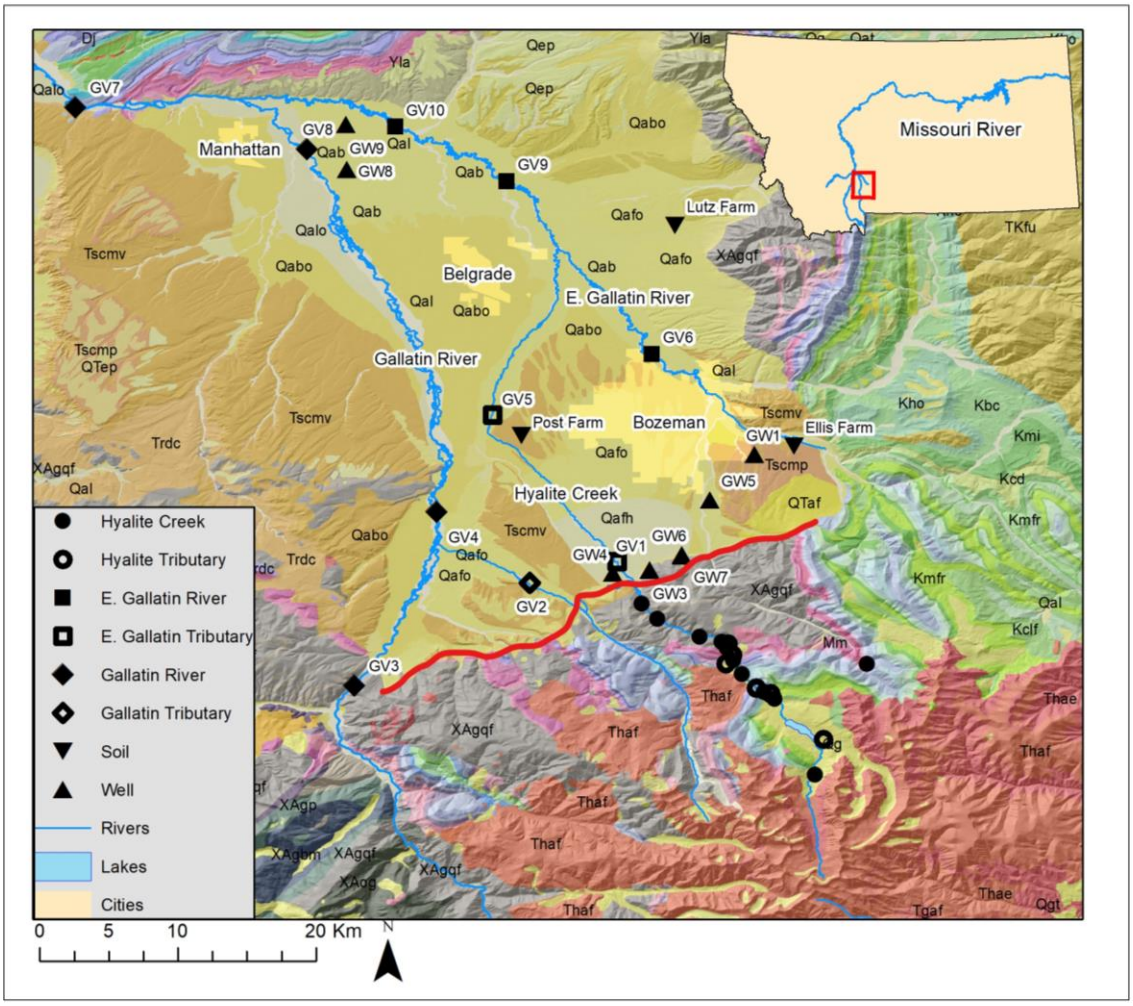

Figure 4.1b. Gallatin Valley sample site locations. The mountain front boundary for the Gallatin Range is highlighted with a red line. Hyalite Canyon site numbers are detailed in Figure 3.1

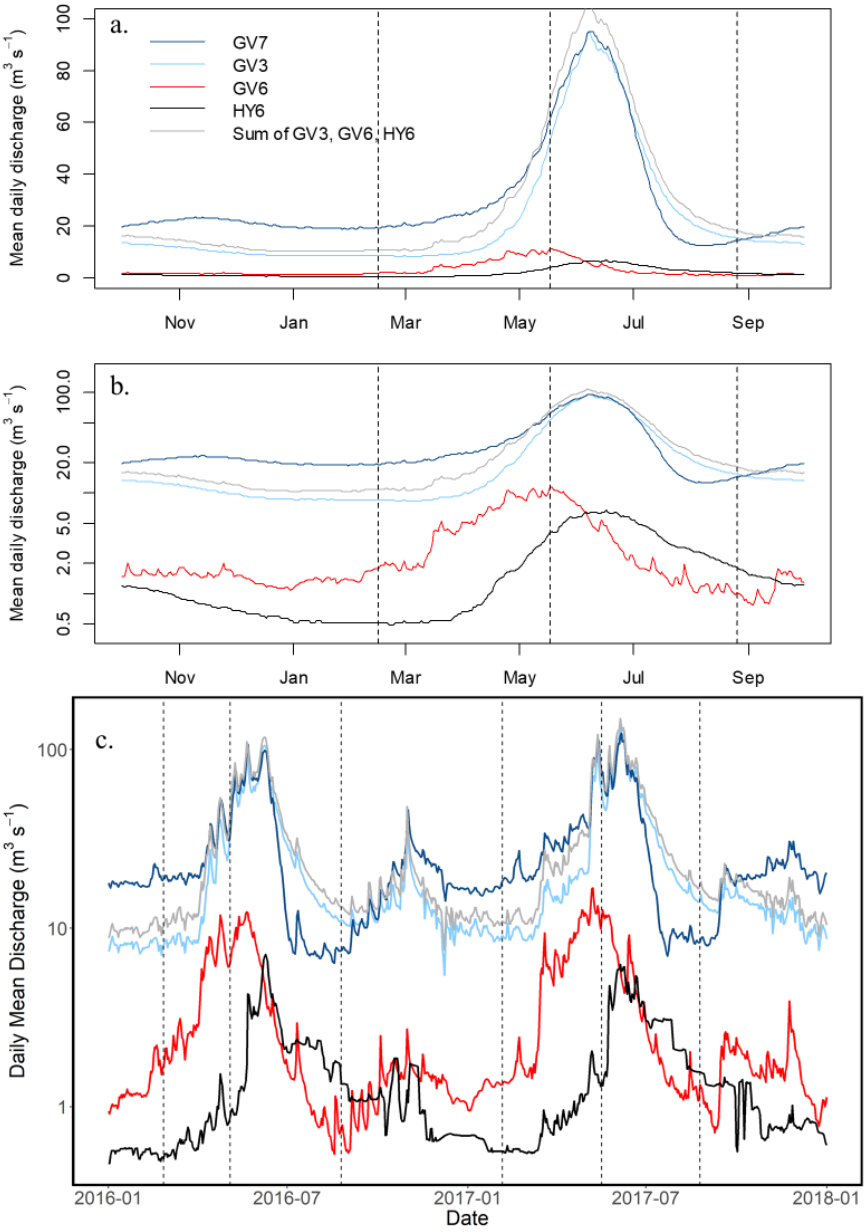

Figure 4.2. Mean daily and daily mean discharge for gauges in the Gallatin Valley and Hyalite Canyon. (a-b) Mean daily values averaged for each calendar day over a 24-year period from 1994 to 2018 from USGS gauges in logarithmic (a) and arithmetic (b) forms; (c) daily mean discharge for USGS gauges measured during the sampling period of 1/1/2016 to 1/1/2018 in logarithmic form. For all plots the Gallatin River at Gallatin Gateway (GV3) is represented in light blue, the Gallatin River at Logan (GV7) is dark blue, the East Gallatin River (GV6) is red, Hyalite Creek (HY6) is black, and the sum of the discharge from GV3, GV6, and HY6 is gray. Dotted vertical lines indicate dates sites were sampled for geochemical analyses.

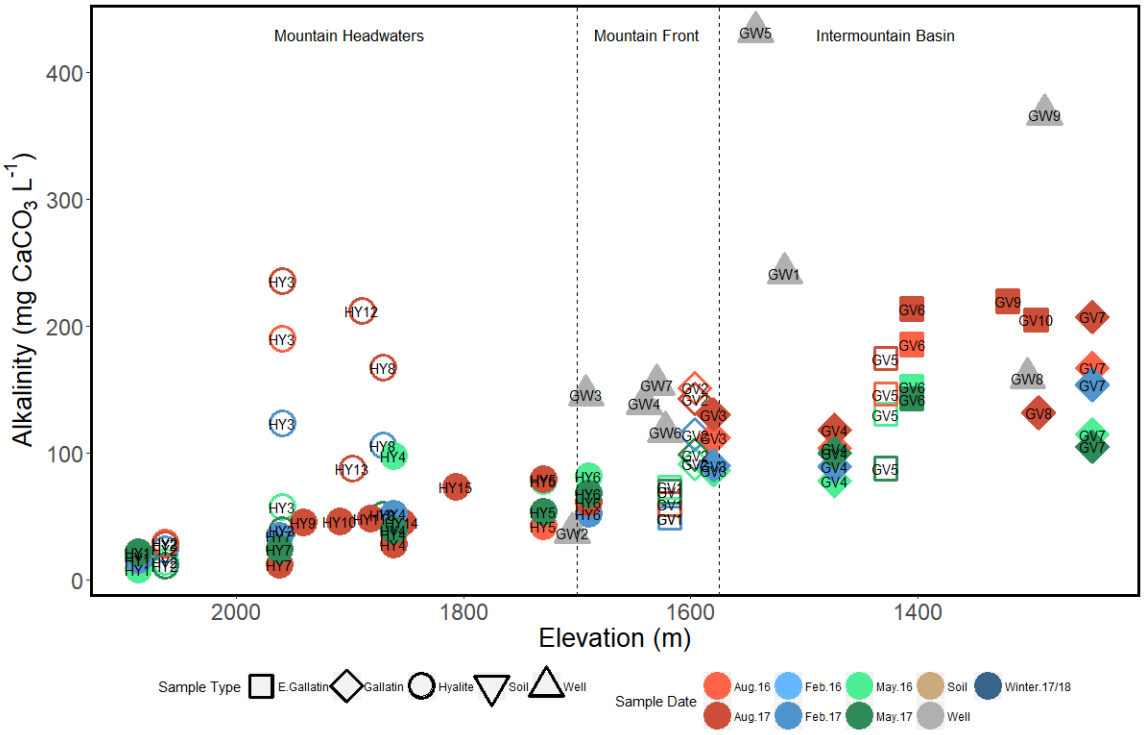

Figure 4.3. Alkalinity of surface water and groundwater plotted against site elevation. Samples of mainstem flow are shown as solid symbols and samples of tributary flow are shown as open circles with colors indicating sampling dates. Vertical dashed lines represent approximate boundaries between different process domains labeled at the top of the plot.

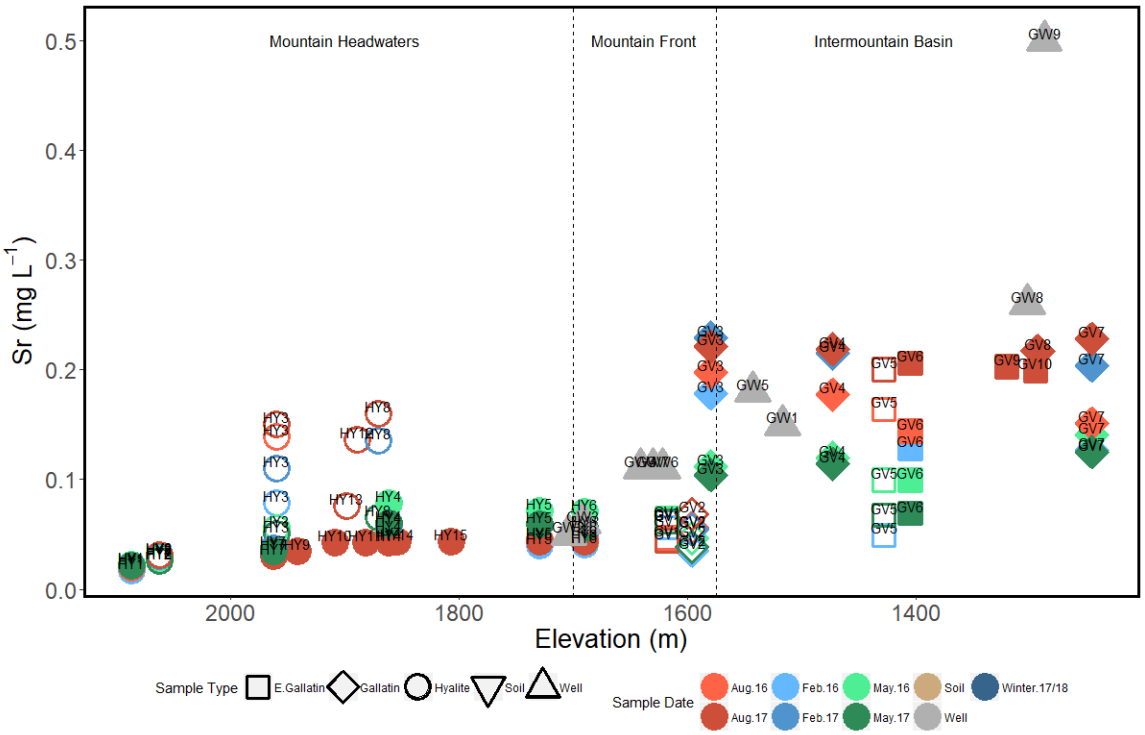

Figure 4.4. Sr concentration of surface water and groundwater plotted against site elevation. Samples of mainstem flow are shown as solid symbols and samples of tributary flow are shown as open circles with colors indicating sampling dates. Vertical dashed lines represent approximate boundaries between different process domains labeled at the top of the plot.

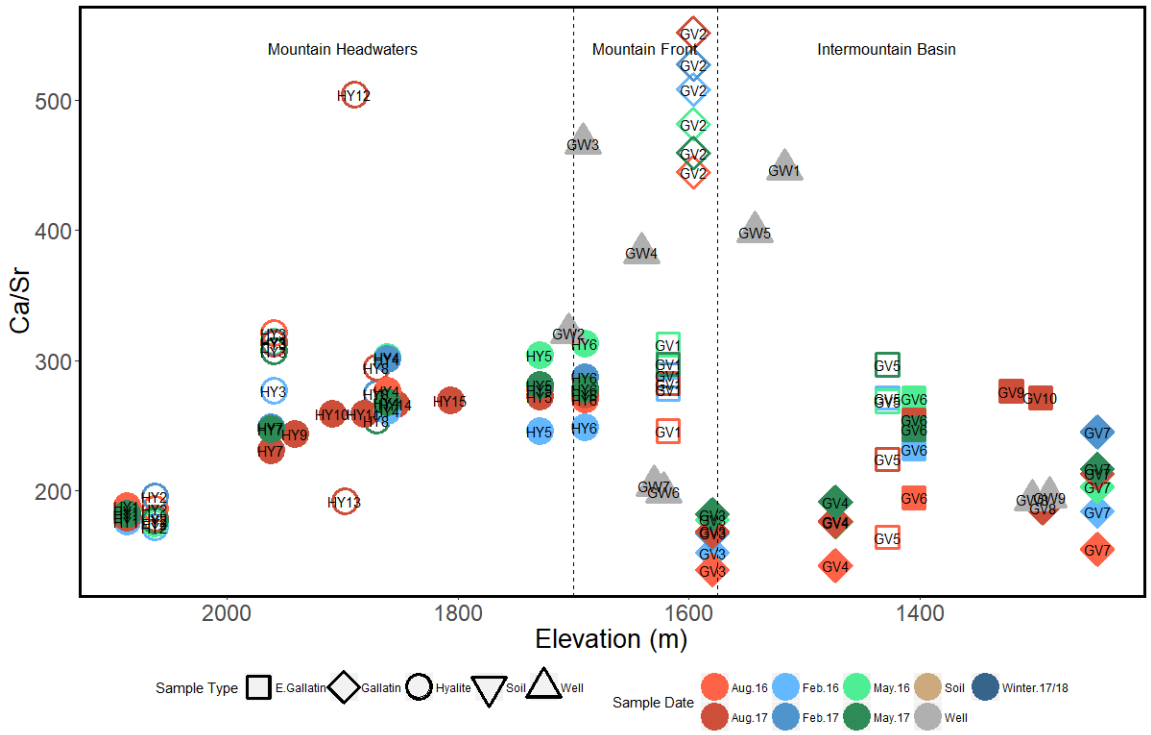

Figure 4.5. Ca/Sr of surface water and groundwater plotted against site elevation. Samples of mainstem flow are shown as solid symbols and samples of tributary flow are shown as open circles with colors indicating sampling dates. Vertical dashed lines represent approximate boundaries between different process domains labeled at the top of the plot.

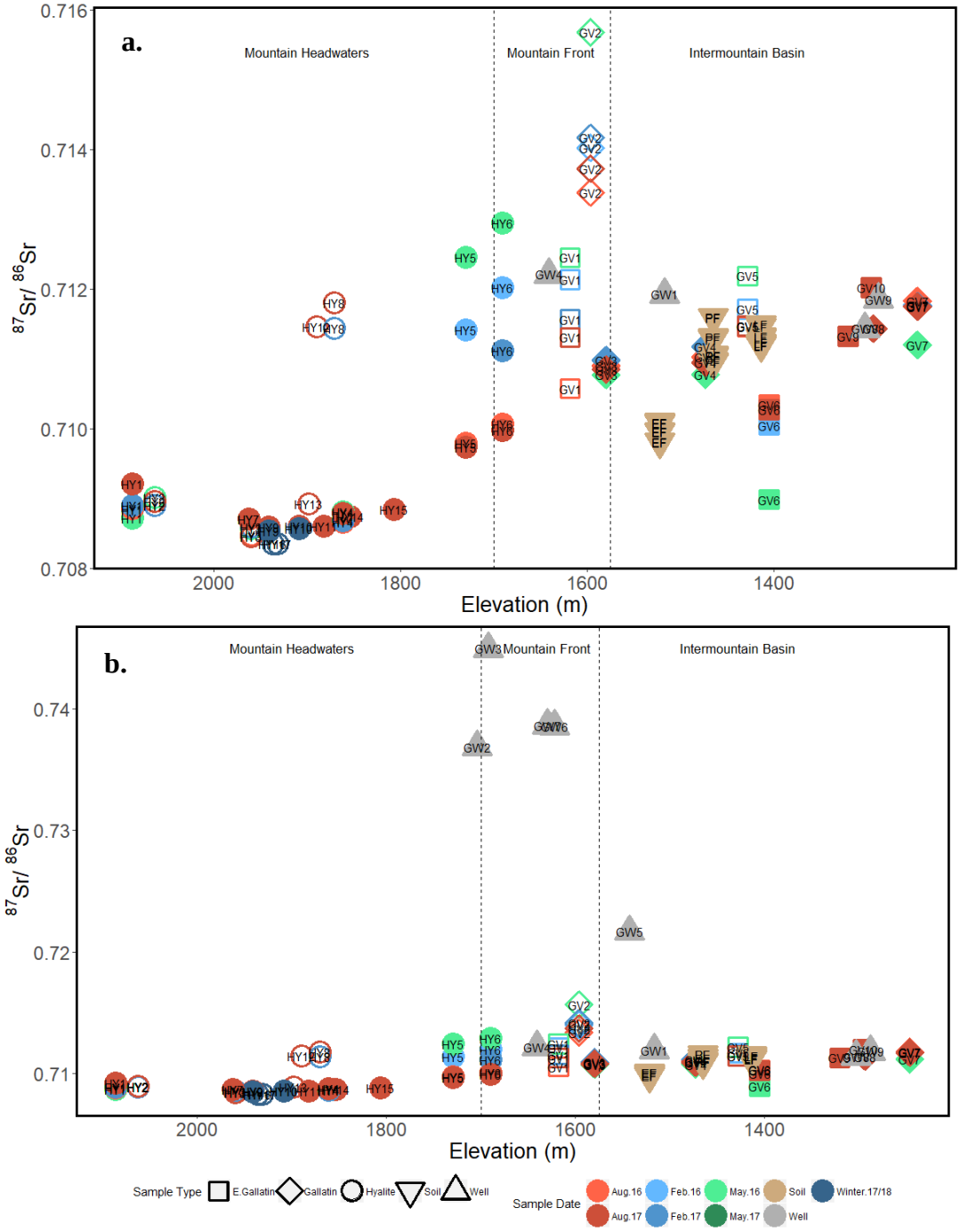

Figure 4.6. $^{87}Sr/^{86}Sr$ isotope ratios of surface water, groundwater, and soils plotted against site elevation. (a) $^{87}Sr/^{86}Sr$ isotope ratio trends with elevation, excluding high $^{87}Sr/^{86}Sr$ mountain front wells; (b) $^{87}Sr/^{86}Sr$ isotope ratio trends with elevation, including high $^{87}Sr/^{86}Sr$ mountain front wells. Samples of mainstem flow are shown as solid symbols and samples of tributary flow are shown as open circles with colors indicating sampling dates. Vertical dashed lines represent approximate boundaries between different process domains labeled at the top of the plot.

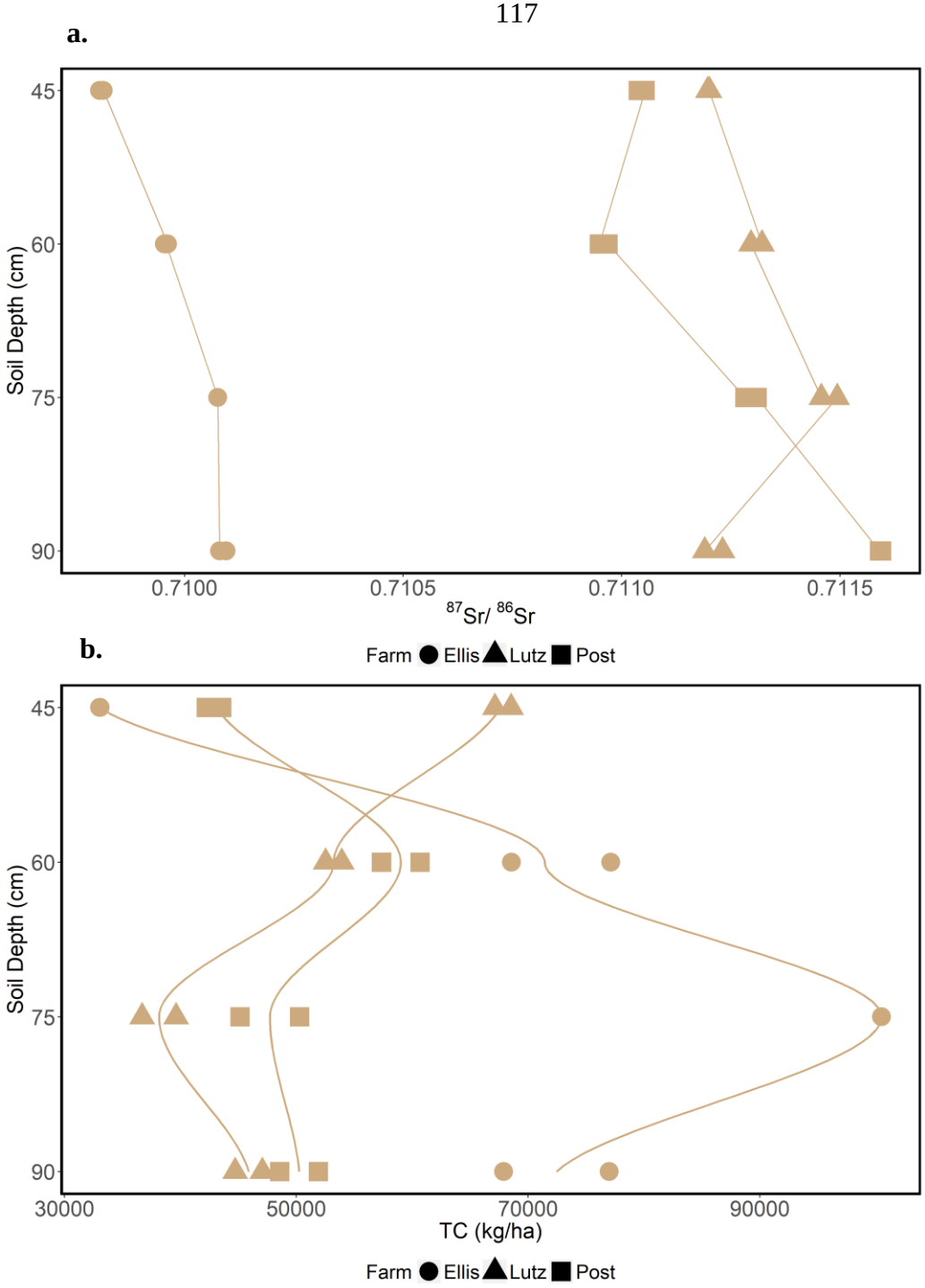

Figure 4.7. Soil $^{87}Sr/^{86}Sr$ isotope ratio and total carbon content plotted against depth. **(**a) $^{87}Sr/^{86}Sr$ isotope composition and (b) total carbon % of soils from Ellis (circle), Lutz (triangle), and Post (square) Farms in the Gallatin Valley at 15 cm depth intervals.

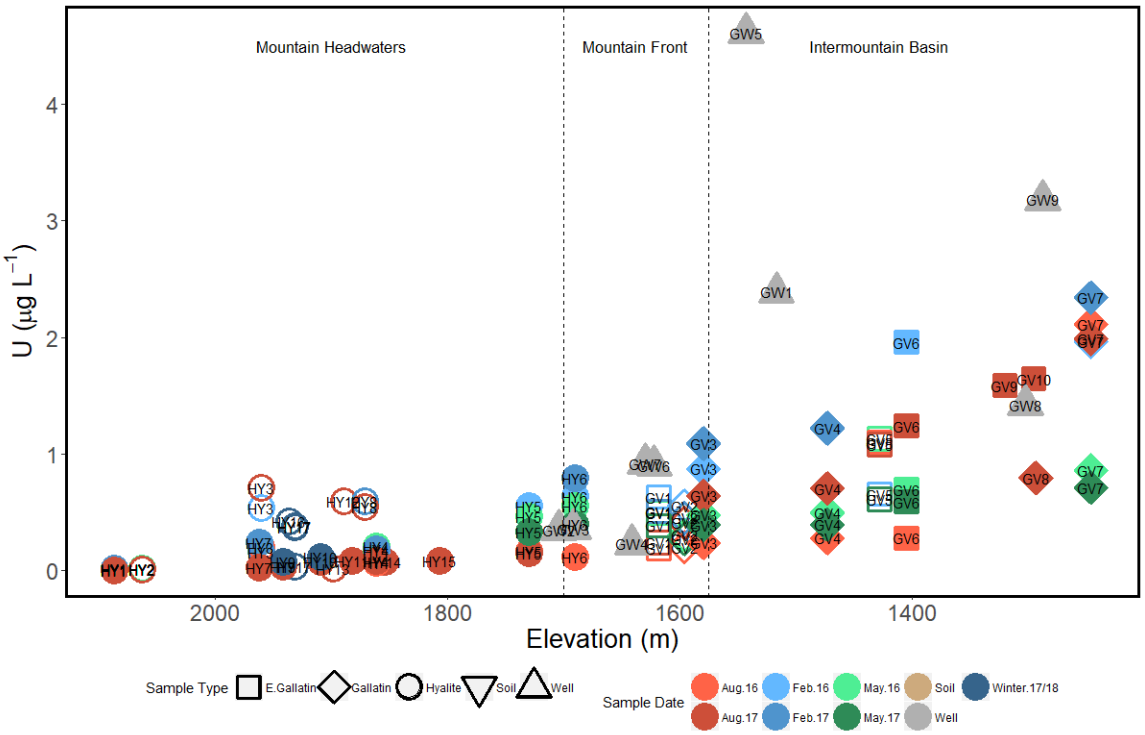

Figure 4.8. U concentration of surface water and groundwater plotted against site elevation. Samples of mainstem flow are shown as solid symbols and samples of tributary flow are shown as open circles with colors indicating sampling dates. Vertical dashed lines represent approximate boundaries between different process domains labeled at the top of the plot.

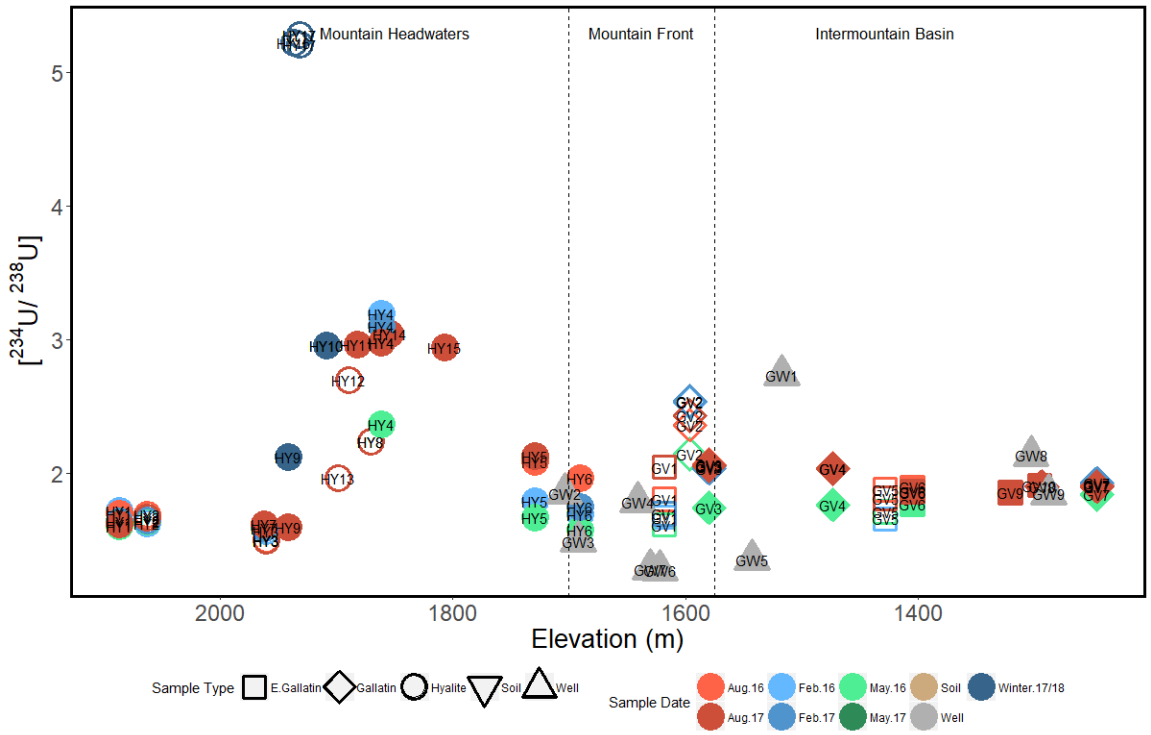

Figure 4.9. [$^{234}U/^{238}U$] of surface water and groundwater plotted against site elevation. Samples of mainstem flow are shown as solid symbols and samples of tributary flow are shown as open circles with colors indicating sampling dates. Vertical dashed lines represent approximate boundaries between different process domains labeled at the top of the plot.

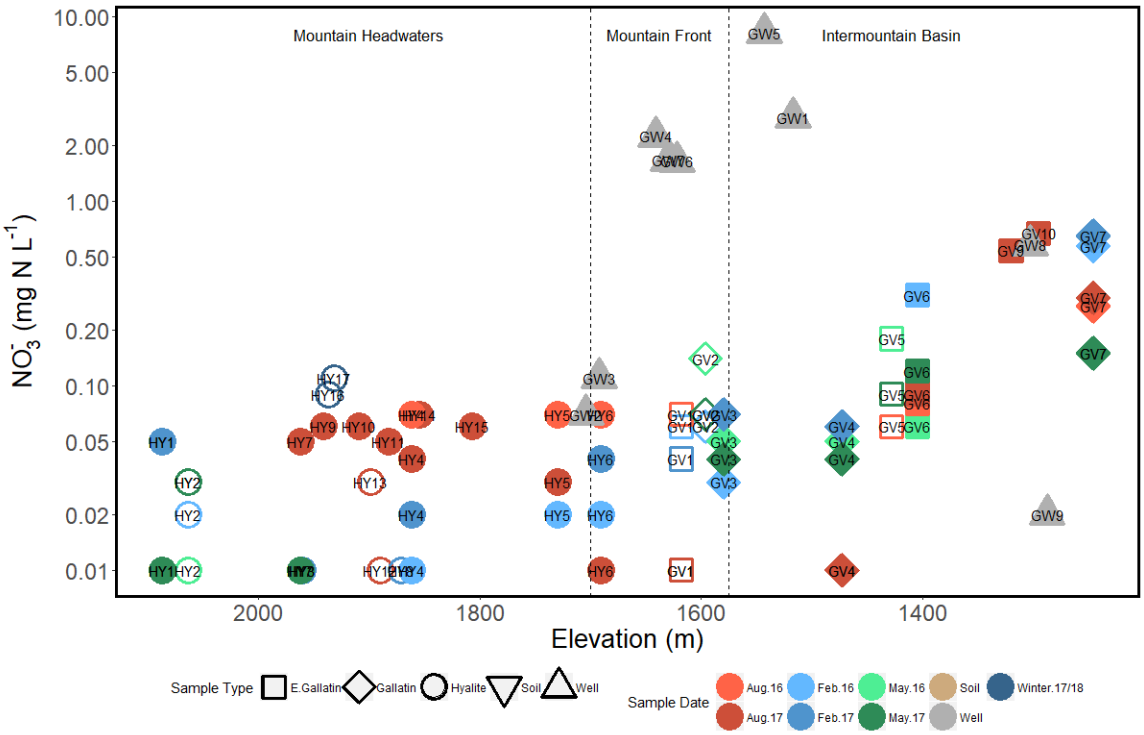

Figure 4.10. NO_3^- concentration of surface water and groundwater plotted against site elevation. Concentration of NO_3^--N shown on a log scale. Samples of mainstem flow are shown as solid symbols and samples of tributary flow are shown as open circles with colors indicating sampling dates. Vertical dashed lines represent approximate boundaries between different process domains labeled at the top of the plot.

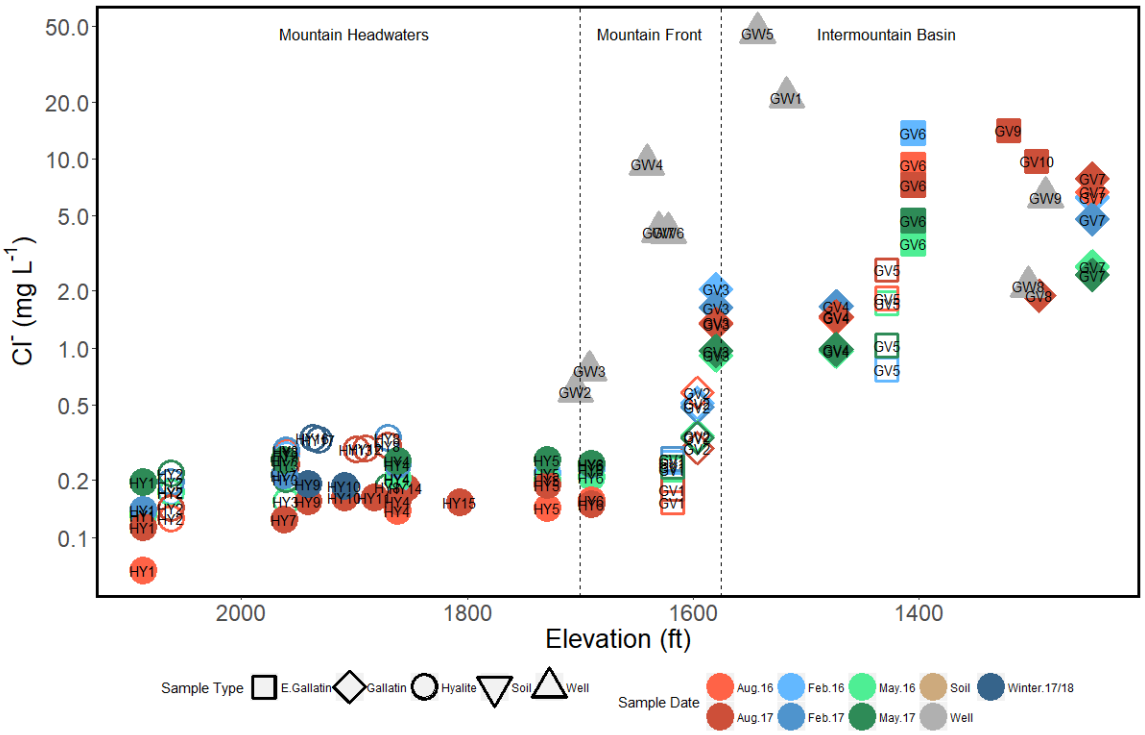

Figure 4.11. Cl^- concentration of surface water and groundwater plotted against site elevation. Concentration of Cl^- shown on a log scale. Samples of mainstem flow are shown as solid symbols and samples of tributary flow are shown as open circles with colors indicating sampling dates. Vertical dashed lines represent approximate boundaries between different process domains labeled at the top of the plot.

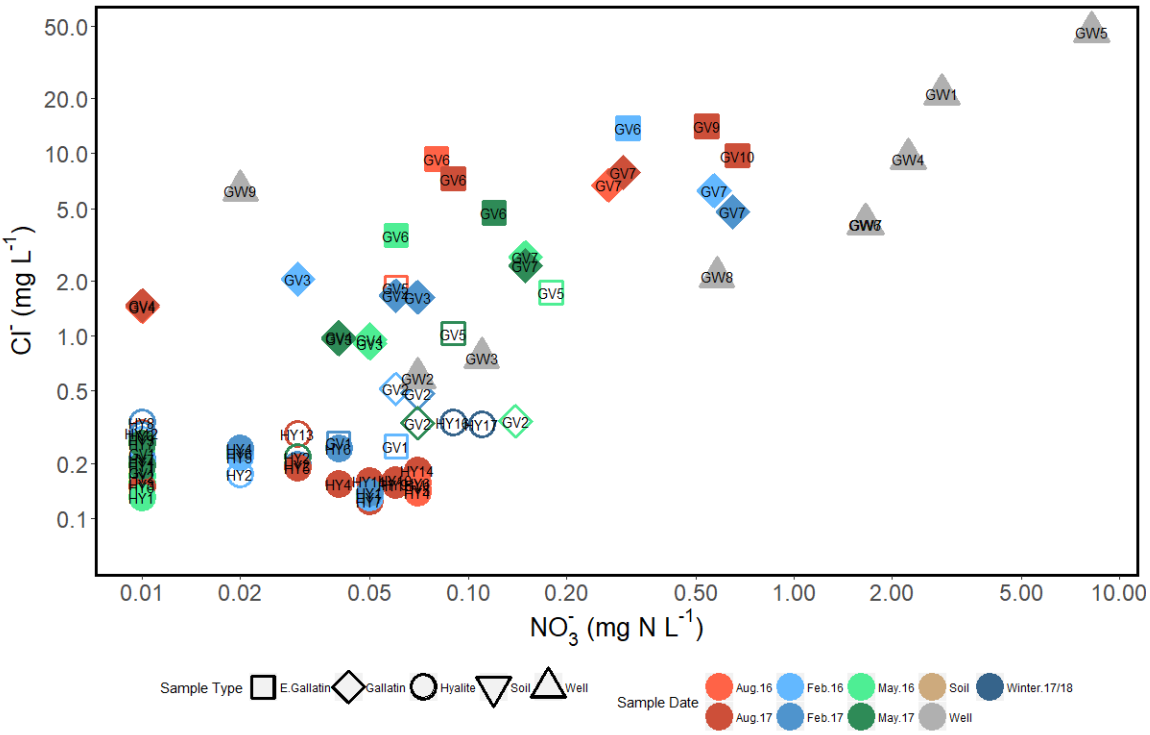

Figure 4.12. Concentration of NO_3^- plotted against concentration of Cl^-. Concentration of NO_3^- and Cl^- shown on a log scale. Samples of mainstem flow are shown as solid symbols and samples of tributary flow are shown as open circles with colors indicating sampling dates.

CHAPTER FIVE

GENERAL CONCLUSIONS

We used geochemical tracers to evaluate water/rock and water/substrate interactions indicative of water flow path and storage dynamics in mountain headwaters and intermountain basin process domains, using Hyalite Creek and the Gallatin Valley as a case study. This thesis includes two manuscripts in preparation for publication. The first, (Chapter 3) evaluates baseflow and surface subsurface water interactions along the mountain headwaters stream Hyalite Creek. The second, (Chapter 4) examines the transition from a convergent flow found in mountain headwater catchments to divergent flow found just below the mountain front within intermountain basins. This transition facilitates alluvial aquifer recharge which, combined with water infiltration through soils, ultimately controls the quality and quantity of surface and groundwater moving through intermountain basins.

In Hyalite Creek, geochemical tracers $^{87}Sr/^{86}Sr$ and [$^{234}U/^{238}U$] were used as sensitive indicators of distinct groundwater inflows in a lithologically diverse catchment, providing quantification of groundwater inflows and thus baseflow generation. The longitudinal sampling applied in Chapter 3 further allows the use of geochemical tracers to explore groundwater sources that would likely have been below detection limits if assessed only at the watershed outlet. Geochemical results from longitudinal sampling were used in mixing models combining tracer concentrations and isotope ratios to quantify the fractional contributions from groundwater sources. Contribution from the Madison

aquifers was consistent with previous research (~3.7% of local streamflow) (Kirk 2002). Isotopic results also revealed baseflow contributions from the Archean gneiss fracture flow in the lower canyon, which contributed ~2% of local streamflow during August baseflow conditions and ~8% of local streamflow during February baseflow conditions. This interaction of fracture flow with streamflow was not evident in solute chemistry or discharge rates but is clearly indicated by $^{87}Sr/^{86}Sr$ ratios in streamflow. Ultimately this research has enhanced understanding of groundwater inflows along Hyalite Canyon and developed sensitive geochemical tracers of common rock units in the region.

In the Gallatin Valley, we sought to understand how the interaction of mountain front recharge with intermountain basin soils, rivers and aquifers defines the geochemistry of waters that supply the Missouri River system. As mountain front water enters the intermountain basin, geochemical trends between the mountain front and the Gallatin River downgradient in the intermountain basin suggest several key processes that define the resulting transformation of water character. First, moderation of Ca/Sr, $^{87}Sr/^{86}Sr$, and $[^{234}U/^{238}U]$ to more intermediate values suggest the mixing of surface, soil, and groundwater moving down gradient in the Gallatin Valley. Second, higher concentrations of Sr and U, higher alkalinity, higher Ca/Sr ratios, lower $[^{234}U/^{238}U]$ values and $^{87}Sr/^{86}Sr$ ratios consistent with soil carbonates suggest that water movement through soil facilitated the influence of soil secondary carbonates on the geochemical composition of the water. Finally, the increased water movement through soils in the Gallatin Valley facilitated the increase in anthropogenic solutes in surface and groundwaters. Extensive cultivation and development in the valley enhances water movement through soils by eliminating native

vegetation and wetlands. In addition, the presence of an extensive canal and associated irrigation system in the Gallatin Valley creates seepage and return flow that increase water infiltration through soil to shallow aquifers, magnifying the influence of fertilizers, septic systems, and anthropogenic activity.

We suggest that these patterns are typical of dynamics across mountain-basin transitions in the intermountain west region of the United States, where water originating from mountain headwaters carries a distinct geochemical signature of water-rock interaction. As urban areas in intermountain basins expand and predicted changes in temperature and precipitation patterns decrease snowpack storage (Silverman & Maneta 2016), it is increasingly important to understand and quantify ground water storage, residence time, inflow, and exchange in mountain stream systems and their resulting influence on the hydrology of intermountain basins. At the mountain front, mountain stream water recharges valley aquifers and, as shallow groundwater moves through the valley, mixes with infiltration through soils. The movement of shallow groundwater transforms both its quality and its quantity as a function of agricultural practices, municipal redistribution, density of septic systems and mobilization of secondary weathering products from soils and deeper substrate weathering environments. Using the Gallatin River Watershed, a headwaters to the Upper Missouri River basin, as a case study, we observed distinct trends in the geochemical composition of waters that further understanding of water movement and storage in the mountain headwaters and intermountain basin systems characteristic of the intermountain west.

REFERENCES CITED

Amundson, R. et al., 2015. Hillslope soils and vegetation. *Geomorphology*, 234, pp.122–132. Available at: http://dx.doi.org/10.1016/j.geomorph.2014.12.031.

Andersen, M.B., Stirling, C.H. & Weyer, S., 2017. Uranium Isotope Fractionation. *Reviews in Mineralogy & Geochemistry*, 82, pp.799–850.

Arendt, C.A., Aciego, S.M. & Hetland, E.A., 2015. An open source Bayesian Monte Carlo isotope mixing model with applications in Earth surface processes. *Geochemistry, Geophysics, Geosystems*, 16(5), pp.1274–1292.

Banner, J.L., 1995. Application of the isotope and trace element geochemistry of strontium to studies of diagenesis in carbonate systems. *Sedimentology*, 42(42), pp.805–824.

Barbieri, M. et al., 2005. Stable isotope (2H , 18O and 87Sr/86Sr) and hydrochemistry monitoring for groundwater hydrodynamics analysis in a karst aquifer (Gran Sasso , Central Italy). *Applied Geochemistry*, 20, pp.2063–2081.

Barbieri, M. & Morotti, M., 2003. Hydrogeochemistry and strontium isotopes of spring and mineral waters from Monte Vulture volcano , Italy. *Applied Geochemistry*, 18, pp.117–125.

Basu, A. et al., 2015. Isotopic and geochemical tracers for U(VI) reduction and U mobility at an in situ recovery U mine. *Environmental Science and Technology*, 49(10), pp.5939–5947.

Berg, R.B., Lonn, J.D. & Locke, W.W., 1999. *Geologic Map of the Gardiner 30' by 60' Quadrangle, South- Central Montana*,

Berg, R.B., Lopez, D.A. & Lonn, J.D., 2000. *Geologic Map of the Livingston 30' x 60' Quadrangle South-Central Montana*,

Bohlke, J.K. & Denver, J.M., 1995. Combined use of ground- water dating, chemical, and isotopic analyses to resolve the history and fate of nitrate contamination in two agricultural watersheds, atlantic coastal Plain, Maryland. *Water Resources Research*, 31(9), pp.2319–2339.

Böhlke, J.K., Verstraeten, I.M. & Kraemer, T.F., 2007. Effects of surface-water irrigation on sources, fluxes, and residence times of water, nitrate, and uranium in an alluvial aquifer. *Applied Geochemistry*, 22(1), pp.152–174.

Bourdon, B. et al., 2003. Introduction to U-Series Geochemistry. In *U-Series Geochemistry*. pp. 1–17.

Brown, S.T. et al., 2016. Isotopic Evidence for Reductive Immobilization of Uranium Across a Roll-Front Mineral Deposit. *Environmental Science and Technology*,

50(12), pp.6189–6198.

Brown, S.T. et al., 2018. Uranium isotope fractionation by abiotic reductive precipitation. *Proceedings of the National Academy of Sciences*, 2(Vi), p.201805234. Available at: http://www.pnas.org/lookup/doi/10.1073/pnas.1805234115.

Bullen, T.D. et al., 1997. Chemical weathering of soil chronosequence on granitoid alluviun: II. Mineralogic and isotopic constraints on the behaviour os strontium. *Geochim. Chosmo chim. Acta*, 60(2), pp.1807–1821.

Burow, K.R. et al., 2010. Nitrate in groundwater of the United States, 1991 - 2003. *Environmental Science & Technology*, 44(13), pp.4988–4997. Available at: http://dx.doi.org/10.1021/es100546y.

Capell, R. et al., 2011. Using hydrochemical tracers to conceptualise hydrological function in a larger scale catchment draining contrasting geologic provinces. *Journal of Hydrology*, 408(1–2), pp.164–177. Available at: http://dx.doi.org/10.1016/j.jhydrol.2011.07.034.

Capo, R.C. & Chadwick, O.A., 1999. Sources of strontium and calcium in desert soil and calcrete. , 170, pp.61–72.

Capo, R.C., Stewart, B.W. & Chadwick, O.A., 1998. Strontium isotopes as tracers of ecosystem processes : Theory and methods processes : theory and methods. *Geoderma*, 82, pp.197–225.

Chabaux, F., Riotte, J. & Dequincey, O., 2003. U-Th-Ra Fractionation During Weathering and River Transport. *Reviews in Mineralogy & Geochemistry*, 52, pp.533–576.

Chadwick, O.A. et al., 2009. Changing sources of strontium to soils and ecosystems across the Hawaiian Islands. *Chemical Geology*, 267(1–2), pp.64–76. Available at: http://dx.doi.org/10.1016/j.chemgeo.2009.01.009.

Cheng, H. et al., 2013. Improvements in230Th dating,230Th and234U half-life values, and U-Th isotopic measurements by multi-collector inductively coupled plasma mass spectrometry. *Earth and Planetary Science Letters*, 371–372, pp.82–91. Available at: http://dx.doi.org/10.1016/j.epsl.2013.04.006.

Covino, T.P. & McGlynn, B.L., 2007. Stream gains and losses across a mountain-to-valley transition: Impacts on watershed hydrology and stream water chemistry. *Water Resources Research*, 43(10), pp.1–14.

Depaolo, D.J. et al., 2006. Sediment transport time measured with U-series isotopes : Results from ODP North Atlantic drift site 984. *Earth and Planetary Science Letters*, 248, pp.394–410.

Depaolo, D.J. et al., 2012. Uranium comminution ages: Sediment transport and deposition time scales. *Comptes rendus - GeoscienceGeoscience*, 344(11–12), pp.678–687. Available at: http://dx.doi.org/10.1016/j.crte.2012.10.014.

Dixon, J.L., Chadwick, O.A. & Vitousek, P.M., 2016. Climate-driven thresholds for chemical weathering in postglacial soils of New Zealand. *Journal of Geophysical Research: Earth Surface*, 121, pp.1619–1634.

DNRC, M., 2014. *Middle Creek Dam (Hyalite) Fact Sheet*,

Dosseto, A., Bourdon, B. & Turner, S.P., 2008. *Uranium-series isotopes in river materials: Insights into the timescales of erosion and sediment transport*,

Dosseto, A., Buss, H.L. & Chabaux, F., 2014. Age and weathering rate of sediments in small catchments: The role of hillslope erosion. *Geochimica et Cosmochimica Acta*, 132, pp.238–258.

Drexler, J.Z. et al., 2014. 234U/238U and delta87Sr in peat as tracers of paleosalinity in the Sacramento-San Joaquin Delta of California, USA. *Applied Geochemistry*, 40, pp.164–179. Available at: http://dx.doi.org/10.1016/j.apgeochem.2013.10.011.

Emanuel, R.E. et al., 2014. Vegetation and topographic influences on the connectivity of shallow groundwater between hillslopes and streams. *Ecohydrology*, 7(2), pp.887–895.

Ewing, S.A. et al., 2015. ScienceDirect Uranium isotopes and dissolved organic carbon in loess permafrost: Modeling the age of ancient ice. *Geochimica et Cosmochimica Acta*, 152, pp.143–165.

Faure, G. & Mensing, T.M., 2005. *Isotopes Principles and Applications 3rd Edition*, Hoboken, New Jersey: John Wiley & Sons.

Feeley, T.C. & Cosca, M.A., 2003. Time vs . composition trends of magmatism at Sunlight volcano , Absaroka volcanic province , Wyoming. *Geological Society of America, Bulletin*, (6), pp.714–728.

Frost, C.D. & Toner, R.N., 2004. Strontium isotopic identification of Water-Rock Interaction and Ground Water Mixing. *Ground Water*, 42(3), pp.418–432.

Gardner, W.P. et al., 2011. Using terrigenic 4He to identify and quantify regional groundwater discharge to streams. *Water Resources Research*, 47(November 2010), pp.1–13.

Gedeon, J., 2015. Tourist traffic skyrockets in popular Bozeman recreation area. *NBC Montana*.

Gordon, R.P. et al., 2015. Sources and pathways of stream generation in tropical proglacial valleys of the Cordillera Blanca , Peru. *JOURNAL OF HYDROLOGY*, 522, pp.628–644. Available at: http://dx.doi.org/10.1016/j.jhydrol.2015.01.013.

Green, K.C., Brardinoni, F. & Alila, Y., 2013. Geomorphology Channel morphology and bed-load yield in fl uvial , formerly-glaciated headwater streams of the Columbia Mountains , Canada. *Geomorphology*, 188, pp.96–109. Available at: http://dx.doi.org/10.1016/j.geomorph.2012.05.004.

Hackett, B.O.M., Visher, F.N. & Mcmurtrey, R.G., 1960. Geology and Ground-Water Resources of the Gallatin Valley Gallatin County Montana.

Hart, W.S. et al., 2004. The 87Sr/86Sr ratios of lacustrine carbonates and lake-level history of the Bonneville paleolake system. *Bulletin of the Geological Society of America*, 116(9–10), pp.1107–1119.

Hinckley, E.L.S. et al., 2014. Aspect control of water movement on hillslopes near the rain-snow transition of the Colorado Front Range. *Hydrological Processes*, 28(1), pp.74–85.

Hiza, M.M., 1999. *The geochemistry and geochronology of the Eocene Absaroka volcanic province, northern Wyoming and southwest Montana, USA*. Oregon State University.

Hogan, J.F. & Blum, J.D., 2003. Tracing hydrologic flow paths in a small forested watershed using variations in 87 Sr/ 86 Sr, [Ca]/[Sr], [Ba]/[Sr] and δ 18 O. *Water Resources Research*, 39(10), p.1282. Available at: http://www.agu.org/pubs/crossref/2003/2002WR001856.shtml.

Horton, T.W. et al., 1999. Chemical weathering and lithologic controls of water chemistry in a high-elevation river system: Clark's Fork of the Yellowstone river, Wyoming and Montana. *Water Resources Research*, 35(5), pp.1643–1655.

Hoylman, Z.H. et al., 2018. Hillslope Topography Mediates Spatial Patterns of Ecosystem Sensitivity to Climate. *Journal of Geophysical Research: Biogeosciences*, 123(2), pp.353–371.

Jacobson, A.D. et al., 2003. Climatic and etctonic controls on chemical weathering in the New Zealand Southern Alps. *Geochimica et Cosmochimica Acta*, 67(1), pp.29–46.

Jacobson, A.D., Blum, J.D. & Walter, L.M., 2002. Reconciling the elemental and Sr isotope composition of Himalayan weathering fluxes: Insights from the carbonate geochemistry of stream waters. *Geochimica et Cosmochimica Acta*, 66(19), pp.3417–3429.

Jaffey, A.H. et al., 1971. Precision measurement of half-lives and specific activities of

U235 and U238. *Physical Review C*, 4(5), pp.1889–1906.

Jasechko, S., 2016. Partitioning young and old groundwater with geochemical tracers. *Chemical Geology*, 427, pp.35–42. Available at: http://dx.doi.org/10.1016/j.chemgeo.2016.02.012.

Jasechko, S. & Kirchner, J.W., 2016. Substantial proportion of global streamflow less than three months old. *Nature Geoscience*, (January).

Jencso, K.G. et al., 2009. Hydrologic connectivity between landscapes and streams: Transferring reach- and plot-scale understanding to the catchment scale. *Water Resources Research*, 45(4).

Jencso, K.G. & McGlynn, B.L., 2011. Hierarchical controls on runoff generation: Topographically driven hydrologic connectivity, geology, and vegetation. *Water Resources Research*, 47(11). Available at: file:///G:/CAOS (2)/Citavi Attachments/Jencso, McGlynn 2011 - Hierarchical controls on runoff generation.pdf.

Kelley, C.J. et al., 2017. Water and nitrogen movement through a semiarid dryland agricultural catchment: Seasonal and decadal trends. *Hydrological Processes*, 31(10), pp.1889–1899.

Kellogg, K.S. & Williams, V.S., 2006. *Geologic Map of the Ennis 30' by 60' Quadrangle Madison and Gallatin Counties, Montana, Park County, Wyoming*,

Kendy, E., 2001. *Ground-Water Resources of the Gallatin Local Water Quality District Southwestern Montana*,

Kharaka, Y.K. et al., 1991. Geochemical Investigations of Hydraulic connections between the Corwin Springs Know Geothermal Resources Area and Adjacent Parts of Yellowstone National Park, in Sorrey, M.L., Effects of potential geothermal development in the Corwin Springs Known Geother. *USGS Water Resources Investigations Report 91-4052*, pp.F1–F38.

Kirk, K.B., 2002. *A preliminary investigation of the Madison aquifer for a drinking water supply in Bozeman , Montana Abstract :* Montana State University.

Knowles, N., Park, M. & Dettinger, M.D., 2005. Trends in Snowfall versus Rainfall in the Western United States Trends in Snowfall versus Rainfall in the Western United States. *Journal of Climate*, 19, pp.4545–4559.

Kohl, C.A.K. et al., 2014. Strontium Isotopes Test Long-Term Zonal Isolation of Injected and Marcellus Formation Water after Hydraulic Fracturing. *Environmental Science & Technology*, 48, pp.9867–9873.

Kramer, C., 2013. A History of Bozeman's Water System Part III. *Bozeman Magazine*.

Land, M. et al., 2000. Ba/Sr, Ca/Sr and 87Sr/86Sr ratios in soil water and groundwater: implications for relative contributions to stream water discharge. *Applied Geochemistry*, 15(3), pp.311–325.

Leeman, W.P. et al., 1977. Radiogenic and stable isotope studies of hot-spring deposits in Yellowstone National Park and their genetic implications. *Geochemical Journal*, 11(2), pp.65–74.

Lindsay, C.R. & Feeley, T.C., 2003. Magmagenesis at the Eocene Electric Peak – Sepulcher Mountain complex , Absaroka Volcanic Province , USA. , 67, pp.53–76.

Liu, W. et al., 2016. Chemical and strontium isotopic characteristics of the rivers around the Badain Jaran Desert , northwest China : implication of river solute origin and chemical weathering. *Environmental Earth Sciences*, 75(15), pp.1–16.

Ludwig, K.R., Wallace, A.R. & Simmons, K.R., 1985. The Schwartzwalder uranium deposit, II: Age of uranium mineralization and lead isotope constraints on genesis. *Economic Geology*, 80(7), pp.1858–1871.

Maher, K. et al., 2003. Vadose zone infiltration rate at Hanford , Washington , inferred from Sr isotope measurements. *Water Resources Research*, 39(8), p.1204.

Maher, K., Depaolo, D.J. & Christensen, J.N., 2006. U – Sr isotopic speedometer : Fluid flow and chemical weathering rates in aquifers. , 70, pp.4417–4435.

Maher, K., DePaolo, D.J. & Christensen, J.N., 2006. U–Sr isotopic speedometer: Fluid flow and chemical weathering rates in aquifers. *Geochimica et Cosmochimica Acta*, 70(17), pp.4417–4435.

Martin, J.B. & Moore, P.J., 2008. Sr concentrations and isotope ratios as tracers of ground-water circulation in carbonate platforms : Examples from San Salvador Island and Long Island , Bahamas. , 249, pp.52–65.

May, K.A., 1985. *Archean geology of a part of the northern Gallatin Range, southwest Montana*. Montana State University.

McArthur, J.M. et al., 2006. A revised Pliocene record for marine-87Sr/86Sr used to date an interglacial event recorded in the Cockburn Island Formation, Antarctic Peninsula. *Palaeogeography, Palaeoclimatology, Palaeoecology*, 242(1–2), pp.126–136.

McArthur, J.M., Howarth, R.J. & Bailey, T.R., 2001. Strontium Isotope Stratigraphy: LOWESS Version 3: Best Fit to the Marine Sr-Isotope Curve for 0–509 Ma and Accompanying Look-up Table for Deriving Numerical Age. *The Journal of*

Geology, 109(2), pp.155–170. Available at: http://www.journals.uchicago.edu/doi/10.1086/319243.

McGlynn, B.L. & McDonnell, J.J., 2003. Quantifying the relative contributions of riparian and hillslope zones to catchment runoff. *Water Resources Research*, 39(11).

McGuire, K.J. et al., 2005. The role of topography on catchment-scale water residence time. *Water Resources Research*, 41(5), pp.1–14.

Montana DNRC, 2018, Montana Bureau of Mines and Geology Surface Water and Assessment and Monitoring Program data available on the World Wide Web, accessed [August 13, 2018], at URL [http://data.mbmg.mtech.edu/swamp/reports/GageReport.asp?SiteId=321&agency=mbmg&reqby=P&]

Montgomery, C.W. & Lytwyn, J.N., 1984. Rb-Sr Systematics and Ages of Principal Precambrian Lithologies in the South Snowy Block, Beartooth Mountains. *The Journal of Geology*, 92(1), pp.103–112.

Montgomery, D.R., 1999. Process domains and the river continuum. *Journal Of The American Water Resources Association*, 35(2), pp.397–410.

Moore-Nall, A.L., 2016. *Structural controls and chemical characterization of brecciation and uranium vanadium mineralization in the northern Bighorn Basin*. Montana State University.

Négrel, P., Petelet-giraud, E. & Widory, D., 2004. Strontium isotope geochemistry of alluvial groundwater: a tracer for groundwater resources characterisation. *Hydrology & Earth System Sciences*, 8(5), pp.959–972.

Paces, J.B., Long, A.J. & Koth, K., 2015. Potential Application of Radiogenic Isotopes and Geophysical Methods to Understand the Hydrothermal System of the Upper Geyser Basin , Yellowstone National Park. *National Park Service - Natural Resource Report*, p.57.

Paces, J.B. & Wurster, F.C., 2014. Natural uranium and strontium isotope tracers of water sources and surface water-groundwater interactions in arid wetlands - Pahranagat Valley, Nevada, USA. *Journal of Hydrology*, 517, pp.213–225.

Payn, R.A. et al., 2009. Channel water balance and exchange with subsurface flow along a mountain headwater stream in Montana, United States. *Water Resources Research*, 45(11).

Payn, R.A. et al., 2012. Exploring changes in the spatial distribution of stream baseflow generation during a seasonal recession. *Water Resources Research*, 48(October 2011), pp.1–15.

Pierret, M.C. et al., 2014. Chemical and U – Sr isotopic variations in stream and source waters of the Strengbach watershed (Vosges mountains, France). *Hydrological Processes*, 18, pp.3969–3985.

PRISM Climate Group, Oregon State University, http://prism.oregonstate.edu, created 24 Aug 2004.

Roback, R.C. et al., 2001. Uranium isotopic evidence for groundwater chemical evolution and flow patterns in the eastern Snake River Plain aquifer, Idaho. *Geological Society of America, Bulletin*, 113(9), pp.1133–1141.

Ross, M.R.V. et al., 2015. Designer Ecosystems: Incorporating Design Approaches into Applied Ecology. *Annual Review of Environment and Resources*, 40(1), pp.419–443. Available at: http://www.annualreviews.org/doi/10.1146/annurev-environ-121012-100957.

Roy, S., Gaillardet, J. & Allègre, C.J., 1999. Geochemistry of dissolved and suspended loads of the Seine river, France: Anthropogenic impact, carbonate and silicate weathering. *Geochimica et Cosmochimica Acta*, 63(9), pp.1277–1292.

Ryu, J. et al., 2009. Uranium isotopes as a tracer of sources of dissolved solutes in the Han River , South Korea. *Chemical Geology*, 258(3–4), pp.354–361. Available at: http://dx.doi.org/10.1016/j.chemgeo.2008.10.039.

Scanlon, B.R. et al., 2005. Impact of land use and land cover change on groundwater recharge and quality in the southwestern US. *Global Change Biology*, 11(10), pp.1577–1593.

Sigler, W.A. et al., 2018. Connections among soil, ground, and surface water chemistries characterize nitrogen loss from an agricultural landscape in the upper Missouri River Basin. *Journal of Hydrology*, 556, pp.247–261. Available at: https://doi.org/10.1016/j.jhydrol.2017.10.018.

Silverman, N.L. et al., 2013. Dynamically downscaled winter precipitation over complex terrain of the Central Rockies of Western Montana , USA. *Water Resources Research*, 49(458), pp.458–470.

Silverman, N.L. & Maneta, M.P., 2016. Detectability of change in winter precipitation within mountain landscapes: Spatial patterns and uncertainty. *Water Resources Research*, 52, pp.4301–4320.

Smedes, H.W. & Prostka, H.J., 1972. Stratigraphic Framework of the Absaroka Volcanic Supergroup in the Yellowstone National Park Region. *Geological Survey Professional Paper 729-C*, pp.1–43.

Somers, L.D. et al., 2016. Quantifying groundwater – surface water interactions in a

proglacial valley, Cordillera Blanca, Peru. *Hydrological Processes*, 30, pp.2915–2929.

Soulsby, C. & Tetzlaff, D., 2008. Towards simple approaches for mean residence time estimation in ungauged basins using tracers and soil distributions. *Journal of Hydrology*, 363(1–4), pp.60–74. Available at: http://dx.doi.org/10.1016/j.jhydrol.2008.10.001.

Steiger, R.H. & Jager, E., 1977. SUBCOMMISSION ON GEOCHRONOLOGY : CONVENTION ON THE USE OF DECAY CONSTANTS IN GEO- AND COSMOCHRONOLOGY compded by On August 24 , 1976 the lUGS Subcommlsslon on Geochronology met in Sydney , Australia , during the 25th International Geological Congress . It. , 36, p.1977.

Stylo, M. et al., 2015. Uranium isotopes fingerprint biotic reduction. *Proceedings of the National Academy of Sciences*, 112(18).

Suksi, J., Rasilainen, K. & Pitkanen, P., 2006. Variations in 234U/238 U activity ratios in groundwater — A key to flow system characterisation? *Physics and Chemistry of the Earth*, 31, pp.556–571.

U.S. ClimateData, 2018. Climate Bozeman - Montana and Weather averages Bozeman. *U.S. Climate Data*, p.2018. Available at: https://www.usclimatedata.com/climate/bozeman/montana/united-states/usmt0040 [Accessed June 7, 2018].

U.S. Department of Agriculture, 2015. *2012 National Resources Inventory*, Available at: http://www.nrcs.usda.gov/technical/nri/12summary.

United States Census Bureau, 2018. Quick Facts Bozeman city, Montana. *United States Census Bureau*.

United States Department of Agriculture, 1996. *MT622 - Soil Survey of Gallatin County Area, Montana Part 1*,

United States Department of Agriculture, N.R.C.S., 1996. *Soil Survey of Gallatin National Forest, Montana*,

U.S. Geological Survey, 2018, National Water Information System data available on the World Wide Web (USGS Water Data for the Nation), accessed [August 13, 2018], at URL[https://waterdata.usgs.gov/mt/nwis/uv/?site_no=06050000&agency_cd=USGS &]

Vuke, S.M. et al., 2007. Geologic Map of Montana - edition 1.0. *Montana Bureau of Mines and Geology - Open File Report*.

Vuke, S.M. et al., 2014. *Geologic map of the bozeman 30' x 60' Quadrangle Southwestern Montana*,

Weber, M., 1965. *General geology and geomorphology of the Middle Creek area, Gallatin County, Montana*. Montana State University.

White, A.F. et al., 2009. Chemical weathering of a marine terrace chronosequence, Santa Cruz, California. Part II: Solute profiles, gradients and the comparisons of contemporary and long-term weathering rates. *Geochimica et Cosmochimica Acta*, 73(10), pp.2769–2803. Available at: http://dx.doi.org/10.1016/j.gca.2009.01.029.

White, A.F. et al., 1996. Chemical Weathering of a Soil Chronosequence on Granite Alluvium I. Reaction Rates Based on Changes in Soil Mineralogy. *Geochimica et Cosmochimica Acta*, 60(14), pp.2533–2550.

White, A.F. et al., 2005. The ubiquitous nature of accessory calcite in granitoid rocks: Implications for weathering, solute evolution, and petrogenesis. *Geochimica et Cosmochimica Acta*, 69(6), pp.1455–1471.

Williams, M.R. et al., 2015. Linking Nitrogen Management, Seep Chemistry, and Stream Water Quality in Two Agricultural Headwater Watersheds. *Journal of Environment Quality*, 44(3), p.910. Available at: https://dl.sciencesocieties.org/publications/jeq/abstracts/44/3/910.

Wilson, J.L. & Guan, H., 2004. Mountain-Block Hydrology and Mountain Front Recharge. In J. F. Hogan, F. M. Phillips, & B. R. Scanlon, eds. *Groundwater Recharge in a Desert Environment: The Southwestern United States*. American Geophysical Union, pp. 113–138.

Wooden, J.L. & Mueller, P.A., 1988. Pb, Sr, and Nd isotopic compositions of a suite of Late Archean, igneous rocks, eastern Beartooth Mountains: implications for crust-mantle evolution. *Earth and Planetary Science Letters*, 87, pp.59–72.

Yang, J., Mcmillan, H. & Zammit, C., 2017. Modelling Surface water-groundwater interaction in New Zealand: Model development and application. *Hydrological Processes*, 31(4), pp.1099–1085.

APPENDICES

APPENDIX A

SR BLANK ANALYSIS

There was some concern of sporadically high Sr blanks (contributions of exogenous Sr not inherent to a sample being analyzed) in the isotopic dry down procedure. Samples collected for Sr-isotope analyses typically consisted of 1000 ml of water with concentrations of 0.02 to 0.2 mg Sr L^{-1} (Table X). After evaporating the entire sample to dryness, a total of 20 to 200 µg (2×10^{-5} to 2×10^{-4} g) of Sr inherent to the water sample was available for analysis.

Blanks were routinely processed along with samples to evaluate whether contributions from exogenous sources of Sr were significant. Analyses included a milli-Q water procedural blank of 260,048 pg (2.6×10^{-7} g) and a field blank of 183,288 pg (1.8×10^{-7} g). Those analyses imply that as much as 0.1 to 1 percent of the Sr analyzed did not originate in the water sample. Another field blank contained a more reasonable value of 1,879 pg (1.9×10^{-9} g) of Sr, indicating that only about 0.001 to 0.01 percent of the total Sr was exogenous. The high blanks were examined with utmost concern and importance.

A sample of 1000 mL deionized water produced from the MSU Soil Biogeochemistry lab was sent to SWIRL for analysis where it was found that lab water contributes only about ~100 pg (1×10^{-10} g) of Sr blank. Total process blanks (blank Sr added from all dry-down and chemical procedures) using trace metal grade nitric acid (Trace Metal Grade (TMG) HNO_3) indicated a maximum contribution of 1470 to 2170 pg (1.5×10^{-9} to 2.2×10^{-9} g) of Sr throughout the procedure of evaporating water, refluxing, and dissolving solutes. Blanks using both TMG and Optima HNO_3 at the MSU

Soil Biogeochemistry lab showed similar results, with 746 – 1160 pg of Sr for the TMG HNO_3 blanks and 677 pg for the Optima HNO_3 blanks.

With water and acid eliminated as potential sources of exogenous Sr, the column chemistry was examined next. Total process blanks prepared and ran through columns at the MSU Soil Biogeochemistry lab contained both acceptable (1,879 pg) and high levels (~200,000 pg) of Sr. Similar results were obtained for Sr blanks evaporated at MSU and ran through column chemistry at SWIRL. Consequently, we do not believe that column chemistry conducted at MSU is the likely cause of the sporadically elevated Sr blanks.

Consequently, we interpret the pattern of unpredictable blank levels as not being caused by contaminated chemical reagents, but rather by introduction of atmospheric dust that was sporadically introduced into samples during the dry down process or cleaning and drying of labware at the MSU Soil Biogeochemistry lab. During this step, samples in open vessels were exposed to the laboratory environment, albeit under laminar air flow, for 24 to 72 hours.

Results are interpreted to indicate that elevated blank levels were not an issue of mass contamination, but rather a sporadic introduction of ambient lab dust into some samples. No attempt was made to characterize the $^{87}Sr/^{86}Sr$ composition. However, because of the large sample sizes, blank contributions remain small relative to large $^{87}Sr/^{86}Sr$ differences between sample sites observed in different samples. Consistencies of $^{87}Sr/^{86}Sr$ signal between samples collected at different times from the same sites as well as sites from the same lithologic groupings and their correspondence to $^{87}Sr/^{86}Sr$ values with expected values, confirm that measured $^{87}Sr/^{86}Sr$ values characterize real

compositional differences rather than anomalies attributable to contamination. That being said, all efforts are being taken to fully understand the quantity and isotopic signature of lab dust and to minimize the introduction of lab dust to future analyses.

APPENDIX B

FILTER CROSS CONTAMINATION

Upon examining contamination of Sr blanks, we noticed that field blanks (milli-Q water blanks transported to the field, filtered in the field, and processed in the lab) were consistently contained greater amounts of Sr contamination than laboratory blanks (milli-Q water blanks processed in the lab). In the field, filters were frequently re-used. While care was taken to flush out water from the previous sample site and purge water the filter with water from the new sample site, the disparity between field blanks and laboratory blanks raised concern about Sr contamination due to filter re-use.

To fully examine the possibility of cross-contamination with filter reuse during sample collection, the effects of filter reuse were evaluated. We collected a stream sample from Cottonwood Creek (site GV2) using a new filter. A second water sample was then collected from Hyalite Creek (site GV1) using the same filter after rinsing continuously for several minutes with water from the Hyalite site, as per standard procedures. An additional sample was taken from Hyalite Creek at the same time, but this time using a new filter. The two samples from Hyalite Creek were compared to see if any isotopic signature from Cottonwood Creek contaminated the Hyalite Creek sample when the same filter was used.

It was found that re-using the same filter did not introduce significant variation in $^{87}Sr/^{86}Sr$ isotope ratio of the sample. In the Cottonwood Creek sample (GV2) $^{87}Sr/^{86}Sr$ isotope ratio was measured to be 0.714260. Using the same filter, Hyalite Creek sample (GV1) had $^{87}Sr/^{86}Sr$ isotope ratios of 0.711088 and 0.711090. Using a new filter, Hyalite Creek sample (GV1) had an $^{87}Sr/^{86}Sr$ isotope ratio of 0.711087. Due to variations being

within sixth decimal place, it is unlikely that filter re-use had a noticeable influence on the $^{87}Sr/^{86}Sr$ composition of water samples.

APPENDIX C

MONTE CARLO TABLE OF END MEMBERS

Table C. 1 End Members, means and standard deviations used for Monte Carlo analysis. This table defines 8/23/2017 sampling of site HY10 as a mixture between 12/14/2017, 1/29/2018, and 3/27/2017 sampling of the Madison springs (HY16, HY17) and 8/23/2017 sampling Hyalite Creek below the reservoir (HY7); 8/24/2017 sampling of site HY5 is defined as a mixture between Archean gneiss wells (GW2, GW3) and 8/24/2017 sampling of the middle reaches of Hyalite Creek (HY14, HY15); and 2/4/2017 sampling of HY6 is defined as a mixture between Archean gneiss wells (GW2, GW3) and 2/4/2017 sampling of the middle reaches of Hyalite Creek (HY4).

End Member	Site ID	Sample Date	Sr (mg L^{-1})	U (µg L^{-1})	$^{87}Sr/^{86}Sr$	$[^{234}U/^{238}U]$
Madison:	HY16	12/14/2017	0.13	0.4239	0.708352	5.226
	HY17	12/14/2017	0.12		0.708349	5.285
	HY17	1/29/2018	0.15	0.3820		5.282
	HY17	3/27/2017	0.15	0.3720	0.708357	5.215
Mean:			0.14	0.3926	0.7083527	5.2520
SD:			0.015	0.0275	0.000004	0.037
Below Reservoir:	HY7	8/23/2017	0.0303	0.023	0.708701	1.6209
Mean:			0.0303	0.023	0.708701	1.6209
SD*:			0.005	0.02	0.00005	0.03
Madison/Below Reservoir Mixture:	HY10	8/23/2017	0.0424	0.079	0.708602	2.9576
Archean Gneiss:	GW2	5/18/2017	0.0477	0.353	0.736865	1.8486
	GW3	5/18/2017	0.0578	0.364	0.744966	1.4885
Mean:			0.05275	0.3585	0.7409155	1.66855
SD:			0.00714	0.00779	0.005728	0.2546292
Middle Hyalite Creek (Aug):	HY14	8/24/2017	0.0435	0.077	0.708736	3.0469
	HY15	8/24/2017	0.0430	0.083	0.708847	2.9439
Mean:			0.04325	0.0800	0.7087915	2.99540
SD:			0.00035	0.00042	0.000078	0.072832
Archean/Middle Hyalite Mixture (Aug):	HY5	8/24/2017	0.0437	0.152	0.709734	2.1284
Middle Hyalite Creek (Feb):	HY4	2/4/2017	0.0585	0.186	0.7086785	3.0997

Mean:			0.0585	0.186	0.7086785	3.0997
SD*:			0.01	0.03	0.0001	0.01
Archean/Middle Hyalite Mixture (Feb):	HY6	2/4/2017	0.0501	0.791	0.7111241	1.747

*Standard deviation estimated based off of other sampling dates/similar sites.

APPENDIX D

PROBABILITY DENSITY PLOTS OF FRACTIONAL CONTRIBUTIONS OF INFLOWS TO HYALITE CREEK

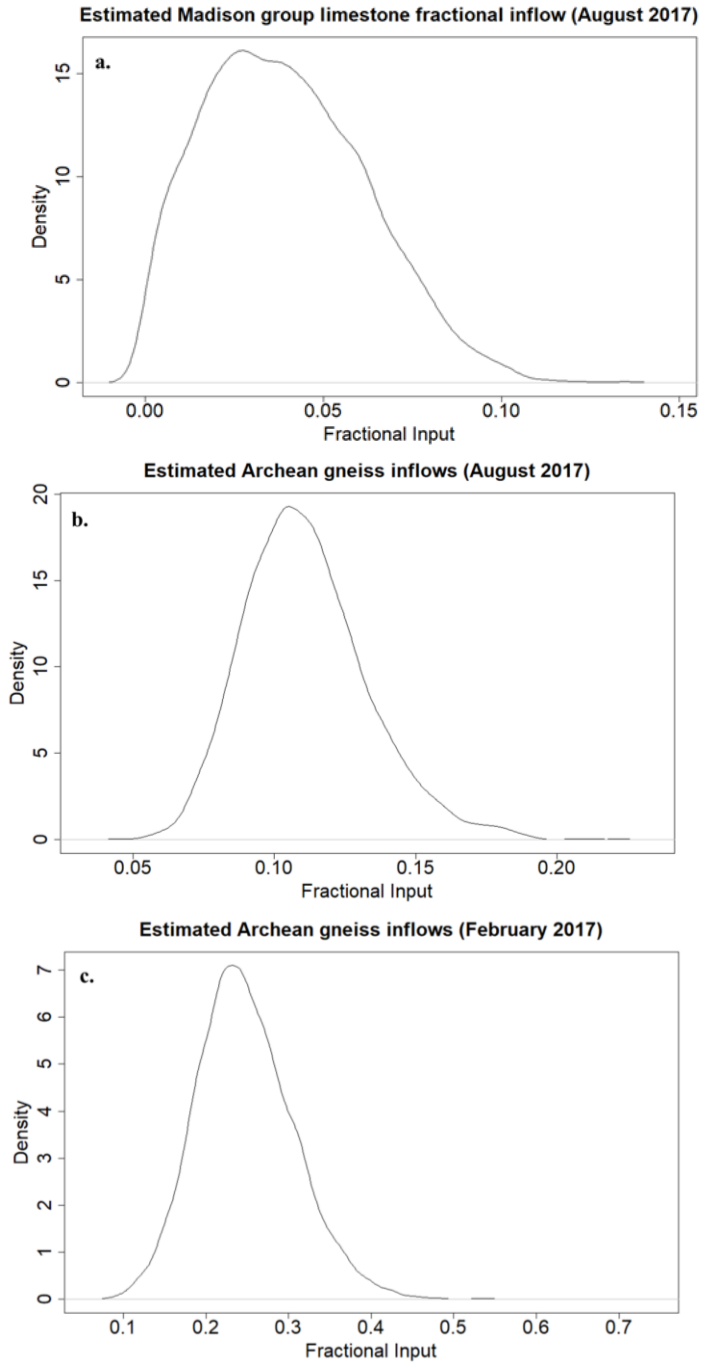

Figure D.1 Probability density plots of fractional contributions of inflows to Hyalite Creek. Panels (c), (b), and (c) are probability density plots summarizing the distributions of the ensemble of estimated aquifer contributions to stream flow (i.e. locations of beige circles on semi-transparent black lines in Figure 3.7). Contributions are estimated for discreet segments of Hyalite Creek from: (a) the Madison group limestone aquifer at 1920 m elevation in August 2017; (c) the Archean gneiss aquifer in lower Hyalite Canyon in August 2017; and (e) the Archean gneiss aquifer in February 2017.

APPENDIX E

R-CODE FOR MONTE CARLO REALIZATIONS AND MAXIMUM LIKLIHOOD OPTIMIZATION

The following code example uses a 2-component mixture of springs from the Madison Group Limestones (sites HY16, HY17) and Hyalite Creek below Hyalite Reservoir (site HY7) to form a mixture at site HY10. The code takes a normal distribution, based on the variation within sample sites and sample dates, of the Sr and U concentration and isotopic composition of each end member. A mixing line realization is constructed sampling from the normal distributions U and Sr concentration and isotopic composition of each end member. A monte carlo analysis repeats the construction of a mixing line realization 5,000 times. A maximum likelihood optimization function is performed on each mixing line realization to find the point on the mixing line most like the defined mixture composition.

```
#Set working directory and get CSV
setwd("~/GRW/CSV")
HY.Mixing <- read.csv("180305_GRW_Mixing.csv", stringsAsFactors = FALSE)
attach(HY.Mixing)

# Calculate the discreet fractions of end members
# from the cumulative fractions
disFrac <- function(f)
{
  remaining <- 1 - f[1];
  if (length(f)>=2)
  {
    for (i in 2:length(f))
    {
      f[i] <- remaining * f[i];
      remaining <- remaining - f[i];
    }
  }
  return(c(f, remaining));
}

# Mixing function to calculate chemical composition
# based on fractional composition of end members
#f = fraction, v=vector of values
#adding isotope, if just concentration run old mix
#if isotope True, if just concentrations NA
mix <- function(
  f,
  endMembers,
  is.isotope=numeric(length = 0),
  endMembers.isotopes=NA
)
{
```

```
 results <- apply(
  endMembers,
  2,
  function(v, f) {
   return(sum (v * f));
  },
  f = f
 )

 if(!length(is.isotope)==0)
 {

  for(index in 1:length(is.isotope))
  {
   if(is.isotope[index])
   {
    product <- sum(f*endMembers[,index]*endMembers.isotopes[,index])
    results <- c(results, product/results[index]) #to get just it iso not iso*conc
   }
  }
 }
 return(results)
}


#Defining mainstem upstream of Archean endmember##
#Just using Aug.17 and sites HY14 and HY15, in Archean above the shear zone#
Middle.Sr.conc <- c(HY.Mixing$Srppm[SampleID=="GRW_20170824_HY014"],
                    HY.Mixing$Srppm[SampleID=="GRW_20170824_HY015"])

Middle.U.conc <- c(HY.Mixing$TIMSU[SampleID=="GRW_20170824_HY014"],
                   HY.Mixing$TIMSU[SampleID=="GRW_20170824_HY015"])

Middle.Sr.iso <- c(HY.Mixing$Sr8786[SampleID=="GRW_20170824_HY014"],
                   HY.Mixing$Sr8786[SampleID=="GRW_20170824_HY015"])

Middle.U.iso <- c(HY.Mixing$UAR[SampleID=="GRW_20170824_HY014"],
                  HY.Mixing$UAR[SampleID=="GRW_20170824_HY015"])

#Defining Gneiss endmember#
#Using wells GW2 and GW3 from May.17 sampling#
Gneiss.Sr.conc <- c(HY.Mixing$Srppm[SampleID=="GRW_20170518_GW002"],
                    HY.Mixing$Srppm[SampleID=="GRW_20170518_GW003"])
```

```
Gneiss.U.conc <- c(HY.Mixing$TIMSU[SampleID=="GRW_20170518_GW002"],
                   HY.Mixing$TIMSU[SampleID=="GRW_20170518_GW003"])

Gneiss.Sr.iso <- c(HY.Mixing$Sr8786[SampleID=="GRW_20170518_GW002"],
                   HY.Mixing$Sr8786[SampleID=="GRW_20170518_GW003"])

Gneiss.U.iso <- c(HY.Mixing$UAR[SampleID=="GRW_20170518_GW002"],
                  HY.Mixing$UAR[SampleID=="GRW_20170518_GW003"])

##Run as mean value for each endmember###
#Define the tracer concentrations for the end members
#mean of endmembers
endMembers.conc.mean <- data.frame(
  Sr.conc = c(mean(Middle.Sr.conc), mean(Gneiss.Sr.conc)),
  U.conc = c(mean(Middle.U.conc), mean(Gneiss.U.conc)),
  row.names = c("Middle", "Gneiss")
);

endMembers.isotopes.mean <- data.frame(
  Sr.iso = c(mean(Middle.Sr.iso), mean(Gneiss.Sr.iso)),
  U.iso = c(mean(Middle.U.iso), mean(Gneiss.U.iso)),
  row.names = c("Middle", "Gneiss")
);

#Generally agree with sds, keeping sds instead of choosing them#
endMembers.conc.sd <- data.frame(
  Sr.conc = c(sd(Middle.Sr.conc), sd(Gneiss.Sr.conc)),
  U.conc = c(sd(Middle.U.conc), sd(Gneiss.U.conc)),
  row.names = c("Middle", "Gneiss")
);

endMembers.isotopes.sd <- data.frame(
  Sr.iso = c(sd(Middle.Sr.iso), sd(Gneiss.Sr.iso)),
  U.iso = c(sd(Middle.U.iso), sd(Gneiss.U.iso)),
  row.names = c("Middle", "Gneiss")
);

###Mixture###
#From HY5 on Aug.17#
sample <- c(
  Sr.conc = HY.Mixing$Srppm[SampleID=="GRW_20170824_HY005"],
  U.conc = HY.Mixing$TIMSU[SampleID=="GRW_20170824_HY005"],
  Sr.iso = HY.Mixing$Sr8786[SampleID=="GRW_20170824_HY005"],
  U.iso = HY.Mixing$UAR[SampleID=="GRW_20170824_HY005"]
```

```
);


optimmix <- function(cumf, endMembers, obs, sd, is.isotope=NA,
endMembers.isotopes=NA)
{
 # Calculate the prediction using the mixing function
 pred <- mix(f = disFrac(cumf),
          endMembers = endMembers,
          is.isotope = is.isotope,
          endMembers.isotopes = endMembers.isotopes);

 #Return the max liklihood#
 return(sum(-(dnorm(obs, mean=pred, sd=sd, log = TRUE))));
}

realizations <- 10000

ensemble <- data.frame(Middle = rep(NaN, realizations),
                Gneiss = rep(NaN, realizations),
                Mix.Sr.conc = rep(NaN, realizations),
                Mix.U.conc = rep(NaN, realizations),
                Mix.Sr.iso = rep(NaN, realizations),
                Mix.U.iso = rep(NaN, realizations),
                Middle.Sr.conc = rep(NaN, realizations),
                Gneiss.Sr.conc = rep(NaN, realizations),
                Middle.U.conc = rep(NaN, realizations),
                Gneiss.U.conc = rep(NaN, realizations),
                Middle.Sr.iso = rep(NaN, realizations),
                Gneiss.Sr.iso = rep(NaN, realizations),
                Middle.U.iso = rep(NaN, realizations),
                Gneiss.U.iso = rep(NaN, realizations))

for (realization in 1:realizations){

 #sample from normal distribution with mean and standard deviation
 endMembers.conc <- data.frame(
   Sr.conc = rnorm(n=2, mean = endMembers.conc.mean$Sr.conc, sd =
endMembers.conc.sd$Sr.conc),
   U.conc = rnorm(n=2, mean = endMembers.conc.mean$U.conc, sd =
endMembers.conc.sd$U.conc),
   row.names = c("Middle", "Gneiss")
 );
```

```
  endMembers.isotopes <- data.frame(
    Sr = rnorm(n=2, mean = endMembers.isotopes.mean$Sr.iso, sd =
endMembers.isotopes.sd$Sr.iso),
    U = rnorm(n=2, mean = endMembers.isotopes.mean$U.iso, sd =
endMembers.isotopes.sd$U.iso),
    row.names = c("Middle", "Gneiss")
  );


  optimr <- optim(
    par = c(0.5),
    fn = optimmix,
    endMembers = endMembers.conc,
    obs = sample,
    sd = c(0.01, 0.01, 0.00001, 0.001),
    is.isotope = c(TRUE,TRUE),
    endMembers.isotopes = endMembers.isotopes,
    method = "L-BFGS-B",
    lower = rep(0, 1),
    upper = rep(1, 1)
  );

  fractions <- disFrac(optimr$par);
  ensemble[realization,] <- c(fractions,
                              mix(
                                f = fractions,
                                endMembers = endMembers.conc,
                                is.isotope = c(TRUE, TRUE),
                                endMembers.isotopes = endMembers.isotopes),
                              as.vector(as.matrix(endMembers.conc)),
                              as.vector(as.matrix(endMembers.isotopes)));

}


#To Visually represent model#
###Function for Mixng lines#####
##function##
mixingline <- function(
  em,
  Fa = seq(from = 0, to = 1, length.out = 100),
  Fb = seq(from = 1, to = 0, length.out = 100)
){
```

```
  line.Sr <-
(Fa*em["Middle.Sr.iso"]*em["Middle.Sr.conc"]+Fb*em["Gneiss.Sr.iso"]*em["Gneiss.Sr
.conc"])/(Fa*em["Middle.Sr.conc"]+Fb*em["Gneiss.Sr.conc"])
  line.U <-
(Fa*em["Middle.U.iso"]*em["Middle.U.conc"]+Fb*em["Gneiss.U.iso"]*em["Gneiss.U.c
onc"])/(Fa*em["Middle.U.conc"]+Fb*em["Gneiss.U.conc"])
  return(data.frame(Fa, line.U, line.Sr))
}

row <- as.numeric(ensemble[1,])
names(row) <- names(ensemble)
df <- mixingline(row)

#baseplot#
plot(x=df$line.U, y=df$line.Sr, type="l", col=rgb(0,0,0, alpha=0.01),
     xlim = c(1,3.5), ylim = c(0.708,0.75),
     xlab = expression(paste("["^{234}, "U/ ", phantom()^{238}, "U]")),
     ylab = expression(paste(phantom()^{87}, "Sr/ ", phantom()^{86}, "Sr"))
)

#add mixing lines#
for(index in 2:realizations)
{
  row <- as.numeric(ensemble[index,])
  names(row) <- names(ensemble)
  df <- mixingline(row)
  lines(x=df$line.U, y=df$line.Sr, col=rgb(0,0,0, alpha = 0.01))
}

#add fraction points#
points(x=ensemble$Mix.U.iso, y=ensemble$Mix.Sr.iso, col=rgb(1,1,1))

##Make data frame of points to plot###
plot.U.iso <- c(HY.Mixing$UAR[SiteID=="HY14"],
                HY.Mixing$UAR[SiteID=="HY15"],
                HY.Mixing$UAR[SiteID=="GW2"],
                HY.Mixing$UAR[SiteID=="GW3"],
                HY.Mixing$UAR[SiteID=="HY5"],
                HY.Mixing$UAR[SiteID=="HY6"])

plot.Sr.iso <- c(HY.Mixing$Sr8786[SiteID=="HY14"],
                 HY.Mixing$Sr8786[SiteID=="HY15"],
                 HY.Mixing$Sr8786[SiteID=="GW2"],
                 HY.Mixing$Sr8786[SiteID=="GW3"],
```

```
            HY.Mixing$Sr8786[SiteID=="HY5"],
            HY.Mixing$Sr8786[SiteID=="HY6"])

#add endmember points#
points(x=plot.U.iso, y=plot.Sr.iso,
      col=c('dodgerblue4', 'dodgerblue4',
          'tomato3', 'tomato3',
          'slateblue3', 'slateblue3', 'slateblue3','slateblue3','slateblue3', 'slateblue3'),
      pch=16, cex=1.5)
text(x=plot.U.iso, y=plot.Sr.iso,
    labels = c("HY14", "HY15", "GW2", "GW3","HY5", "", "HY5", "HY6",
            "HY6", "HY6"),
    cex=0.8, pos=3)
```

APPENDIX F

DATA STRUCTURE AND CONTENT OF ALL SUPPORTING AND ADDITIONAL DATA STORED ON THE EWING LAB SERVER

- Gallatin-Hyalite Waters
  - Field Sites
  - Field Data *Field data and discharge sheets for surface water and groundwater sampling*
    - Field Photos *Photos of sampling trips*
    - Location Data *Summary of spatial data for all site locations*
    - GWIC Well Summaries *MBMG GWIC well summaries for wells sampled*
    - Home Owner Emails *Drafts of emails sent to homeowners whose wells were sampled*
  - Soils *Bulk density, milling, and chemical data associated with soils sampled for GRW project*
  - Presentations
    - Ewing Presentations 2017 *GRW presentations by Dr. Ewing in 2017*
    - GRW Meetings *Miller led presentations for GRW meetings*
    - EGU 2018 *Dr. Ewing's EGU presentation in 2018*
    - Lab Meetings *Miller led presentations for Ewing lab meetings*
  - Grants, Reports, Proposals
    - GRW annual reports
      - GRW annual report 2018
      - GRW annual report 2017
    - USGS 104g grant
    - Media
  - Chemical Data *Includes GRW Master Data and Sample Inventory*
    - U and Sr Purification *Data for preparations and results of U and Sr isotopic analysis*
    - Raw Data Files
      - Dionex *Data files for water samples ran at MSU EAL on the Dionex*
      - ICP Data *Data files for water samples ran at MSU EAL and MBMG on the ICP*
      - Shimadzu *Data files for water samples ran at MSU EAL on the Shimadzu*
  - Literature *Literature related to the GRW project in general*
    - Local Sr Values *Literature referencing $^{87}Sr/^{86}Sr$ values for local rock units*
    - Gallatin theses & related *Theses relating the water in Hyalite and the Gallatin Valley*
    - U and Sr-related articles
    - Weathering
    - Alkalinity in rivers
  - R *Additional plots on the GRW project not used for Miller thesis*
    - Runoff *Plots on runoff conditions*
    - HY Plots *Hyalite Radon plots and old Hyalite isotope plots*
    - Mixing *Old drafts of mixing models, showing evolution of the model*
    - GV Plots *Old Gallatin Valley isotopic plots*

- Michalek_Data_Exercise *PCA from MBMG data*
- GRWGIS *All information related to Miller's GIS work on GRW project*
  - Hillshades *Data files used for hillshades*
  - Watershed Analysis *All data files relating to Miller's Hyalite watershed analysis*
  - Glacial Extent *Pinedale and Bulllake glacial extents in Hyalite*
  - WorkingDrafts *All maps made during GRW project work by Miller*
  - Water *All water GIS data including rivers, lakes, streams, and waterways*
  - Geology *All geologic layers used for mapping*
    - gallatin_valley_48k
    - bozeman09_100k *USGS quadrangle*
    - w_gallatin_50k
    - livingston_100k *USGS quadrangle*
    - ennis_100k *USGS quadrangle*
    - gardiner_100k *USGS quadrangle*
    - hebgen_lake_100k *USGS quadrangle*
    - MTgeol_dd
    - MTseamless *Map layer used for Hyalite paper figures*
  - Data *Location and chemical data used for GIS mapping*
  - MontanaStateBoundary_shp *Boundary of Montana used for location inset*
- Bozeman Area Geology and Maps
- Noble_Gas_Sampling
- ESturn Work
- Water Isotopes

MillerEwing
- Miller_Thesis
  - GV Paper *All drafts, data, code, and references related to the Ch.4 Gallatin Valley paper*
    - References *PDFs of all papers referenced in the Gallatin paper*
    - Figures *All code and associated CSVs used for figures of the Gallatin paper*
    - Tables *Excel files of all tables made for Gallatin paper*
    - Gallatin GIS *All GIS layers and maps used for Gallatin paper GIS figures*
  - HY Paper *All drafts, data, code and reference related to the Ch.3 Hyalite Canyon Paper*
    - LocalSr *Steve Custer's compilation of local Sr values*
    - Figures *All code and associated CSVs used for figures and models of the Hyalite paper*
    - Hyalite Data Set *Complete data set of all data used for Hyalite paper*
    - Tables *Excel files of all tables made for Hyalite paper*
    - References *PDFs of all papers referenced in the Hyalite paper*

- Hyalite GIS *All GIS layers and maps used for Hyalite paper GIS figures*
- Conclusion *All drafts related to Miller Thesis Conclusions*
- Appendices *All drafts related to Miller Thesis Appendices*
- Lit Review *All drafts and references related to Miller Thesis Literature Review*
  - References *PDFs of all papers referenced in Miller Thesis Literature Review*
- Introduction *All drafts and references related to Miller Thesis Introduction*
  - References *PDFs of all papers referenced in Miller Thesis Introduction*

MillerF_Presentations

- LRESColloqium2018 *Presentation for 2018 LRES Research Colloqium*
- AWRA 2017 GRW *Presentation for 2017 AWRA Conference*
- Seminar2017 *Presentation for Fall 2017 LRES Seminar class*
- Nielsen Fellowship *Write up summarizing work completed as part of the Nielsen Fellowship*

APPENDIX G

COMPLETE CHEMICAL DATA ANALYZED FROM THE GRW STUDY TO DATE

Table G.1 Water analysis of total carbon (TC), inorganic carbon (IC), NPOC, and total nitrogen (TN) analyzed at the MSU-EAL.

Sample ID	Site ID	Sampling Date	TC (mg C L^{-1})	uncertainty	flag*	IC (mg C L^{-1})	uncertainty	flag*	NPOC (mg C L^{-1})	uncertainty	flag*	TN (mg N L^{-1})	uncertainty	flag*
GRW_20170831_GV010	GV10	8/31/2017	43.17	3.45	ok	0.00	0.00	bdl	0.70	0.07	ok	0.87	0.04	ok
GRW_20170831_GV009	GV9	8/31/2017	45.99	3.68	ok	32.44	2.60	ok	1.21	0.12	ok	0.85	0.04	ok
GRW_20170825_GV008	GV8	8/25/2017	27.74	2.22	ok	19.62	3.14	bql	0.19	0.00	bql	0.08	0.01	bdl
GRW_20160226_GV007	GV7	2/26/2016	42.31			38.66						0.51	0.74	
GRW_20160506_GV007	GV7	5/6/2016	27.87	1.95	ok	24.41	1.71	ok	3.10	0.22	ok	0.20	0.10	ok
GRW_20160707_GV007	GV7	7/7/2016	34.56	1.73	ok	32.11	1.61	ok	1.58	0.11	ok	0.14	0.01	ok
GRW_20160826_GV007	GV7	8/26/2016	37.51	1.88	ok	35.41	1.77	ok	1.45	0.07	ok	0.3299	0.03	ok
GRW_20170205_GV007	GV7	2/5/2017							0.92	0.05	ok	0.08	0.00	ok
GRW_20170517_GV007	GV7	5/17/2017	28.01	1.40	ok	24.36	1.22	ok	2.62	0.13	ok	0.30	0.03	ok
GRW_20170825_GV007	GV7	8/25/2017	37.98	3.04	ok	26.84	2.15	ok	0.78	0.08	ok	0.52	0.03	ok
GRW_20160226_GV006	GV6	2/26/2016	51.30			47.33						0.39	0.64	
GRW_20160506_GV006	GV6	5/6/2016	34.88	2.44	ok	31.65	2.22	ok	3.18	0.22	ok	0.14	0.10	ok
GRW_20160707_GV006	GV6	7/7/2016	42.97	2.15	ok	40.11	2.01	ok	1.92	0.13	ok	0.11	0.01	ok
GRW_20160826_GV006	GV6	8/26/2016	44.76	2.24	ok	43.41	2.17	ok	2.00	0.10	ok	0.1604	0.02	ok
GRW_20170517_GV006	GV6	5/17/2017	36.44	1.82	ok	32.24	1.61	ok	2.94	0.15	ok	0.30	0.03	ok
GRW_20170825_GV006	GV6	8/25/2017	43.81	3.50	ok	29.57	2.37	ok	2.70	0.27	ok	0.38	0.02	ok
GRW_20160226_GV005	GV5	2/26/2016	24.09			20.81						0.19	0.37	
GRW_20160506_GV005	GV5	5/6/2016	30.32	2.12	ok	26.34	1.84	ok	3.01	0.21	ok	0.25	0.10	ok
GRW_20160707_GV005	GV5	7/7/2016	25.06	1.25	ok	23.30	1.17	ok	1.32	0.09	ok	0.00	0.01	bql
GRW_20160826_GV005	GV5	8/26/2016	30.44	1.52	ok	29.15	1.46	ok	1.21	0.06	ok	0.0987	0.02	ok
GRW_20170517_GV005	GV5	5/17/2017	26.35	1.32	ok	22.45	1.12	ok	2.81	0.14	ok	0.25	0.02	ok
GRW_20170825_GV005	GV5	8/25/2017	32.64	2.61	ok	22.42	3.59	bql	1.12	0.11	ok	0.15	0.01	ok
GRW_20160506_GV004	GV4	5/6/2016	21.08	1.48	ok	16.59	1.16	ok	3.88	0.27	ok	0.12	0.10	ok
GRW_20160707_GV004	GV4	7/7/2016	22.10	1.11	ok	20.55	1.03	ok	1.25	0.09	ok	0.00	0.01	bql
GRW_20160826_GV004	GV4	8/26/2016	25.55	1.28	ok	21.30	1.07	ok				0.00	0.02	bql

GRW_20170205_GV004	GV4	2/5/2017							0.95	0.05	ok	0.08	0.00	ok
GRW_20170517_GV004	GV4	5/17/2017	21.92	1.10	ok	18.26	0.91	ok	2.83	0.14	ok	0.17	0.02	ok
GRW_20170825_GV004	GV4	8/25/2017	24.86	1.99	ok	17.28	2.76	bql	0.22	0.02	ok	0.09	0.00	ok
GRW_20160226_GV003	GV3	2/26/2016	30.37			26.72						0.23	0.37	
GRW_20160506_GV003	GV3	5/6/2016	20.43	1.43	ok	15.52	1.09	ok	3.86	0.27	ok	0.14	0.10	ok
GRW_20160707_GV003	GV3	7/7/2016	21.10	1.06	ok	19.65	0.98	ok	1.22	0.09	ok	0.00	0.01	bql
GRW_20160826_GV003	GV3	8/26/2016	24.78	1.24	ok	22.87	1.14	ok	0.91	0.05	ok	0.00	0.02	bql
GRW_20170205_GV003	GV3	2/5/2017							1.77	0.09	ok	0.08	0.00	ok
GRW_20170517_GV003	GV3	5/17/2017	21.53	1.08	ok	17.71	0.89	ok	2.91	0.15	ok	0.17	0.02	ok
GRW_20170825_GV003	GV3	8/25/2017	24.02	1.92	ok	16.16	2.59	bql	0.49	0.05	ok	0.16	0.01	ok
GRW_20160226_GV002	GV2	2/26/2016	37.59			35.76						0.23	0.39	
GRW_20160506_GV002	GV2	5/6/2016	22.98	1.61	ok	20.60	1.44	ok	1.63	0.11	ok	0.15	0.10	ok
GRW_20160707_GV002	GV2	7/7/2016	38.93	1.95	ok	37.75	1.89	ok	1.36	0.10	ok	0.00	0.01	bql
GRW_20160825_GV002	GV2	8/25/2016	34.17	1.71	ok	33.06	1.65	ok	1.08	0.05	ok	0.00	0.02	bql
GRW_20170205_GV002	GV2	2/5/2017							0.62	0.03	ok	0.07	0.00	ok
GRW_20170517_GV002	GV2	5/17/2017	23.96	1.20	ok	21.00	1.05	ok	1.72	0.09	ok	0.16	0.02	ok
GRW_20170825_GV002	GV2	8/25/2017	30.27	2.42	ok	0.00	0.00	bdl	0.14	0.00	bql	0.07	0.01	bdl
GRW_20160226_GV001	GV1	2/26/2016	21.78			18.24						0.19	0.37	
GRW_20160506_GV001	GV1	5/6/2016	22.81	1.60	ok	16.74	1.17	ok	4.39	0.31	ok	0.00	0.10	bdl
GRW_20160707_GV001	GV1	7/7/2016	12.26	0.61	ok	10.88	0.54	ok	1.39	0.10	ok	0.00	0.01	bql
GRW_20160825_GV001	GV1	8/25/2016	12.99	0.65	ok	11.45	0.57	ok	1.49	0.07	ok	0.1393	0.02	ok
GRW_20170205_GV001	GV1	2/5/2017							0.60	0.03	ok	0.08	0.00	ok
GRW_20170517_GV001	GV1	5/17/2017	21.95	1.10	ok	18.03	0.90	ok	3.36	0.17	ok	0.14	0.01	ok
GRW_20170825_GV001	GV1	8/25/2017	12.11	0.97	ok	7.64	1.22	bql	0.55	0.05	ok	0.13	0.01	ok
GRW_20180327_HY017	HY17	3/27/2018	35.59	3.56	ok	37.01	3.70	ok	0.48	0.10	ok	0.28	0.03	ok
GRW_20170824_HY015	HY15	8/24/2017	11.09	0.89	ok	6.74	1.08	bql	0.58	0.06	ok	0.17	0.01	ok
GRW_20170824_HY014	HY14	8/24/2017	11.12	0.89	ok	6.79	1.09	bql	0.59	0.06	ok	0.21	0.01	ok
GRW_20170824_HY013	HY13	8/24/2017	14.19	1.14	ok	9.24	1.48	bql	0.12	0.00	bql	0.06	0.01	bdl

GRW_20170823_HY012	HY12	8/23/2017	47.15	3.77	ok	33.50	2.68	ok	0.92	0.09	ok	0.15	0.01	ok
GRW_20170823_HY011	HY11	8/23/2017	10.61	0.85	ok	6.39	1.02	bql	0.55	0.05	ok	0.22	0.01	ok
GRW_20170823_HY010	HY10	8/23/2017	10.55	0.84	ok	6.32	1.01	bql	0.61	0.06	ok	0.20	0.01	ok
GRW_20180327_HY010	HY10	3/27/2018	18.79	1.88	ok	15.46	1.55	ok	1.54	0.08	ok	0.41	0.07	ok
GRW_20170823_HY009	HY9	8/23/2017	8.41	0.67	ok	4.81	0.77	bdl	0.58	0.06	ok	0.21	0.01	ok
GRW_20180327_HY009	HY9	3/27/2018	13.42	1.34	ok	11.86	1.19	ok	1.37	0.07	ok	0.16	0.01	ok
GRW_20170204_HY008	HY8	2/4/2017							0.68	0.03	ok	0.72	0.04	ok
GRW_20170516_HY008	HY8	5/16/2017	24.49	1.22	ok	17.41	0.87	ok	5.55	0.28	ok	0.21	0.02	ok
GRW_20170823_HY008	HY8	8/23/2017	30.91	2.47	ok	23.70	3.79	bql	1.25	0.13	ok	0.10	0.00	ok
GRW_20180327_HY008	HY8	3/27/2018	23.93	2.39	ok	18.03	1.80	ok	4.83	0.48	aql	0.52	0.07	ok
GRW_20170204_HY007	HY7	2/4/2017							0.58	0.03	ok	0.11	0.01	ok
GRW_20170516_HY007	HY7	5/16/2017	12.96	0.65	ok	9.28	0.46	ok	3.19	0.16	ok	0.13	0.01	ok
GRW_20170823_HY007	HY7	8/23/2017	8.03	0.64	ok	3.90	0.62	bdl	0.58	0.06	ok	0.24	0.01	ok
GRW_20180327_HY007	HY7	3/27/2018	12.08	1.21	ok	9.67	0.97	ok	1.56	0.08	ok	0.51	0.08	ok
GRW_20160209_HY006	HY6	2/9/2016	18.21			17.03						0.16	0.30	
GRW_20160219_HY006	HY6	2/19/2016	22.08			17.90						0.20	0.38	
GRW_20160518_HY006	HY6	5/18/2016	22.18	1.55	ok	16.74	1.17	ok	4.42	0.31	ok	0.00	0.10	bdl
GRW_20160706_HY006	HY6	7/6/2016	12.20	0.61	ok	10.27	0.51	ok	1.68	0.12	ok	0.00	0.01	bql
GRW_20160825_HY006	HY6	8/25/2016	12.18	0.61	ok	11.08	0.55	ok	1.50	0.07	ok	0.1466	0.02	ok
GRW_20170204_HY006	HY6	2/4/2017							0.56	0.03	ok	0.12	0.01	ok
GRW_20170516_HY006	HY6	5/16/2017	22.16	1.11	ok	17.33	0.87	ok	3.61	0.18	ok	0.15	0.01	ok
GRW_20170824_HY006	HY6	8/24/2017	11.95	0.96	ok	6.66	1.07	bql	0.60	0.06	ok	0.13	0.01	ok
GRW_20180327_HY006	HY6	3/27/2018	19.31	1.93	ok	17.49	1.75	ok	1.42	0.07	ok	0.27	0.04	ok
GRW_20160209_HY005	HY5	2/9/2016	17.94			16.94						0.16	0.31	
GRW_20160219_HY005	HY5	2/19/2016	21.43			17.93						0.23	0.37	
GRW_20160518_HY005	HY5	5/18/2016	22.37	1.57	ok	17.06	1.19	ok	4.56	0.32	ok	0.00	0.10	bdl
GRW_20160706_HY005	HY5	7/6/2016	11.90	0.60	ok	11.19	0.56	ok	1.42	0.10	ok	0.00	0.01	bql
GRW_20160825_HY005	HY5	8/25/2016	11.84	0.59	ok	10.70	0.54	ok	1.33	0.07	ok	0.1430	0.02	ok

GRW_20170516_HY005	HY5	5/16/2017	22.14	1.11	ok	17.51	0.88	ok	3.55	0.18	ok	0.14	0.01	ok
GRW_20170824_HY005	HY5	8/24/2017	12.20	0.98	ok	6.77	1.08	bql	0.66	0.07	ok	0.14	0.01	ok
GRW_20180327_HY005	HY5	3/27/2018	19.01	1.90	ok	17.61	1.76	ok	1.42	0.07	ok	0.20	0.01	ok
GRW_20160209_HY004	HY4	2/9/2016	16.06			16.12						0.15	0.28	
GRW_20160219_HY004	HY4	2/19/2016	21.40			17.54						0.24	0.40	
GRW_20160518_HY004	HY4	5/18/2016	23.04	1.61	ok	18.61	1.30	ok	3.97	0.28	ok	0.00	0.10	bdl
GRW_20160706_HY004	HY4	7/6/2016	11.76	0.59	ok	10.32	0.52	ok	1.65	0.12	ok	0.00	0.01	bql
GRW_20160825_HY004	HY4	8/25/2016	11.88	0.59	ok	10.66	0.53	ok	1.36	0.07	ok	0.1620	0.02	ok
GRW_20170204_HY004	HY4	2/4/2017							0.46	0.02	ok	0.12	0.01	ok
GRW_20170516_HY004	HY4	5/16/2017	23.02	1.15	ok	18.44	0.92	ok	3.25	0.16	ok	0.14	0.01	ok
GRW_20170823_HY004	HY4	8/23/2017	11.39	0.91	ok	6.34	1.01	bql	0.60	0.06	ok	0.17	0.01	ok
GRW_20180327_HY004	HY4	3/27/2018	18.01	1.80	ok	18.09	1.81	ok	1.19	0.06	ok	0.14	0.01	ok
GRW_20160209_HY003	HY3	2/9/2016	40.14			38.88						0.17	0.31	
GRW_20160219_HY003	HY3	2/19/2016	41.02			36.45						0.25	0.39	
GRW_20160518_HY003	HY3	5/18/2016	18.35	1.28	ok	12.90	0.90	ok	6.40	0.45	aql	0.00	0.10	bdl
GRW_20160706_HY003	HY3	7/6/2016	40.14	2.01	ok	36.23	1.81	ok	2.64	0.19	ok	0.00	0.01	bql
GRW_20160825_HY003	HY3	8/25/2016	42.15	2.11	ok	39.94	2.00	ok	1.83	0.09	ok	0.00	0.02	bql
GRW_20170204_HY003	HY3	2/4/2017							0.89	0.04	ok	0.09	0.00	ok
GRW_20170516_HY003	HY3	5/16/2017	21.58	1.08	ok	14.51	0.73	ok	5.67	0.28	ok	0.19	0.02	ok
GRW_20170823_HY003	HY3	8/23/2017	45.61	3.65	ok	29.61	2.37	ok	1.18	0.12	ok	0.13	0.01	ok
GRW_20180327_HY003	HY3	3/27/2018	34.21	3.42	ok	31.69	3.17	ok	2.93	0.29	aql	0.24	0.03	ok
GRW_20160209_HY002	HY2	2/9/2016	6.96			6.27						0.15	0.29	
GRW_20160219_HY002	HY2	2/19/2016	10.31			6.60						0.20	0.39	
GRW_20160518_HY002	HY2	5/18/2016	7.72	0.54	ok	5.34	0.37	ok	1.83	0.13	ok	0.00	0.10	bdl
GRW_20160706_HY002	HY2	7/6/2016	0.00	0.50	bql	5.41	0.27	ok	1.19	0.08	ok	0.00	0.01	bql
GRW_20160825_HY002	HY2	8/25/2016	0.00	0.00	bql	5.971	0.30	ok	0.88	0.04	ok	0.00	0.02	bql
GRW_20170204_HY002	HY2	2/4/2017							0.17	0.01	ok	0.01	0.00	bql
GRW_20170516_HY002	HY2	5/16/2017	7.53	0.38	ok	5.42	0.27	ok	1.83	0.09	ok	0.09	0.01	ok

GRW_20170823_HY002	HY2	8/23/2017	7.22	0.58	ok	3.51	0.56	bdl	0.07	0.00	bdl	0.07	0.01	bdl
GRW_20160209_HY001	HY1	2/9/2016	5.14			4.09						0.18	0.31	
GRW_20160219_HY001	HY1	2/19/2016	6.85			4.28						0.20	0.37	
GRW_20160518_HY001	HY1	5/18/2016	6.36	0.44	ok	4.40	0.31	ok	1.76	0.12	ok	0.00	0.10	bdl
GRW_20160706_HY001	HY1	7/6/2016	0.00	0.50	bql			bql	1.03	0.07	ok	0.00	0.01	bql
GRW_20160825_HY001	HY1	8/25/2016	0.00	0.00	bql	4.365	0.22	ok	1.00	0.05	ok	0.00	0.02	bql
GRW_20170204_HY001	HY1	2/4/2017							1.99	0.10	ok	0.10	0.01	ok
GRW_20170516_HY001	HY1	5/16/2017	6.97	0.35	ok	5.18	0.26	ok	1.78	0.09	ok	0.09	0.01	ok
GRW_20170823_HY001	HY1	8/23/2017	5.28	0.42	ok	2.20	0.35	bdl			bdl	0.07	0.01	bdl
GRW_20180327_HY001	HY1	3/27/2018	6.80	0.68	ok	4.66	0.47	ok	1.31	0.07	ok	0.42	0.04	ok
GRW_20170622_GW001	GW1	6/22/2017	48.37	4.84	ok	43.33	4.33	ok	2.22	0.22	ok	2.86	0.29	aql
GRW_20170518_GW002	GW2	5/18/2017	17.31	0.87	ok	14.72	0.74	ok	4.28	0.21	ok	0.20	0.02	ok
GRW_20170518_GW003	GW3	5/18/2017	31.94	1.60	ok	31.91	1.60	ok	0.39	0.02	ok	0.16	0.02	ok
GRW_20170620_GW004	GW4	6/20/2017	33.15	3.32	ok	30.52	3.05	ok	0.95	0.09	ok	2.49	0.25	aql
GRW_20170622_GW005	GW5	6/22/2017	101.60	10.16	aql	93.39	9.34	aql	1.17	0.12	ok	8.70	0.87	aql
GRW_20170622_GW006	GW6	6/22/2017	27.91	2.79	ok	25.77	2.58	ok	0.49	0.05	ok	1.73	0.17	ok
GRW_20170622_GW007	GW7	6/22/2017	27.94	2.79	ok	25.92	2.59	ok	0.35	0.03	ok	1.52	0.15	ok
GRW_20170720_GW008	GW8	7/20/2017	35.42	2.83	ok			bdl			bdl	0.72	0.04	ok
GRW_20170720_GW009	GW9	7/20/2017	77.21	12.35	aql			bdl	0.62	0.06	ok	0.15	0.01	ok

*ok: sample within instrument detection limit, bdl: below detection limit, bql: below quantification limit, aql: above quantification limit.

Table G.2 Water analysis of Cl^-, SO_4^{2-}, and NO_3^- analyzed at the MSU-EAL.

Sample ID	Site ID	Sampling Date	Cl^- (mg L^{-1})	uncertainty	flag*	SO_4^{2-} (mg S L^{-1})	uncertainty	flag*	NO_3^- (mg N L^{-1})	uncertainty	flag*
GRW_20180524_GV012	GV12	5/24/2018	0.72	0.07	ok	2.41	0.36	ok	0.038	0.006	ok
GRW_20180524_GV011	GV11	5/24/2018	0.31	0.03	ok	0.36	0.05	ok	0.018	0.010	bql
GRW_20170831_GV010	GV10	8/31/2017	9.72	1.94	ok	6.93	1.39	aql	0.670	0.134	ok
GRW_20180524_GV010	GV10	5/24/2018	4.60	0.46	ok	3.32	0.50	ok	0.373	0.056	ok
GRW_20170831_GV009	GV9	8/31/2017	14.12	2.82	ok	6.55	1.31	ok	0.541	0.108	ok
GRW_20180524_GV009	GV9	5/24/2018	4.55	0.45	ok	2.63	0.39	ok	0.295	0.044	ok
GRW_20170825_GV008	GV8	8/25/2017	1.89	0.38	ok	10.04	2.01	aql	0.002	0.010	bql
GRW_20160226_GV007	GV7	2/26/2016	6.26	0.31	ok	11.42	1.14	aql	0.565	0.057	aql
GRW_20160506_GV007	GV7	5/6/2016	2.70	0.13	ok	6.17	0.31	ok	0.155	0.008	ok
GRW_20160707_GV007	GV7	7/7/2016	6.72	0.67	aql	8.08	0.40	ok	0.057	0.003	ok
GRW_20160826_GV007	GV7	8/26/2016	6.69	0.67	aql	9.53	0.95	aql	0.265	0.013	ok
GRW_20170205_GV007	GV7	2/5/2017	4.79	0.24	ok	11.60	1.16	aql	0.648	0.065	aql
GRW_20170517_GV007	GV7	5/17/2017	2.43	0.12	ok	5.49	0.27	ok	0.145	0.007	ok
GRW_20170825_GV007	GV7	8/25/2017	7.89	1.58	ok	9.87	1.97	aql	0.297	0.059	ok
GRW_20180524_GV007	GV7	5/24/2018	1.84	0.18	ok	3.34	0.50	ok	0.113	0.017	ok
GRW_20160226_GV006	GV6	2/26/2016	13.73	1.37	aql	6.53	0.33	ok	0.310	0.015	ok
GRW_20160506_GV006	GV6	5/6/2016	3.56	0.18	ok	2.85	0.14	ok	0.056	0.003	ok
GRW_20160707_GV006	GV6	7/7/2016	7.64	0.76	aql	5.74	0.29	ok	0.012	0.001	ok
GRW_20160826_GV006	GV6	8/26/2016	9.32	0.93	aql	6.51	0.33	ok	0.077	0.004	ok
GRW_20170517_GV006	GV6	5/17/2017	4.73	0.24	ok	3.07	0.15	ok	0.124	0.006	ok
GRW_20170825_GV006	GV6	8/25/2017	7.28	1.46	ok	6.56	1.31	ok	0.092	0.018	ok
GRW_20180524_GV006	GV6	5/24/2018	2.93	0.29	ok	2.44	0.37	ok	0.150	0.023	ok
GRW_20160226_GV005	GV5	2/26/2016	0.77	0.04	ok	1.31	0.07	ok	0.004	0.000	bql
GRW_20160506_GV005	GV5	5/6/2016	1.73	0.09	ok	2.97	0.15	ok	0.184	0.009	ok
GRW_20160707_GV005	GV5	7/7/2016	1.25	0.06	ok	8.38	0.42	ok	0.017	0.001	ok

GRW_20160826_GV005	GV5	8/26/2016	1.84	0.09	ok	12.43	1.24	aql	0.056	0.003	ok
GRW_20170517_GV005	GV5	5/17/2017	1.03	0.05	ok	1.91	0.10	ok	0.093	0.005	ok
GRW_20170825_GV005	GV5	8/25/2017	2.59	0.52	ok	11.21	2.24	aql	0.002	0.010	bql
GRW_20180524_GV005	GV5	5/24/2018	0.34	0.03	ok	0.47	0.07	ok	0.024	0.005	bql
GRW_20160506_GV004	GV4	5/6/2016	0.96	0.05	ok	4.74	0.24	ok	0.047	0.002	ok
GRW_20160707_GV004	GV4	7/7/2016	1.02	0.05	ok	8.69	0.87	aql	0.004	0.000	bql
GRW_20160826_GV004	GV4	8/26/2016	1.45	0.07	ok	14.45	1.44	aql	0.005	0.001	bql
GRW_20170205_GV004	GV4	2/5/2017	1.66	0.08	ok	15.32	1.53	aql	0.064	0.003	ok
GRW_20170517_GV004	GV4	5/17/2017	0.99	0.05	ok	4.86	0.24	ok	0.042	0.002	ok
GRW_20170825_GV004	GV4	8/25/2017	1.47	0.29	ok	13.37	2.67	aql	0.011	0.010	bql
GRW_20180524_GV004	GV4	5/24/2018	0.67	0.07	ok	2.24	0.34	ok	0.045	0.007	ok
GRW_20160226_GV003	GV3	2/26/2016	2.05	0.10	ok	18.20	1.82	aql	0.034	0.002	ok
GRW_20160506_GV003	GV3	5/6/2016	0.92	0.05	ok	4.65	0.23	ok	0.049	0.002	ok
GRW_20160707_GV003	GV3	7/7/2016	0.98	0.05	ok	8.74	0.87	aql	0.007	0.001	bql
GRW_20160826_GV003	GV3	8/26/2016	1.36	0.07	ok	14.89	1.49	aql	n.a.		aql
GRW_20170205_GV003	GV3	2/5/2017	1.64	0.08	ok	16.50	1.65	aql	0.068	0.003	ok
GRW_20170517_GV003	GV3	5/17/2017	0.96	0.05	ok	4.92	0.25	ok	0.041	0.002	ok
GRW_20170825_GV003	GV3	8/25/2017	1.34	0.27	ok	13.16	2.63	aql	0.001	0.010	bql
GRW_20180524_GV003	GV3	5/24/2018	0.65	0.06	ok	2.22	0.33	ok	0.033	0.005	ok
GRW_20160226_GV002	GV2	2/26/2016	0.51	0.03	ok	1.04	0.05	ok	0.064	0.003	ok
GRW_20160506_GV002	GV2	5/6/2016	0.34	0.02	ok	0.85	0.04	ok	0.135	0.007	ok
GRW_20160707_GV002	GV2	7/7/2016	0.79	0.04	ok	0.94	0.05	ok	0.066	0.003	ok
GRW_20160825_GV002	GV2	8/25/2016	0.58	0.03	ok	0.94	0.05	ok	n.a.		aql
GRW_20170205_GV002	GV2	2/5/2017	0.49	0.02	ok	1.15	0.06	ok	0.072	0.004	ok
GRW_20170517_GV002	GV2	5/17/2017	0.33	0.02	ok	0.82	0.04	ok	0.074	0.004	ok
GRW_20170825_GV002	GV2	8/25/2017	0.30	0.06	ok	0.56	0.11	ok	n.a.		bdl
GRW_20180524_GV002	GV2	5/24/2018	0.30	0.03	ok	0.52	0.08	ok	0.053	0.008	ok
GRW_20160226_GV001	GV1	2/26/2016	0.25	0.01	ok	1.14	0.06	ok	0.057	0.003	ok

GRW_20160506_GV001	GV1	5/6/2016	0.23	0.02	bql	1.02	0.05	ok	0.011	0.001	bql
GRW_20160707_GV001	GV1	7/7/2016	0.17	0.02	bql	0.53	0.03	ok	0.002	0.000	bql
GRW_20160825_GV001	GV1	8/25/2016	0.15	0.02	bql	0.56	0.03	ok	0.073	0.004	ok
GRW_20170205_GV001	GV1	2/5/2017	0.26	0.01	ok	1.04	0.05	ok	0.038	0.002	ok
GRW_20170517_GV001	GV1	5/17/2017	0.24	0.01	ok	1.00	0.05	ok	0.004	0.000	ok
GRW_20170825_GV001	GV1	8/25/2017	0.18	0.04	ok	0.56	0.11	ok	0.009	0.010	bql
GRW_20180524_GV001	GV1	5/24/2018	0.26	0.03	ok	0.40	0.06	ok	0.001	0.010	bdl
GRW_20171214_HY017	HY17	12/14/2017	0.33	0.07	ok	4.32	0.86	ok	0.110	0.022	ok
GRW_20180129_HY017	HY17	1/29/2018	0.38	0.03	ok	4.58	0.46	ok	0.123	0.012	ok
GRW_20171214_HY016	HY16	12/14/2017	0.34	0.07	ok	4.30	0.86	ok	0.093	0.019	ok
GRW_20170824_HY015	HY15	8/24/2017	0.15	0.03	ok	0.51	0.10	ok	0.055	0.011	ok
GRW_20170824_HY014	HY14	8/24/2017	0.18	0.04	ok	0.52	0.10	ok	0.069	0.014	ok
GRW_20180129_HY014	HY14	1/29/2018	0.27	0.02	ok	1.25	0.12	ok	28.685	4.303	aql
GRW_20170824_HY013	HY13	8/24/2017	0.29	0.06	ok	0.43	0.09	ok	0.031	0.006	ok
GRW_20170823_HY012	HY12	8/23/2017	0.30	0.06	ok	0.63	0.13	ok	0.013	0.010	bql
GRW_20170823_HY011	HY11	8/23/2017	0.16	0.03	ok	0.51	0.10	ok	0.053	0.011	ok
GRW_20170823_HY010	HY10	8/23/2017	0.16	0.03	ok	0.51	0.10	ok	0.061	0.012	ok
GRW_20171214_HY010	HY10	12/14/2017	0.19	0.04	ok	0.76	0.15	ok	n.a.		bdl
GRW_20180129_HY010	HY10	1/29/2018	0.31	0.02	ok	1.23	0.12	ok	0.017	0.010	bql
GRW_20170823_HY009	HY9	8/23/2017	0.15	0.03	ok	0.29	0.06	ok	0.058	0.012	ok
GRW_20171214_HY009	HY9	12/14/2017	0.19	0.04	ok	0.60	0.12	ok	0.001	0.010	bql
GRW_20180129_HY009	HY9	1/29/2018	0.26	0.02	ok	0.82	0.08	ok	0.042	0.010	ok
GRW_20180517_HY009	HY9	5/17/2018	0.20	0.02	ok	0.52	0.05	ok	0.002	0.010	bdl
GRW_20170204_HY008	HY8	2/4/2017	0.34	0.02	ok	1.32	0.07	ok	0.014	0.001	ok
GRW_20170516_HY008	HY8	5/16/2017	0.18	0.01	ok	0.48	0.02	ok	0.004	0.000	ok
GRW_20170823_HY008	HY8	8/23/2017	0.31	0.06	ok	0.70	0.14	ok	0.002	0.010	bql
GRW_20180517_HY008	HY8	5/17/2018	0.19	0.02	ok	0.35	0.03	ok	0.000	0.010	bdl
GRW_20170204_HY007	HY7	2/4/2017	0.21	0.01	ok	0.41	0.02	ok	0.006	0.000	ok

GRW_20170516_HY007	HY7	5/16/2017	0.26	0.01	ok	0.61	0.03	ok	0.006	0.000	ok
GRW_20170823_HY007	HY7	8/23/2017	0.12	0.02	ok	0.22	0.04	ok	0.051	0.010	ok
GRW_20180517_HY007	HY7	5/17/2018	0.19	0.02	ok	0.41	0.04	ok	0.001	0.010	bdl
GRW_20160209_HY006	HY6	2/9/2016	0.21	0.02	bql	1.00	0.05	ok	0.026	0.001	ok
GRW_20160219_HY006	HY6	2/19/2016	0.23	0.02	bql	1.09	0.05	ok	0.018	0.001	ok
GRW_20160518_HY006	HY6	5/18/2016	0.21	0.02	bql	0.93	0.05	ok	0.002	0.000	bql
GRW_20160706_HY006	HY6	7/6/2016	0.16	0.02	bql	0.50	0.03	ok	0.001	0.000	bql
GRW_20160825_HY006	HY6	8/25/2016	0.16	0.02	bql	0.53	0.03	ok	0.067	0.003	ok
GRW_20170204_HY006	HY6	2/4/2017	0.24	0.01	ok	1.01	0.05	ok	0.035	0.002	ok
GRW_20170516_HY006	HY6	5/16/2017	0.24	0.01	ok	1.01	0.05	ok	0.005	0.000	ok
GRW_20170824_HY006	HY6	8/24/2017	0.15	0.03	ok	0.47	0.09	ok	0.011	0.010	bql
GRW_20180517_HY006	HY6	5/17/2018	0.20	0.02	ok	0.60	0.06	ok	0.000	0.010	bdl
GRW_20160209_HY005	HY5	2/9/2016	0.21	0.02	bql	0.97	0.05	ok	0.023	0.001	ok
GRW_20160219_HY005	HY5	2/19/2016	0.22	0.02	bql	1.05	0.05	ok	0.015	0.001	ok
GRW_20160518_HY005	HY5	5/18/2016	0.20	0.02	bql	0.91	0.05	ok	0.002	0.000	bql
GRW_20160706_HY005	HY5	7/6/2016	0.16	0.02	bql	0.49	0.02	ok	0.001	0.000	bql
GRW_20160825_HY005	HY5	8/25/2016	0.14	0.01	bql	0.52	0.03	ok	0.070	0.004	ok
GRW_20170516_HY005	HY5	5/16/2017	0.26	0.01	ok	0.99	0.05	ok	0.004	0.000	ok
GRW_20170824_HY005	HY5	8/24/2017	0.19	0.04	ok	0.52	0.10	ok	0.026	0.005	ok
GRW_20180129_HY005	HY5	1/29/2018	0.29	0.02	ok	1.32	0.13	ok	0.043	0.010	ok
GRW_20180517_HY005	HY5	5/17/2018	0.21	0.02	ok	0.62	0.06	ok	0.001	0.010	bdl
GRW_20160209_HY004	HY4	2/9/2016	0.20	0.02	bql	0.92	0.05	ok	0.007	0.001	bql
GRW_20160219_HY004	HY4	2/19/2016	0.20	0.02	bql	1.00	0.05	ok	0.008	0.001	bql
GRW_20160518_HY004	HY4	5/18/2016	0.20	0.02	bql	0.98	0.05	ok	0.002	0.000	bql
GRW_20160706_HY004	HY4	7/6/2016	0.16	0.02	bql	0.48	0.02	ok	0.001	0.000	bql
GRW_20160825_HY004	HY4	8/25/2016	0.14	0.01	bql	0.50	0.03	ok	0.075	0.004	ok
GRW_20170204_HY004	HY4	2/4/2017	0.24	0.01	ok	0.95	0.05	ok	0.019	0.001	ok
GRW_20170516_HY004	HY4	5/16/2017	0.25	0.01	ok	1.03	0.05	ok	0.005	0.000	ok

GRW_20170823_HY004	HY4	8/23/2017	0.16	0.03	ok	0.48	0.10	ok	0.042	0.008	ok
GRW_20180517_HY004	HY4	5/17/2018	0.21	0.02	ok	0.63	0.06	ok	0.001	0.010	bdl
GRW_20160209_HY003	HY3	2/9/2016	0.25	0.01	ok	2.00	0.10	ok	0.024	0.001	ok
GRW_20160219_HY003	HY3	2/19/2016	0.27	0.01	ok	1.93	0.10	ok	0.013	0.001	ok
GRW_20160518_HY003	HY3	5/18/2016	0.16	0.02	bql	0.60	0.03	ok	0.013	0.001	ok
GRW_20160706_HY003	HY3	7/6/2016	0.16	0.02	bql	0.95	0.05	ok	0.021	0.001	ok
GRW_20160825_HY003	HY3	8/25/2016	0.28	0.01	ok	1.33	0.07	ok	0.003	0.000	bql
GRW_20170204_HY003	HY3	2/4/2017	0.29	0.01	ok	2.58	0.13	ok	0.007	0.000	ok
GRW_20170516_HY003	HY3	5/16/2017	0.20	0.01	ok	0.73	0.04	ok	0.003	0.001	bql
GRW_20170823_HY003	HY3	8/23/2017	0.24	0.05	ok	1.22	0.24	ok	0.004	0.010	bql
GRW_20180517_HY003	HY3	5/17/2018	0.18	0.01	ok	0.57	0.06	ok	0.000	0.010	bdl
GRW_20160209_HY002	HY2	2/9/2016	0.18	0.02	bql	0.33	0.03	bql	0.034	0.002	ok
GRW_20160219_HY002	HY2	2/19/2016	0.18	0.02	bql	0.33	0.03	bql	0.020	0.001	ok
GRW_20160518_HY002	HY2	5/18/2016	0.17	0.02	bql	0.22	0.02	bql	0.013	0.001	bql
GRW_20160706_HY002	HY2	7/6/2016	0.11	0.01	bql	0.20	0.02	bql	0.006	0.001	bql
GRW_20160825_HY002	HY2	8/25/2016	0.13	0.01	bql	0.26	0.03	bql	0.003	0.000	bql
GRW_20170204_HY002	HY2	2/4/2017	0.20	0.01	ok	0.34	0.02	ok	0.033	0.002	ok
GRW_20170516_HY002	HY2	5/16/2017	0.22	0.01	ok	0.25	0.01	ok	0.028	0.001	ok
GRW_20170823_HY002	HY2	8/23/2017	0.14	0.03	ok	0.26	0.05	ok	0.001	0.010	bql
GRW_20180517_HY002	HY2	5/17/2018	0.20	0.02	ok	0.23	0.02	ok	0.018	0.010	bql
GRW_20160209_HY001	HY1	2/9/2016	0.13	0.01	bql	0.15	0.02	bql	0.064	0.003	ok
GRW_20160219_HY001	HY1	2/19/2016	0.13	0.01	bql	0.15	0.02	bql	0.046	0.002	ok
GRW_20160518_HY001	HY1	5/18/2016	0.13	0.01	bql	0.15	0.01	bql	0.006	0.001	bql
GRW_20160706_HY001	HY1	7/6/2016	0.06	0.01	bql	0.10	0.01	bql	0.003	0.000	bql
GRW_20160825_HY001	HY1	8/25/2016	0.07	0.01	bql	0.11	0.01	bql	n.a.		aql
GRW_20170204_HY001	HY1	2/4/2017	0.14	0.01	ok	0.16	0.01	ok	0.047	0.002	ok
GRW_20170516_HY001	HY1	5/16/2017	0.20	0.01	ok	0.19	0.01	ok	0.013	0.001	ok
GRW_20170823_HY001	HY1	8/23/2017	0.11	0.02	ok	0.11	0.02	ok	0.003	0.010	bql

GRW_20180129_HY001	HY1	1/29/2018	0.16	0.01	ok	0.21	0.02	ok	0.041	0.010	ok
GRW_20180517_HY001	HY1	5/17/2018	0.15	0.01	ok	0.16	0.02	ok	0.011	0.010	bql
GRW_20171213_SD001	SD1	12/13/2017	0.16	0.03	ok	0.40	0.08	ok	0.028	0.006	ok
GRW_20170622_GW001	GW1	6/22/2017	21.18	1.06	ok	13.14	0.66	ok	2.855	0.143	ok
GRW_20180607_GW001	GW1	6/1/2018	21.11	2.22	aql	12.99	1.95	aql	2.974	0.297	ok
GRW_20170518_GW002	GW2	5/18/2017	0.59	0.03	ok	1.74	0.09	ok	0.069	0.003	ok
GRW_20170518_GW003	GW3	5/18/2017	0.76	0.04	ok	2.23	0.11	ok	0.108	0.005	ok
GRW_20180525_GW003	GW3	5/25/2018	0.77	0.08	ok	2.09	0.31	ok	0.110	0.016	ok
GRW_20170620_GW004	GW4	6/20/2017	9.39	0.47	ok	1.37	0.07	ok	2.255	0.113	ok
GRW_20170622_GW005	GW5	6/22/2017	46.37	4.64	aql	3.18	0.16	ok	8.200	0.410	ok
GRW_20180525_GW005	GW5	5/25/2018	79.31	11.90	aql	4.17	0.63	ok	10.074	2.267	aql
GRW_20170622_GW006	GW6	6/22/2017	4.09	0.20	ok	1.44	0.07	ok	1.647	0.082	ok
GRW_20170622_GW007	GW7	6/22/2017	4.10	0.21	ok	1.45	0.07	ok	1.665	0.083	ok
GRW_20170720_GW008	GW8	7/20/2017	2.12	0.42	ok	12.87	2.57	aql	0.577	0.115	ok
GRW_20180525_GW008	GW8	5/25/2018	5.40	0.54	ok	14.79	2.22	ok	6.467	1.455	aql
GRW_20170720_GW009	GW9	7/20/2017	6.27	1.25	ok	37.64	7.53	aql	0.018	0.010	bql
GRW_20180525_GW009	GW9	5/25/2018	5.84	0.58	ok	30.72	4.61	ok	0.019	0.010	bql

*ok: sample within instrument detection limit, bdl: below detection limit, bql: below quantification limit, aql: above quantification limit

Table G.3 Water analysis of cations analyzed by ICP-OES and ICP-MS at MBMG and MSU-EAL.

Sample ID	Site ID	Sampling Date	Al (mg L^{-1})	As (mg L^{-1})	B (mg L^{-1})	Ba (mg L^{-1})	Ca (mg L^{-1})	Cu (mg L^{-1})	Fe (mg L^{-1})	K (mg L^{-1})	Mb (mg L^{-1})	Mg (mg L^{-1})	Mn (mg L^{-1})	Na (mg L^{-1})	P (mg L^{-1})	Pb (mg L^{-1})	Se (mg L^{-1})	Si (mg L^{-1})	Sr (mg L^{-1})
GRW_20180524_GV012	GV12	5/24/2018	0.03			0.03	15.70		0.02	1.07		4.59		2.75	0.05			3.93	0.08
GRW_20180524_GV011	GV11	5/24/2018				0.02	20.40			1.08		3.04		1.98	0.06			3.00	0.05
GRW_20170831_GV010	GV10	8/31/2017				0.08	54.00			3.22		16.60		9.01				6.98	0.20
GRW_20180524_GV010	GV10	5/24/2018	0.03			0.04	30.80		0.04	1.89		10.70		6.30				4.01	0.10
GRW_20170831_GV009	GV9	8/31/2017				0.06	56.10			3.52		17.80		11.60				5.53	0.20
GRW_20180524_GV009	GV9	5/24/2018	0.05		0.02	0.04	35.80		0.05	1.74		9.73		6.45	0.05			3.15	0.12
GRW_20170825_GV008	GV8	8/25/2017				0.06	40.50			1.94		11.70		4.81				5.83	0.22
GRW_20160226_GV007	GV7	2/26/2016		0.001		0.03	23.25			2.46		13.18		7.80		0.001	0.003	0.00	0.13
GRW_20160506_GV007	GV7	5/6/2016				0.04	28.60			1.73		8.89		5.76				6.20	0.14
GRW_20160707_GV007	GV7	7/7/2016				0.03	26.70			3.27		14.50		10.00				6.08	0.17
GRW_20160826_GV007	GV7	8/26/2016				0.03	23.40			3.55		14.90		9.66				7.91	0.15
GRW_20170205_GV007	GV7	2/5/2017				0.05	50.00			2.53		14.20		7.85				4.60	0.20
GRW_20170517_GV007	GV7	5/17/2017				0.03	27.10			1.45		8.89		5.62				6.15	0.13
GRW_20170825_GV007	GV7	8/25/2017				0.07	48.60			3.51		15.40		9.90	0.02			7.58	0.23
GRW_20180524_GV007	GV7	5/24/2018				0.04	23.50		0.02	2.12		7.12	0.01	4.68				4.58	0.11
GRW_20160226_GV006	GV6	2/26/2016				0.03	29.72			2.00		15.37		10.24			0.004	0.00	0.13
GRW_20160506_GV006	GV6	5/6/2016				0.03	26.90			1.04		9.77		6.61				4.96	0.10
GRW_20160707_GV006	GV6	7/7/2016				0.03	26.80			1.69		15.70		9.99				4.95	0.14
GRW_20160826_GV006	GV6	8/26/2016				0.03	28.00			2.56		16.60		7.67				6.64	0.14
GRW_20170517_GV006	GV6	5/17/2017				0.02	17.10			1.23		9.42		7.37				4.04	0.07
GRW_20170825_GV006	GV6	8/25/2017				0.06	52.40			2.86		15.90		8.51	0.08			7.11	0.21
GRW_20180524_GV006	GV6	5/24/2018	0.02			0.04	34.90			1.24		9.61		6.44				3.92	0.11
GRW_20160226_GV005	GV5	2/26/2016				0.02	13.32			1.55		5.70		2.53				0.00	0.05
GRW_20160506_GV005	GV5	5/6/2016				0.04	26.70			1.99		8.88		5.54				7.13	0.10
GRW_20160707_GV005	GV5	7/7/2016				0.02	16.80	0.01		1.63		9.74		5.08				5.93	0.11

GRW_20160826_GV005	GV5	8/26/2016			0.03	26.90		2.09		12.50	5.76				5.88	0.16
GRW_20170517_GV005	GV5	5/17/2017			0.03	20.00		1.57		7.01	4.26	0.02			6.49	0.07
GRW_20170825_GV005	GV5	8/25/2017			0.06	44.80		2.49		13.10	6.48				6.50	0.20
GRW_20180524_GV005	GV5	5/24/2018	0.06		0.02	11.20	0.06	1.85		3.20	2.21				7.27	0.04
GRW_20160506_GV004	GV4	5/6/2016			0.03	21.10	0.02	1.25		6.10	3.90				5.49	0.12
GRW_20160707_GV004	GV4	7/7/2016			0.02	20.60		1.41		8.88	4.15				5.52	0.14
GRW_20160826_GV004	GV4	8/26/2016			0.02	25.20		1.69		11.80	4.74				4.46	0.18
GRW_20170205_GV004	GV4	2/5/2017			0.03	37.90		1.57		12.80	4.91				4.34	0.22
GRW_20170517_GV004	GV4	5/17/2017			0.03	21.80		1.14		6.70	3.95				5.64	0.11
GRW_20170825_GV004	GV4	8/25/2017			0.05	38.60		1.51		11.60	4.37	0.02			4.59	0.22
GRW_20180524_GV004	GV4	5/24/2018	0.03		0.03	17.60	0.04	1.17		4.74	2.82				4.29	0.09
GRW_20160226_GV003	GV3	2/26/2016		0.001	0.03	27.21		1.45	0.001	11.75	4.51		0.001	0.001		0.18
GRW_20160506_GV003	GV3	5/6/2016			0.03	19.90		1.19		5.86	3.71				5.21	0.11
GRW_20160707_GV003	GV3	7/7/2016			0.03	22.80		1.32		8.70	4.26				5.28	0.15
GRW_20160826_GV003	GV3	8/26/2016			0.02	27.50		1.67		12.10	4.68				4.60	0.20
GRW_20170205_GV003	GV3	2/5/2017			0.03	38.30		1.50		13.30	4.92				5.32	0.23
GRW_20170517_GV003	GV3	5/17/2017			0.03	18.90		1.09		6.59	4.00	0.02			5.33	0.10
GRW_20170825_GV003	GV3	8/25/2017			0.04	37.30		1.51		11.60	4.51				4.70	0.22
GRW_20180524_GV003	GV3	5/24/2018	0.02		0.03	17.40	0.02	1.13		4.71	3.02				3.94	0.08
GRW_20160226_GV002	GV2	2/26/2016			0.01	17.91		1.02		10.00	1.48					0.04
GRW_20160506_GV002	GV2	5/6/2016			0.02	22.30		1.22		6.01	1.54				6.30	0.05
GRW_20160707_GV002	GV2	7/7/2016			0.04	29.10		1.52		10.50	3.11				8.15	0.07
GRW_20160825_GV002	GV2	8/25/2016			0.02	24.90		1.55		9.88	2.08				7.29	0.06
GRW_20170205_GV002	GV2	2/5/2017			0.00	28.70		1.18		11.70	1.40				4.37	0.05
GRW_20170517_GV002	GV2	5/17/2017			0.01	17.60		1.23		6.14	2.25				6.24	0.04
GRW_20170825_GV002	GV2	8/25/2017			0.04	37.80		1.30		9.54	2.10				6.53	0.07
GRW_20180524_GV002	GV2	5/24/2018			0.02	18.20		1.20		4.36	1.64				4.99	0.04
GRW_20160226_GV001	GV1	2/26/2016			0.02	15.57		1.51		5.22	2.47					0.06

GRW_20160506_GV001	GV1	5/6/2016		0.04	20.20	0.03	1.27	5.33	2.79	0.05	6.66	0.06
GRW_20160707_GV001	GV1	7/7/2016		0.02	11.50		1.69	3.41	2.25	0.03	9.54	0.05
GRW_20160825_GV001	GV1	8/25/2016		0.01	11.50		1.68	3.65	1.83	0.05	9.03	0.05
GRW_20170205_GV001	GV1	2/5/2017		0.02	17.70		1.65	5.61	2.43	0.04	6.90	0.06
GRW_20170517_GV001	GV1	5/17/2017		0.03	18.40		1.22	5.36	3.22	0.05	7.24	0.06
GRW_20170825_GV001	GV1	8/25/2017		0.02	12.50	0.03	1.49	3.61	1.93	0.04	7.95	0.04
GRW_20180524_GV001	GV1	5/24/2018	0.06	0.02	9.76	0.04	1.61	2.69	2.06		6.48	0.04
GRW_20180517_HY019	HY19	5/17/2018	0.06	0.01	13.60	0.04	1.86	3.44	3.27		4.38	0.04
GRW_20180517_HY018	HY18	5/17/2018	0.03	0.02	10.30	0.02	2.77	5.44	3.44		4.44	0.03
GRW_20171214_HY017	HY17	12/14/2017		0.03	26.90		0.60	16.70	0.65	0.03	1.60	0.12
GRW_20180129_HY017	HY17	1/29/2018		0.04	33.70		0.64	17.10	0.82	0.03	1.89	0.15
GRW_20180327_HY017	HY17	3/27/2018		0.04	32.90		0.73	16.40	0.84		1.37	0.15
GRW_20180517_HY017	HY17	5/17/2018		0.03	26.90		0.71	16.80	0.75		2.96	0.12
GRW_20171214_HY016	HY16	12/14/2017		0.03	31.00		0.62	16.60	0.64		2.31	0.13
GRW_20180517_HY016	HY16	5/17/2018		0.03	24.70		0.85	16.90	0.93		2.62	0.11
GRW_20170824_HY015	HY15	8/24/2017		0.02	11.60	0.04	1.33	3.36	1.76	0.06	8.10	0.04
GRW_20170824_HY014	HY14	8/24/2017		0.02	11.60	0.05	1.37	3.31	1.86	0.06	8.31	0.04
GRW_20180129_HY014	HY14	1/29/2018		0.02	19.30	0.03	1.39	5.82	2.69	0.06	0.28	0.06
GRW_20170824_HY013	HY13	8/24/2017		0.03	14.60		2.04	3.26	3.42	0.15	13.00	0.08
GRW_20170823_HY012	HY12	8/23/2017		0.14	68.60		0.92	8.18	2.06		4.90	0.14
GRW_20180517_HY012	HY12	5/17/2018	0.02	0.10	36.50		0.97	4.14	1.33		2.52	0.06
GRW_20170823_HY011	HY11	8/23/2017		0.01	11.00	0.02	1.50	3.26	1.62	0.06	7.66	0.04
GRW_20170823_HY010	HY10	8/23/2017		0.01	11.00	0.04	1.46	3.25	1.64	0.06	7.96	0.04
GRW_20171214_HY010	HY10	12/14/2017		0.02	14.50		1.39	4.62	2.20	0.05	3.88	0.05
GRW_20180129_HY010	HY10	1/29/2018		0.02	15.40		1.36	5.69	2.58	0.05	5.41	0.06
GRW_20180327_HY010	HY10	3/27/2018		0.03	16.60		1.55	5.45	2.78	0.05	2.88	0.06
GRW_20180517_HY010	HY10	5/17/2018		0.03	13.20	0.04	1.35	3.89	2.65		3.81	0.05
GRW_20170823_HY009	HY9	8/23/2017		0.01	8.52	0.06	1.56	2.14	1.78	0.05	8.40	0.04

GRW_20171214_HY009	HY9	12/14/2017		0.02	11.80		1.57	3.39	2.38	0.06		4.24	0.05
GRW_20180129_HY009	HY9	1/29/2018		0.02	13.40	0.02	1.50	3.73	2.87	0.07		4.35	0.05
GRW_20180327_HY009	HY9	3/27/2018		0.02	11.40		1.40	3.33	2.94	0.05		4.20	0.04
GRW_20180517_HY009	HY9	5/17/2018	0.08	0.03	10.90	0.06	1.39	2.89	2.53			6.10	0.05
GRW_20170204_HY008	HY8	2/4/2017		0.08	37.10		1.34	4.22	4.11			6.12	0.14
GRW_20170516_HY008	HY8	5/16/2017		0.03	16.50		0.75	2.40	2.98			8.31	0.06
GRW_20170823_HY008	HY8	8/23/2017		0.11	47.10		1.50	4.94	4.17	0.04		6.32	0.16
GRW_20180327_HY008	HY8	3/27/2018	0.13	0.07	25.20	0.08	1.13	3.13	3.20	0.05		3.19	0.10
GRW_20180517_HY008	HY8	5/17/2018	0.20	0.05	21.80	0.12	1.07	2.28	2.55			7.38	0.08
GRW_20170204_HY007	HY7	2/4/2017		0.00	9.33		1.83	2.30	2.56			5.94	0.04
GRW_20170516_HY007	HY7	5/16/2017		0.01	8.56		1.31	2.38	3.88	0.05		7.94	0.03
GRW_20170823_HY007	HY7	8/23/2017		0.01	7.00	0.09	1.56	1.76	1.57	0.08		8.48	0.03
GRW_20180327_HY007	HY7	3/27/2018		0.01	8.92		1.47	2.48	2.66	0.05		3.91	0.04
GRW_20180517_HY007	HY7	5/17/2018	0.06	0.02	8.46	0.05	1.50	2.25	2.45			7.02	0.04
GRW_20160209_HY006	HY6	2/9/2016		0.02	12.47		1.47	4.87	2.31				0.05
GRW_20160219_HY006	HY6	2/19/2016		0.01	10.05		1.46	5.00	2.39				0.04
GRW_20160518_HY006	HY6	5/18/2016	0.10	0.05	22.00	0.08	1.33	5.32	2.56	0.02		7.38	0.07
GRW_20160706_HY006	HY6	7/6/2016		0.02	12.00		1.76	3.36	1.95	0.04		8.60	0.04
GRW_20160825_HY006	HY6	8/25/2016		0.02	12.70	0.07	1.91	3.94	2.26	0.07		8.37	0.05
GRW_20170204_HY006	HY6	2/4/2017		0.00	14.40		1.63	5.21	2.48			6.84	0.05
GRW_20170516_HY006	HY6	5/16/2017		0.03	15.40		1.26	5.26	3.39	0.03		7.10	0.06
GRW_20170824_HY006	HY6	8/24/2017		0.02	11.80	0.04	1.49	3.36	1.69	0.05		7.36	0.04
GRW_20180327_HY006	HY6	3/27/2018	0.02	0.02	15.30		1.44	5.62	2.59	0.05		3.92	0.05
GRW_20180517_HY006	HY6	5/17/2018	0.07	0.03	13.70	0.03	1.44	3.78	2.50			3.52	0.05
GRW_20160209_HY005	HY5	2/9/2016		0.01	10.68		1.44	4.73	2.24				0.04
GRW_20160219_HY005	HY5	2/19/2016		0.01	9.86		1.43	4.99	2.34				0.04
GRW_20160518_HY005	HY5	5/18/2016		0.04	21.60		1.27	5.28	2.57	0.03		7.38	0.07
GRW_20160706_HY005	HY5	7/6/2016		0.02	12.10		1.67	3.33	1.94	0.03		9.14	0.04

GRW_20160825_HY005	HY5	8/25/2016			0.02	12.60	0.07	1.75	3.73	2.05	0.06		8.86	0.05
GRW_20170516_HY005	HY5	5/16/2017			0.03	16.60		1.22	5.29	3.08	0.04		7.22	0.06
GRW_20170824_HY005	HY5	8/24/2017			0.02	11.90	0.05	1.54	3.42	1.92	0.05		7.25	0.04
GRW_20180129_HY005	HY5	1/29/2018			0.02	17.50		1.49	5.76	2.74	0.05		5.01	0.06
GRW_20180327_HY005	HY5	3/27/2018			0.02	16.40		1.67	6.42	2.99	0.04		5.63	0.06
GRW_20180517_HY005	HY5	5/17/2018	0.06		0.03	15.80	0.04	1.41	3.83	2.36	0.04		6.00	0.06
GRW_20160209_HY004	HY4	2/9/2016		0.001	0.02	13.94		1.38	4.69	2.20		0.001		0.05
GRW_20160219_HY004	HY4	2/19/2016			0.02	13.52		1.36	5.03	2.30				0.05
GRW_20160518_HY004	HY4	5/18/2016	0.11		0.05	23.70	0.08	1.16	5.92	2.76	0.02		7.85	0.08
GRW_20160706_HY004	HY4	7/6/2016			0.02	11.60		1.65	3.28	1.98	0.00		9.44	0.04
GRW_20160825_HY004	HY4	8/25/2016			0.02	12.50	0.09	1.73	3.56	1.79	0.07		8.87	0.05
GRW_20170204_HY004	HY4	2/4/2017			0.02	17.60		1.53	5.25	2.61			6.94	0.06
GRW_20170516_HY004	HY4	5/16/2017			0.03	16.20		1.20	5.74	2.99	0.04		7.33	0.06
GRW_20170823_HY004	HY4	8/23/2017			0.01	11.40	0.06	1.54	3.30	1.62	0.07		7.84	0.04
GRW_20180327_HY004	HY4	3/27/2018			0.02	14.80		1.25	5.36	2.39	0.03		1.78	0.05
GRW_20180517_HY004	HY4	5/17/2018	0.07		0.03	15.70	0.05	1.39	4.04	2.49			7.58	0.06
GRW_20160209_HY003	HY3	2/9/2016			0.07	20.93		0.88	10.62	7.67				0.08
GRW_20160219_HY003	HY3	2/19/2016			0.08	21.65		0.87	9.87	7.11				0.08
GRW_20160518_HY003	HY3	5/18/2016	0.03		0.09	17.50	0.03	0.64	4.02	1.86			4.34	0.06
GRW_20160706_HY003	HY3	7/6/2016			0.20	43.00		1.03	11.40	4.87	0.02		4.72	0.14
GRW_20160825_HY003	HY3	8/25/2016			0.19	44.60		1.04	13.40	7.51	0.02		3.87	0.14
GRW_20170204_HY003	HY3	2/4/2017			0.12	34.50		1.01	11.00	8.11			3.38	0.11
GRW_20170516_HY003	HY3	5/16/2017			0.07	15.50		0.54	4.22	2.23	0.03		3.80	0.05
GRW_20170823_HY003	HY3	8/23/2017			0.20	47.00		0.99	13.20	7.07			3.66	0.15
GRW_20180327_HY003	HY3	3/27/2018	0.04		0.11	28.50	0.04	0.78	10.20	5.19	0.05		2.30	0.09
GRW_20180517_HY003	HY3	5/17/2018			0.08	14.10	0.06	0.66	3.48	1.85			2.77	0.05
GRW_20160209_HY002	HY2	2/9/2016			0.01	4.73		1.90	1.64	1.62				0.03
GRW_20160219_HY002	HY2	2/19/2016			0.01	4.60		1.87	1.63	1.61				0.03

GRW_20160518_HY002	HY2	5/18/2016	0.04		0.01	4.92		0.03	2.23		1.71		1.65	0.07		9.19	0.03
GRW_20160706_HY002	HY2	7/6/2016			0.01	4.74			2.30		1.62		1.60	0.05		12.20	0.03
GRW_20160825_HY002	HY2	8/25/2016			0.01	5.67			2.82		2.10		1.96	0.08		9.88	0.03
GRW_20170204_HY002	HY2	2/4/2017			0.00	5.87			2.10		1.93		2.13	0.05		4.39	0.03
GRW_20170516_HY002	HY2	5/16/2017			0.01	4.59			2.02		1.62		1.92	0.07		7.22	0.03
GRW_20170823_HY002	HY2	8/23/2017			0.01	5.56			2.30		1.90		1.85	0.07		8.14	0.03
GRW_20180517_HY002	HY2	5/17/2018	0.06		0.01	4.53		0.04	1.99		1.59		2.00	0.06		2.58	0.03
GRW_20160209_HY001	HY1	2/9/2016			0.00	3.06			1.47		0.97		1.31				0.02
GRW_20160219_HY001	HY1	2/19/2016			0.00	3.07			1.47		0.98		1.31				0.02
GRW_20160518_HY001	HY1	5/18/2016	0.03		0.00	4.21		0.02	1.52		1.25		1.57	0.04		8.70	0.02
GRW_20160706_HY001	HY1	7/6/2016			0.00	3.39			1.58		1.00		1.25	0.03		6.72	0.02
GRW_20160825_HY001	HY1	8/25/2016			0.00	3.75			1.96		1.24		1.56	0.05		9.15	0.02
GRW_20170204_HY001	HY1	2/4/2017			0.00	3.79			1.68		1.13		1.58	0.04		4.06	0.00
GRW_20170516_HY001	HY1	5/16/2017			0.00	3.90			1.45		1.18		1.48	0.05		6.42	0.02
GRW_20170823_HY001	HY1	8/23/2017			0.00	3.78		0.01	1.73		1.16		1.56	0.05		6.80	0.02
GRW_20180129_HY001	HY1	1/29/2018			0.00	3.77			1.57		1.19		1.57	0.08		2.89	0.02
GRW_20180327_HY001	HY1	3/27/2018			0.00	3.85			1.58		1.26		1.38	0.06		5.08	0.02
GRW_20180517_HY001	HY1	5/17/2018	0.04		0.01	4.07		0.03	1.53		1.24		1.72			2.48	0.02
GRW_20171213_SD001	SD1	12/13/2017			0.01	6.86			1.88		2.14		1.98	0.11		2.76	0.04
GRW_20170622_GW001	GW1	6/22/2017			0.01	68.00			3.80		12.60		9.21	0.04		15.20	0.15
GRW_20180601_GW001	GW1	6/1/2018			0.02	69.40			3.90		12.30		8.07	0.07		5.17	0.16
GRW_20170518_GW002	GW2	5/18/2017			0.01	15.30			1.63		7.34	1.03	4.84	0.03		5.38	0.05
GRW_20170518_GW003	GW3	5/18/2017			0.03	27.00			2.53		10.70		6.28	0.03		7.19	0.06
GRW_20180525_GW003	GW3	5/25/2018			0.03	26.10	0.01		2.62		10.60		5.35			2.22	0.06
GRW_20170620_GW004	GW4	6/20/2017			0.05	42.90			3.63		6.23		7.39	0.10		13.70	0.11
GRW_20170622_GW005	GW5	6/22/2017		0.04	0.17	72.60			3.75		34.30		48.20	0.05		8.95	0.18
GRW_20180525_GW005	GW5	5/25/2018		0.02	0.18	53.30			1.06		13.70		10.50	0.05		2.72	0.13
GRW_20170622_GW006	GW6	6/22/2017			0.03	21.30			2.78		11.80		8.75	0.03		7.82	0.11

GRW_20170622_GW007	GW7	6/22/2017		0.03	22.00	2.71	11.80		8.69	0.04	7.92	0.11
GRW_20170720_GW008	GW8	7/20/2017		0.06	50.30	3.57	13.60		6.35		14.00	0.26
GRW_20180525_GW008	GW8	5/25/2018		0.05	45.30	3.11	18.40		5.59		3.18	0.28
GRW_20170720_GW009	GW9	7/20/2017	0.02	0.10	98.20	6.71	30.10	0.80	34.70	0.02	11.80	0.50
GRW_20180525_GW009	GW9	5/25/2018	0.03	0.07	78.80	6.79	28.90	0.61	33.50	0.00	4.01	0.43

Table G.4 Field water chemical analysis using YSI multimeter.

Sample ID	Site ID	Sampling Date	Alkalinity (mg CaCO3 L-1)	pH	Temperature (°C)	SC	EC	DO (%)	DO (mg L-1)	BP (mmHg)
GRW_20180524_GV012	GV12	5/24/2018	54	9.77	5.32	157	98	72.7	9.20	635.0
GRW_20180524_GV011	GV11	5/24/2018	72	5.18	5.32	169	105	68.2	8.64	632.4
GRW_20170831_GV010	GV10	8/31/2017	205	8.66	18.65	244	214	135.7	12.66	649.6
GRW_20180524_GV010	GV10	5/24/2018	134	8.15	11.52	308	242	63.1	6.87	655.9
GRW_20170831_GV009	GV9	8/31/2017	220	8.54	18.15	261	227	148.2	13.98	649.3
GRW_20180524_GV009	GV9	5/24/2018	144	8.16	11.55	305	227	62.2	6.78	651.7
GRW_20170825_GV008	GV8	8/25/2017	132	8.60	17.18	221	188	120.9	11.50	653.2
GRW_20160226_GV007	GV7	2/26/2016		8.49	5.71	390	246	130.0	16.28	656.8
GRW_20160506_GV007	GV7	5/6/2016	115	8.23	12.79	259	199	77.9	8.24	656.6
GRW_20160707_GV007	GV7	7/7/2016	149	8.76	19.35	591	527	87.3	8.04	653.8
GRW_20160826_GV007	GV7	8/26/2016	167	8.72	16.70	393	331	102.4	9.88	655.2
GRW_20170205_GV007	GV7	2/5/2017	154	5.15	-0.05	370	193	145.8	20.54	648.1
GRW_20170517_GV007	GV7	5/17/2017	105	7.78	7.44	609	164	71.7	8.61	639.2
GRW_20170825_GV007	GV7	8/25/2017	207	8.68	17.86	280	242	139.4	13.22	655.4
GRW_20180524_GV007	GV7	5/24/2018	121	7.88	9.93	213	152	63.2	7.07	657.2
GRW_20160226_GV006	GV6	2/26/2016		8.64	5.09	444	275	141.3	17.91	643.2
GRW_20160506_GV006	GV6	5/6/2016	153	8.32	11.17	296	218	80.1	8.79	643.5
GRW_20160707_GV006	GV6	7/7/2016	201	8.70	18.33	665	580	95.1	8.74	641.9
GRW_20160826_GV006	GV6	8/26/2016	185	8.64	16.10	422	355	91.5	8.90	642.6
GRW_20170517_GV006	GV6	5/17/2017	143	7.74	6.03	285	192	81.5	9.93	640.7
GRW_20170825_GV006	GV6	8/25/2017	214	8.61	18.50	286	250	130.7	12.25	643.3
GRW_20180524_GV006	GV6	5/24/2018	134	8.20	10.10	298	213	63.0	7.09	643.4
GRW_20160226_GV005	GV5	2/26/2016		8.23	0.97	174	94	110.3	15.68	644.3
GRW_20160506_GV005	GV5	5/6/2016	131	8.69	13.39	257	200	90.5	9.37	643.5

GRW_20160707_GV005	GV5	7/7/2016	96	8.46	13.29	436	338	72.6	7.48	640.8
GRW_20160826_GV005	GV5	8/26/2016	146	8.68	11.57	338	251	78.2	8.52	642.7
GRW_20170517_GV005	GV5	5/17/2017	88	7.81	5.10	207	129	76.9	9.83	628.9
GRW_20170825_GV005	GV5	8/25/2017	174	8.72	13.60	239	187	118.4	12.30	644.2
GRW_20180524_GV005	GV5	5/24/2018	68	6.99	8.79	118	81	72.0	8.33	649.5
GRW_20160506_GV004	GV4	5/6/2016	78	7.99	8.43	181	124	79.4	9.31	639.8
GRW_20160707_GV004	GV4	7/7/2016	92	8.27	12.00	398	300	67.4	7.18	639.3
GRW_20160826_GV004	GV4	8/26/2016	104	8.69	11.43	306	226	81.9	8.93	640.0
GRW_20170205_GV004	GV4	2/5/2017	89	6.25	0.30	314	166	105.3	14.66	631.7
GRW_20170517_GV004	GV4	5/17/2017	100	7.68	5.81	194	123	75.9	9.48	630.9
GRW_20170825_GV004	GV4	8/25/2017	118	8.64	13.27	209	162	113.0	11.81	640.3
GRW_20180524_GV004	GV4	5/24/2018	56	7.32	5.80	159	101	76.0	9.44	637.3
GRW_20160226_GV003	GV3	2/26/2016		8.41	2.52	327	186	112.7	15.29	632.9
GRW_20160506_GV003	GV3	5/6/2016	87	8.05	6.90	174	114	93.8	11.15	632.6
GRW_20160707_GV003	GV3	7/7/2016	83	8.29	10.21	384	276	78.1	8.65	631.4
GRW_20160826_GV003	GV3	8/26/2016	112	8.61	10.13	308	221	81.0	9.17	632.9
GRW_20170205_GV003	GV3	2/5/2017	90	5.03	2.34	313	178	84.9	11.62	624.4
GRW_20170517_GV003	GV3	5/17/2017		7.67	5.22	191	118	73.1	9.28	623.1
GRW_20170825_GV003	GV3	8/25/2017	131	8.59	12.13	203	153	105.6	11.34	633.5
GRW_20180524_GV003	GV3	5/24/2018	65	7.11	4.79	152	93	71.4	9.16	1770.0
GRW_20160226_GV002	GV2	2/26/2016		8.43	3.02	278	161	112.4	15.03	632.1
GRW_20160506_GV002	GV2	5/6/2016	92	8.13	6.44	184	119	124.5	14.55	630.8
GRW_20160707_GV002	GV2	7/7/2016	171	8.19	10.37	522	376	63.8	7.13	630.2
GRW_20160825_GV002	GV2	8/25/2016	151	8.70	9.51	279	197	86.4	9.99	634.9
GRW_20170205_GV002	GV2	2/5/2017	115	6.25	2.90	275	159	90.5	12.18	622.1
GRW_20170517_GV002	GV2	5/17/2017	99	7.65	4.17	186	112	73.8	9.62	619.8
GRW_20170825_GV002	GV2	8/25/2017	143	8.39	10.40	182	131	102.1	11.41	630.4
GRW_20180524_GV002	GV2	5/24/2018	71	8.05	4.76	150	92	65.3	8.38	627.0

GRW_20160226_GV001	GV1	2/26/2016		7.80	0.03	152	80	115.2	16.63	630.7
GRW_20160506_GV001	GV1	5/6/2016	73	7.88	7.18	156	103	124.2	11.72	629.0
GRW_20160707_GV001	GV1	7/7/2016	40	8.14	6.22	164	105	72.0	8.96	628.9
GRW_20160825_GV001	GV1	8/25/2016	49	8.27	7.82	103	70	78.9	9.39	633.1
GRW_20170205_GV001	GV1	2/5/2017	49	5.78	0.01	140	73	79.7	11.65	620.2
GRW_20170517_GV001	GV1	5/17/2017	70	7.55	4.84	159	97	78.5	10.20	617.0
GRW_20170825_GV001	GV1	8/25/2017	60	8.00	10.31	71	51	99.1	11.10	628.3
GRW_20180524_GV001	GV1	5/24/2018	78	7.69	6.62	87	57	62.8	7.69	626.1
GRW_20180517_HY017	HY17	5/17/2018	146							
GRW_20180517_HY016	HY16	5/17/2018	166	7.45	7.56	361	241	60.8	7.27	593.1
GRW_20170824_HY015	HY15	8/24/2017	73	8.09	11.96	88	66	96.5	10.40	612.7
GRW_20170824_HY014	HY14	8/24/2017	45	8.04	11.71	88	66	99.0	10.74	610.4
GRW_20180129_HY014	HY14	1/29/2018	85	7.53	3.57	86	51	699.3	92.60	604.0
GRW_20170824_HY013	HY13	8/24/2017	88	7.57	6.65	111	72	92.5	11.30	607.3
GRW_20170823_HY012	HY12	8/23/2017	212	8.40	12.38	554	419	98.5	98.54	609.4
GRW_20180517_HY012	HY12	5/17/2018	167	8.32	5.48	305	192	71.2	8.94	594.4
GRW_20170823_HY011	HY11	8/23/2017	49	8.55	13.55	137	107	100.6	10.44	608.8
GRW_20170823_HY010	HY10	8/23/2017	46	8.36	12.58	138	105	102.0	10.85	609.8
GRW_20180129_HY010	HY10	1/29/2018	79	7.30	4.00	83	50	585.7	76.62	603.8
GRW_20180517_HY010	HY10	5/17/2018	54	8.90	4.80	123	76	74.6	9.56	593.1
GRW_20170823_HY009	HY9	8/23/2017	45	8.11	11.94	107	80	98.5	10.63	607.0
GRW_20180129_HY009	HY9	1/29/2018	65	7.14	3.51	66	39	415.9	55.11	606.9
GRW_20180517_HY009	HY9	5/17/2018	26	5.76	4.72	103	63	71.1	9.14	590.2
GRW_20170204_HY008	HY8	2/4/2017	106	6.03	0.00	244	128	192.7	27.68	577.6
GRW_20170516_HY008	HY8	5/16/2017	51	8.16	4.88	177	109	70.6	9.02	599.8
GRW_20170823_HY008	HY8	8/23/2017	167	8.42	11.05	374	274	90.1	9.92	609.6
GRW_20180517_HY008	HY8	5/17/2018	51	8.63	6.18	149	96	74.8	9.25	601.5
GRW_20170204_HY007	HY7	2/4/2017	35	8.09	3.58	82	49	127.7	16.87	593.5

GRW_20170516_HY007	HY7	5/16/2017	24	8.01	4.38	98	59	73.0	9.46	593.1
GRW_20170823_HY007	HY7	8/23/2017	12	7.76	11.29	90	67	96.6	10.59	606.7
GRW_20180517_HY007	HY7	5/17/2018	21	6.15	4.46	76	46	88.2	11.55	595.1
GRW_20160209_HY006	HY6	2/9/2016		7.92	0.89	142	77	96.0	13.64	628.8
GRW_20160219_HY006	HY6	2/19/2016		8.11	2.06	150	84	101.6	13.89	607.8
GRW_20160518_HY006	HY6	5/18/2016	82	8.28	10.33	155	112	76.8	8.59	619.6
GRW_20160706_HY006	HY6	7/6/2016	50	7.93	11.04	160	117	68.0	7.47	618.8
GRW_20160825_HY006	HY6	8/25/2016		8.44	13.66	103	81	71.6	7.47	625.1
GRW_20170204_HY006	HY6	2/4/2017	52	7.69	0.00	159	83	168.0	24.54	610.8
GRW_20170516_HY006	HY6	5/16/2017	68	8.33	6.75	180	117	72.8	8.87	612.0
GRW_20170824_HY006	HY6	8/24/2017	61	8.23	13.21	90	70	101.5	10.64	623.0
GRW_20180517_HY006	HY6	5/17/2018	56	8.17	7.16	127	84	71.9	8.59	623.0
GRW_20160209_HY005	HY5	2/9/2016		7.98	1.05	141	76	103.5	14.40	625.1
GRW_20160219_HY005	HY5	2/19/2016		8.17	1.85	149	83	103.7	13.93	602.3
GRW_20160518_HY005	HY5	5/18/2016	78	8.25	9.50	158	111	76.0	8.74	618.2
GRW_20160706_HY005	HY5	7/6/2016	57	7.86	10.67	161	117	63.4	7.04	615.8
GRW_20160825_HY005	HY5	8/25/2016	43	8.43	13.73	103	81	72.4	7.51	622.3
GRW_20170516_HY005	HY5	5/16/2017	54	8.33	6.33	181	116	73.6	9.05	610.1
GRW_20170824_HY005	HY5	8/24/2017	79	8.22	12.60	91	69	101.0	10.73	618.6
GRW_20180129_HY005	HY5	1/29/2018	87	7.09	2.44	88	50	768.6	104.29	604.9
GRW_20180517_HY005	HY5	5/17/2018	62	7.81	6.76	124	81	69.0	8.41	613.9
GRW_20160209_HY004	HY4	2/9/2016		8.15	2.83	138	80	96.3	13.02	614.8
GRW_20160219_HY004	HY4	2/19/2016		8.39	3.29	145	85	99.0	13.16	596.0
GRW_20160518_HY004	HY4	5/18/2016	98	8.15	8.40	169	115	76.3	8.94	609.1
GRW_20160706_HY004	HY4	7/6/2016	49	8.07	9.00	157	109	98.8	9.44	606.0
GRW_20160825_HY004	HY4	8/25/2016	37	8.47	13.39	101	79	73.2	7.62	612.3
GRW_20170204_HY004	HY4	2/4/2017	52	8.19	1.64	142	79	165.2	23.06	592.5
GRW_20170516_HY004	HY4	5/16/2017	39	8.26	6.03	190	121	71.5	8.88	600.4

GRW_20170823_HY004	HY4	8/23/2017	28	8.67	14.77	142	114	101.9	10.24	612.3
GRW_20180517_HY004	HY4	5/17/2018	57	8.25	5.30	131	81	71.6	9.06	593.4
GRW_20160209_HY003	HY3	2/9/2016		8.05	0.40	309	164	115.0	16.17	607.2
GRW_20160219_HY003	HY3	2/19/2016		7.81	0.53	289	154	117.6	17.05	590.4
GRW_20160518_HY003	HY3	5/18/2016	57	7.96	3.95	116	69	76.3	10.01	602.4
GRW_20160706_HY003	HY3	7/6/2016	161	8.07	9.60	506	357	61.4	6.99	598.2
GRW_20160825_HY003	HY3	8/25/2016	190	8.70	8.43	309	234	72.5	8.47	604.6
GRW_20170204_HY003	HY3	2/4/2017	123	7.92		317	165	182.3	26.47	588.9
GRW_20170516_HY003	HY3	5/16/2017	39	8.19	2.94	149	86	72.0	9.71	592.6
GRW_20170823_HY003	HY3	8/23/2017	235	8.16	8.98	508	352	93.8	10.83	605.5
GRW_20160209_HY002	HY2	2/9/2016		7.45	0.97	55	30	94.0	13.34	603.0
GRW_20160219_HY002	HY2	2/19/2016		7.66	1.56	54	30	92.2	219.63	590.8
GRW_20160518_HY002	HY2	5/18/2016	15	7.66	3.24	50	29	72.9	9.74	596.0
GRW_20160706_HY002	HY2	7/6/2016	24	7.05	6.33	82	53	78.0	9.30	592.6
GRW_20160825_HY002	HY2	8/25/2016	29	8.15	8.08	58	39	74.1	8.73	598.0
GRW_20170204_HY002	HY2	2/4/2017	24	7.64	1.42	58	32	125.7	17.54	
GRW_20170516_HY002	HY2	5/16/2017	11	7.55	2.28	58	33	71.9	9.85	586.8
GRW_20170823_HY002	HY2	8/23/2017	28	7.42	6.45	82	53	93.4	11.49	
GRW_20180517_HY002	HY2	5/17/2018	33	7.50	3.06	50	29	62.9	8.45	595.0
GRW_20160209_HY001	HY1	2/9/2016		7.36	0.51	37	20	93.4	13.45	600.3
GRW_20160219_HY001	HY1	2/19/2016		7.31	1.00	37	20	96.5	13.68	588.4
GRW_20160518_HY001	HY1	5/18/2016	9	7.91	2.55	40	23	85.3	11.26	594.1
GRW_20160706_HY001	HY1	7/6/2016	16	6.83	6.29	56	37	69.7	8.33	590.5
GRW_20160825_HY001	HY1	8/25/2016	18	7.81	8.37	38	26	74.1	8.69	596.1
GRW_20170204_HY001	HY1	2/4/2017	15	7.95	0.82	40	21	130.7	18.67	585.9
GRW_20170516_HY001	HY1	5/16/2017	22	7.32	1.65	51	28	79.4	11.08	584.2
GRW_20170823_HY001	HY1	8/23/2017	23	7.33	6.73	58	37	92.6	11.32	597.4
GRW_20180129_HY001	HY1	1/29/2018	12	6.88	1.30	22	12	74.2	10.59	595.5

GRW_20180517_HY001	HY1	5/17/2018	45	7.32	2.34	41	23	65.2	8.90	590.6
GRW_20170622_GW001	GW1	6/22/2017	242	7.94	9.33	502	353	68.4	7.74	635.7
GRW_20180607_GW001	GW1	6/1/2018		7.36	9.44	514	360	438.4	49.69	634.2
GRW_20170518_GW002	GW2	5/18/2017	37	7.11	5.50	162	101	38.8	4.90	623.4
GRW_20170518_GW003	GW3	5/18/2017	146	7.40	6.88	313	205	23.6	2.88	623.6
GRW_20180411_GW003	GW3	4/11/2018	120	7.52	6.58	228	147	150.4	18.36	605.7
GRW_20180525_GW003	GW3	5/25/2018	166	7.26	9.47	245	173	68.7	7.83	628.2
GRW_20170620_GW004	GW4	6/20/2017	139	6.97	8.30	355	242	67.2	7.89	625.9
GRW_20170622_GW005	GW5	6/22/2017	432	7.47	8.66	908	624	68.6	7.98	634.9
GRW_20180525_GW005	GW5	5/25/2018		7.11	8.93	1007	698	60.7	5.89	632.0
GRW_20170622_GW006	GW6	6/22/2017	117	7.07	9.38	6	4	74.5	8.53	629.4
GRW_20170622_GW007	GW7	6/22/2017	154	7.03	12.14	3	2	66.1	7.11	628.3
GRW_20170720_GW008	GW8	7/20/2017	159	7.57	11.76	370	277	33.6	3.59	650.7
GRW_20180525_GW008	GW8	5/25/2018	149	7.05	8.28	433	295	33.2	3.91	655.0
GRW_20170720_GW009	GW9	7/20/2017	367	7.41	8.98	785	545	2.5	0.29	650.5

Table G.5 Discharge measured using area-velocity method

Sample ID	Site ID	Sampling Date	Discharge ($m^3 s^{-1}$)
GRW_20170831_GV009	GV9	8/31/2017	2.66
GRW_20170825_GV008	GV8	8/25/2017	1.84
GRW_20160226_GV006	GV6	2/26/2016	1.47
GRW_20160506_GV006	GV6	5/6/2016	7.91
GRW_20160707_GV006	GV6	7/7/2016	1.40
GRW_20160826_GV006	GV6	8/26/2016	0.85
GRW_20170517_GV006	GV6	5/17/2017	11.66
GRW_20170825_GV006	GV6	8/25/2017	1.35
GRW_20160226_GV005	GV5	2/26/2016	0.28
GRW_20160506_GV005	GV5	5/6/2016	0.38
GRW_20160707_GV005	GV5	7/7/2016	0.89
GRW_20160826_GV005	GV5	8/26/2016	0.70
GRW_20170517_GV005	GV5	5/17/2017	0.95
GRW_20170825_GV005	GV5	8/25/2017	0.47
GRW_20160226_GV002	GV2	2/26/2016	8.23
GRW_20160506_GV002	GV2	5/6/2016	1.26
GRW_20160707_GV002	GV2	7/7/2016	0.04
GRW_20160825_GV002	GV2	8/25/2016	0.05
GRW_20170205_GV002	GV2	2/5/2017	0.27
GRW_20170517_GV002	GV2	5/17/2017	1.88
GRW_20170825_GV002	GV2	8/25/2017	0.17
GRW_20160226_GV001	GV1	2/26/2016	0.27
GRW_20160707_GV001	GV1	7/7/2016	1.04
GRW_20160825_GV001	GV1	8/25/2016	0.62
GRW_20170517_GV001	GV1	5/17/2017	0.96
GRW_20170825_GV001	GV1	8/25/2017	0.80
GRW_20170824_HY015	HY15	8/24/2017	1.35
GRW_20170824_HY014	HY14	8/24/2017	1.89
GRW_20170823_HY011	HY11	8/23/2017	1.82
GRW_20170823_HY010	HY10	8/23/2017	1.87
GRW_20170823_HY009	HY9	8/23/2017	1.80
GRW_20170204_HY007	HY7	2/4/2017	0.45
GRW_20170516_HY007	HY7	5/16/2017	0.54
GRW_20170823_HY007	HY7	8/23/2017	1.53
GRW_20160209_HY006	HY6	2/9/2016	0.56
GRW_20160219_HY006	HY6	2/19/2016	0.50
GRW_20160518_HY006	HY6	5/18/2016	1.25

GRW_20160706_HY006	HY6	7/6/2016	2.21
GRW_20160825_HY006	HY6	8/25/2016	1.34
GRW_20170516_HY006	HY6	5/16/2017	1.20
GRW_20170824_HY006	HY6	8/24/2017	1.57
GRW_20160706_HY005	HY5	7/6/2016	2.52
GRW_20170516_HY005	HY5	5/16/2017	1.41
GRW_20170824_HY005	HY5	8/24/2017	2.12
GRW_20160209_HY004	HY4	2/9/2016	0.56
GRW_20160219_HY004	HY4	2/19/2016	0.50
GRW_20160518_HY004	HY4	5/18/2016	0.99
GRW_20160706_HY004	HY4	7/6/2016	2.14
GRW_20160825_HY004	HY4	8/25/2016	1.36
GRW_20170204_HY004	HY4	2/4/2017	0.46
GRW_20170516_HY004	HY4	5/16/2017	1.03
GRW_20170823_HY004	HY4	8/23/2017	1.71
GRW_20160209_HY002	HY2	2/9/2016	0.11
GRW_20160219_HY002	HY2	2/19/2016	0.11
GRW_20160518_HY002	HY2	5/18/2016	0.84
GRW_20160706_HY002	HY2	7/6/2016	0.43
GRW_20160825_HY002	HY2	8/25/2016	0.18
GRW_20170204_HY002	HY2	2/4/2017	0.13
GRW_20170516_HY002	HY2	5/16/2017	1.04
GRW_20170823_HY002	HY2	8/23/2017	0.25
GRW_20160209_HY001	HY1	2/9/2016	0.10
GRW_20160219_HY001	HY1	2/19/2016	0.11
GRW_20160518_HY001	HY1	5/18/2016	1.05
GRW_20160706_HY001	HY1	7/6/2016	0.52
GRW_20160825_HY001	HY1	8/25/2016	0.22
GRW_20170204_HY001	HY1	2/4/2017	0.11
GRW_20170516_HY001	HY1	5/16/2017	1.27